On
two-phase
flow
exchange
between
interacting
hydraulic
channels

T. van der Ros
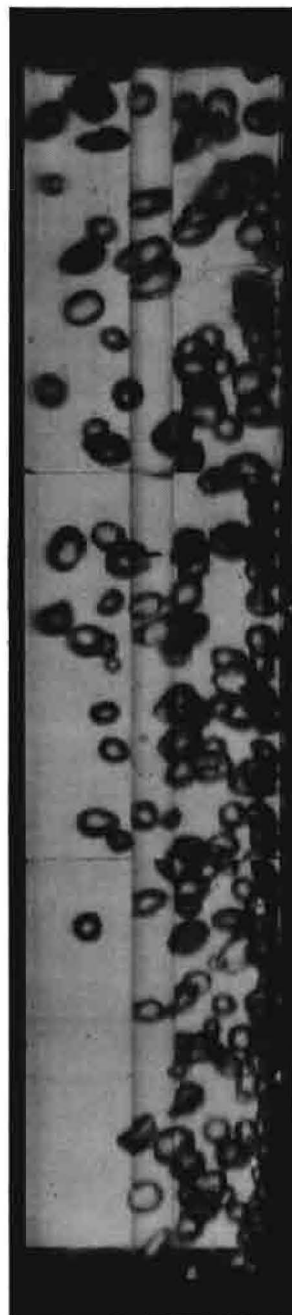
On the cover :

In the photograph gas exchange occurs from the injected channel on the right, through the gap in the middle, to the hydraulic channel on the left.

Note :   In order to obtain a clear view of the mixing phenomenon within this short length of 0.12 m, the inlet liquid velocity was reduced to approx. 0.35 m/s. This resulted in the formation of larger bubbles than obtained during the experimental program.

ON TWO-PHASE FLOW EXCHANGE

BETWEEN

INTERCONNECTED HYDRAULIC CHANNELS

PROEFSCHRIFT

ter verkrijging van de graad van
doctor in de technische wetenschappen
aan de Technische Hogeschool Eindhoven,
op gezag van de rector magnificus
Prof.dr.ir.A.A.Th.M.van Trier,
voor een commissie uit de senaat te verdedigen
op dinsdag 10 november 1970 te 16 uur

door

THEODOOR VAN DER ROS

werktuigbouwkundig ingenieur
geboren te Rotterdam

Dit proefschrift is goedgekeurd door de promotor
PROF. DR. M. BOGAARDT

Aan Helen

SUMMARY

In order to obtain more fundamental knowledge on subchannel mixing, a series of experiments has been carried out on two-phase flow mass exchange in a translucent test section, containing two adjacent simplified reactor subchannels at low pressure.

Bubble generation was simulated by air injection through a porous glass wall into one subchannel. At the exit of the test section, the mass flow leaving each subchannel entered a separator without disturbing the subchannel mixing. The rate of exchange of each separate component as a function of the channel length was determined by measuring void fraction, mass flow, and pressure distributions.

The variables during the experimental program were the simulated channel power, the liquid mass flow rate and the gap width between the subchannels. Each of these parameters was considered to affect substantially the mixing process in the system.

To analyse the observations, a data reduction program was written. Together with the data, correlations for the slip and for the two-phase friction had to be provided as input. Therefore, under the same conditions as the actual mixing measurements, experiments were performed from which these correlations were obtained.

The most important conclusion made from the data is that the experiments have disclosed the mixing mechanism during the observations, all of which were made in the bubble flow regime. Gas mixing behaved as a diffusion mechanism whereas the exchange of liquid rather resulted from the balancing of the axial pressure gradients in the two interacting channels. The liquid cross flow was superimposed on the gas diffusion without interference, although the direction of exchange was often opposite.

Most of the observed effects of the variables during the experiments could be explained by the behaviour of the gas diffusion mechanism.

However, being aware of the limited range of parameters, such as pressure, weight quality, Reynolds' number, type of flow, channel and gap geometry, we do not claim that we have gained more than qualitative effects of the variables used, subject to the experimental conditions.

A mathematical description of the thermo-hydraulic steady-state behaviour of subchannels, including mixing effects, has been added. The theoretical study was based on a solution of the laws of conservation for each subchannel, with the addition of expressions for the two-phase mixing obtained from the observations. The equations were programmed numerically and solved on a computer. The qualitative results of the computations were in reasonable agreement with the experiments.

LIST OF CONTENTS

Chapter 1.   INTRODUCTION

Accurate prediction of the enthalpy distribution in the share of the
coolant system in the core of a nuclear reactor may contribute to
higher reactor performance. The heat removal system of the core consists
of a large number of parallel channels, each divided into interconnect-
ed subchannels formed by a matrix of parallel fuel rods in which the
coolant flows upwards. Since the radial power distribution in a core
is not uniform, the increase in subchannel enthalpy will vary across
the core. Therefore, a hot channel factor has been defined as the ratio
of the maximum local enthalpy increase to the average increase. Since
the turbulent coolant flow in a subchannel mixes with that in neigh-
bouring channels on its journey through the core, reduced maximum en-
thalpy in the hottest subchannel results.

Studies on interchannel mixing have been performed in order to predict
the thermal-hydraulic behaviour of a number of subchannels including
interchannel exchange effects. They may result in a higher critical
heatflux prediction than in many cases where cores have been designed
on the basis of the hottest channel parameters only. Also, it is appar-
ent that by considering interchannel enthalpy exchange correlation of
the results of scaled-down core experiments for critical heatflux data
should improve. Often, such experiments are carried out on the hottest
reactor channel formed by a small number of electrically heated elements
placed within a shroud.
In order to improve the boundary condition for the hottest subchannel,
the number of heating elements in empirical rod clusters tends to be
increased, which requires large power supplies. Subchannel analysis may
eliminate these large bundle experiments. Knudsen (1) reported a better
agreement between experimental critical heatflux data in the hot channel
of small rod clusters by assuming some mixing effects between the sub-
channels of the cluster. Furthermore, a better estimate of the tempe-
rature distribution will ease the structural design of claddings es-
pecially for gas cooled fast reactor elements.

Generally considered are two mechanisms of mixing between semi-open
subchannel which, except in sodium systems, overshadow the effect of
molecular conduction, viz.,

(1) a microscopic transport called turbulent mixing due to the random
    turbulent motions of particles in the gap between the channels.
    Its time-average magnitude of particle exchange at the subchannel
    boundary is always zero; however, when the heat level across the

gap is different, the particles may carry thermal energy from one
channel into the other. The direction of net exchange is such as to
decrease the enthalpy gradient between the subchannels;

(2) a macroscopic transport called cross flow due to different axial
pressure gradients in the subchannels. These gradients may result,
for instance, from different heatflux distributions, changes in
hydraulic diameter or cross-sectional area. Contrary to turbulent
mixing, the local cross flow has a distinct direction corresponding
to a minimum difference between the axial pressure gradients.
A small pressure difference between the channels may be maintained
owing to the frictional pressure drop of the cross flow in the gap.

At present these mechanisms are not understood well enough to derive
reliable theoretical formulae. In order to obtain empirical correla-
tions instead, much experimental work is needed.

1.1.   Single-phase experiments and correlations

During the last decades, many investigators have reported experimental
data on turbulent single-phase liquid mixing. The experiments have been
carried out in two-channel geometries and in clusters by injecting
salts, radio-active fluids, hot water or a dye into a single-phase
fluid system at the inlet of the test section or by heating one or
more channels by electrically heated elements.
Mixing data were obtained by measuring the distribution of the concen-
tration of the injected tracer or of the temperature along the channel
and at the outlet. Figure 1, showing a graph of the number of available
single-phase mixing publications as a function of time, clearly demon-
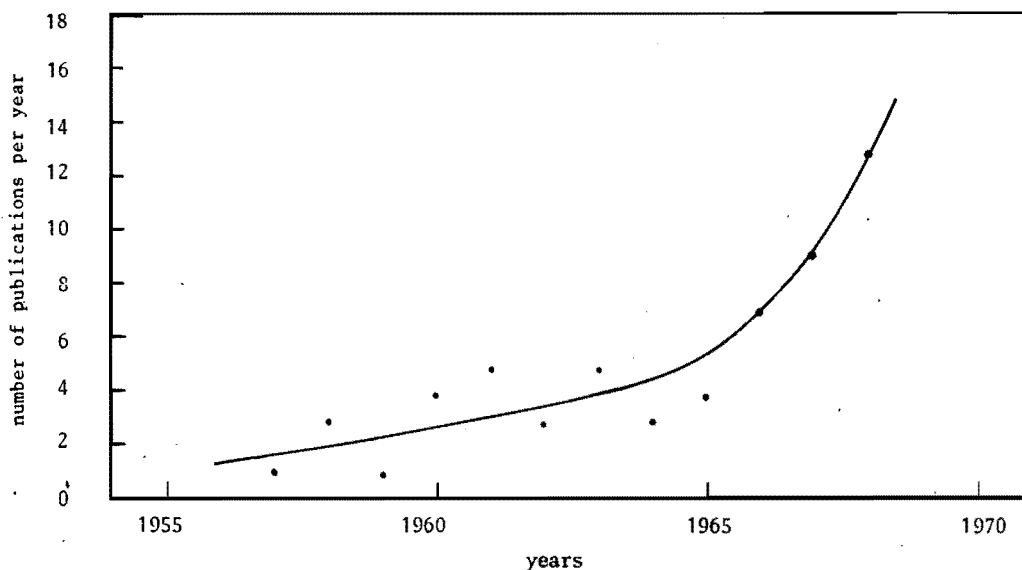strates the increasing interest in this subject.

Fig.1 The increase in single-phase mixing publications

Recent reviews of single-phase mixing data from the literature have been written by Ingesson (2) and Rogers and Todreas (3), primarily directed towards water coolant applications. A survey by Todreas and Wilson (4) is focussed on applications in liquid metal fast reactor systems.

In order to analyse the results, the boundaries of the subchannels considered are usually formed by heating elements or channel surfaces and by division lines thought through the centres of the rods.

Several empirical correlations have been proposed for calculating single-phase mixing rates between subchannels. In all subchannel analyses, the "lumped parameter" approach has been used, averaging parameters such as flow velocity, density and temperature or concentrations, over the flow area of a subchannel.

Ingesson (2) discussed the results arrived at by 16 authors who obtained their single-phase flow data in test sections of different geometrical design of the cross-sectional area: dumb bell, quadratic, triangular, circular 7-rods and 19-rods, row of rods, and tri- and fourcusp.
From these data, including his own experimental results, he obtained a general correlation of the following form, viz., the net amount of heat transferred in the gap between two subchannels per unit length,

$$q' = - s \, \epsilon \, \rho \, c \, \frac{T_i - T_j}{y} \quad , \tag{1.1.}$$

where ϵ denotes the turbulent eddy diffusivity acting as a mixing agent and y stands for the distance between the centroids of the adjacent subchannels.

Correlating the mixing coefficients against the geometrical parameter (pitch to equivalent diameter ratio), he found:

$$\epsilon = 0.05 \sqrt{1/8 \, f} \, (6.12 \, \frac{pitch}{d_h} - 3.03) \, v d_h \quad , \tag{1.2.}$$

Except for few data, the agreement between the mixing predicted by his correlation and the analysed data is reasonable.

A turbulent mixing correlation of coolant in fuel bundles established from experimental results obtained by 9 authors is given by Rogers and Tarasuk (5). They obtained

$$q' = - s \, M_{ij} \, \rho \, v \, c \, (T_i - T_j) \quad , \tag{1.3.}$$

where

$$M_{ij} = \lambda_{ij} \frac{\left\{ 1 + \left(\frac{d_{hj}}{d_{hi}}\right)^{1.13} \right\} \frac{d_{hi}}{D}}{2 \, Re_i^{0.32}} \qquad (1.4.)$$

and

$$\lambda_{ij} = 0.0503 \left(\frac{D}{s}\right)^{1.57} \qquad (1.5.)$$

with a standard deviation of $\pm$ 19 per cent.
Rowe (6) suggested the correlation

$$q' = - s \, \beta \, \rho \, v \, c \, (T_i - T_j) \qquad , \qquad (1.6.)$$

where the mixing coefficient obtained from his own experiments (7) is given by:

$$\beta = 0.0062 \left(\frac{d_h}{s}\right) Re^{-0.1}. \qquad (1.7.)$$

Summarising from the main results obtained from experiments on turbulent single-phase flow liquid mixing between subchannels, we conclude that the rate of exchange increases liniarly with the average mass flow velocity. Further, that the subchannel geometry has some influence, most predominantly the hydraulic channel diameter, but it has been observed that the total amount of turbulent mixing is not a function - or only a weak one - of the gap width s.

Increased mixing with both higher mass flow rates and larger hydraulic diameters can easily be explained by the increased level of turbulence; however, decreased mixing per unit gap width by applying wider gaps between the channels is not easily interpreted. An attempt has been made by Van der Ros and Bogaardt (8), who derived an analytical explanation by using the Prandtl mixing length theory instead of the turbulent eddy diffusivity approach to describe the mixing mechanism. In this theory the rate of transfer per unit area is proportional to the velocity gradient in the gap. This velocity gradient, a mixing promotor, is about inversely proportional to the gap width. The resulting expression for heatexchange between subchannels is:

$$q' = - s \left(\frac{1}{y'}\right)^2 2 \, v \left\{ 1 - 1.35 \left(\frac{s}{d_h}\right)^{0.67} \right\} \rho \, c \, (T_i - T_j) \quad , \qquad (1.8.)$$

where the value of the ratio of the Prandtl mixing length, l, to a
characteristic distance between the channels, y', has been obtained
from a survey of existing data. Expression (1.8.) has been reported
to give fair results with l/y' = 0.1 for gaps formed by round tubes
for s/d$_h$ < 0.5.

It will be clear that in reality the mixing process is much more com-
plex than described by the one-dimensional correlations quoted here.
Large gradients in velocity and in temperature exist in each subchannel,
especially in the neighbourhood of the gap, and the level of turbulence
as well as of mass and heat transport should be described more dimen-
sionally. Studies of these gradients within a hydraulic channel such
as made by Nijsing et al. (9) may contribute significantly to a better
description of inter-subchannel mixing.

1.2.   Two-phase experiments and correlations

Very little information is available on mixing in a boiling system. One
of the causes is, undoubtedly, the difficulty to measure such para-
meters as void fraction, weight quality, mass flow and enthalpy in a
complex two-phase flow system, which quantities should not only be
measured as an average over the cross-section of a bundle or tube, but
should be established for each subchannel individually.

The only experiments performed on mixing rates in a boiling water system
are those by Rowe and Angle (7, 10). In (7) they report on observations
in an electrically heated test section containing two subchannels, one
formed by rods on a square pitch array and located next to another sub-
channel formed by rods on a triangular pitch. All experiments were car-
ried out at 62 bar, with three mass flow rates and for simulated rod
spacings of 0.5 and 2 mm obtained by simultaneously increasing the rod
pitch. The test section was 1.50 m long and designed to allow flow to
enter and leave each channel separately. In reference (10) Rowe and
Angle report on experiments with a different test section, viz., two
equal subchannels formed by rods on a square pitch array. Those measure-
ments were designed to determine the influence of a certain spacer type
on the mixing. A tracer has been used to determine the amount of mass
exchange. Except for the pressure of 27.5 and 52 bar, the same flow
parameters were used as in (7). In the experiments the average amount
of mixing during boiling was determined from enthalpy and mass flow
measurements at the separate exits of each channel. No void fraction
measurements have been taken, however the steam quality could be calculat-
ed from a heat balance. The conclusions made from their experiments are
the following:

(1) Mixing during boiling was found to be not always higher than mix-
    ing without boiling. All of the observed variations in mixing rates
    seem to be related with two-phase flow patterns.
(2) The average mixing varies significantly with exit steam quality.
    Mixing increased with quality to a peak value with steam qualities
    of 0.1-0.2, and decreased by larger qualities.
(3) Increasing the flow rate tends to suppress the variation in mixing
    with steam quality.

15

(4) Rod spacing was found to be an important parameter during boiling. Small gaps do not allow a significant increase in mixing with mass flow rate during boiling, wider gaps allow larger mixing with increasing mass flow rates.

(5) A pressure reduction causes moderate increases in mixing. A shift occurred in the mixing rate against quality consistent with two-phase flow regime boundary shifts that occur in steam-water mixtures.

(6) The effect of spacers was moderate, a small increase at lower qualities and decrease at higher qualities.

Experiments on subchannel mixing in an electrically heated seven-rod cluster during boiling in FREON-12, modelling water at 69 bar, were performed by Bowring and Levy (11). The cluster was thought to incorporate two types of subchannels. One subchannel consisted of six identical equilateral triangular subchannels formed by imaginary lines between the centres of the middle rod and those in the ring of six rods. The other type consisted of six identical subchannels between the outer rods and the shroud. At the exit the flows of the two different types of subchannels were separated. The gap between the tubes was 1.5 mm, the heated channel length 0.9 m. From the observed average mixing, determined from the exit enthalpy values, the conclusions are that mixing decreased when boiling started. With full boiling the average mixing was apparently independent of the exit quality.
Furthermore, the mixing was inversely proportional to mass velocity in the boiling region.

Mixing measurements in an atmospheric air-water system have been performed by Rosuel and Beghin(12) and by Bestenbreur and Spigt (13) who used the same experimental apparatus. The test section, made of plexiglass in order to allow visual observations, consisted of two subchannels simulating reactor channels formed by rods in a square pattern. The gap width was 5 mm, the channel length 1.37 m. Air was injected into the channel at the inlet or at locations downstream of the entrance, through a small tube. The amount of average mixing, measured at one mass flow rate, was determined from the exit conditions of each subchannel where the mass flow of air and water was separated. Furthermore, the volumetric void fraction was measured by means of a gamma ray attenuation method at different locations along the height of the test section, and the pressure distributions in the subchannels were read on a multimanometer. Although their results were influenced by their point injection they found that the amount of mixing, expressed in terms of air qualities, was strongly influenced by the flow regime. Rosuel and Beghin established the effect of twisted tapes used as turbulence promotors and reported very effective results with regard to quality mixing. Bestenbreur and Spigt measured relatively large pressure differences up to 20 mm water column across a 5 mm wide gap between two subchannels, which data were mainly collected in the slug flow regime.

All the described experiments have been performed with flow splitting devices at the exit of each subchannel. To simulate reactor conditions where the subchannels end in a common chimney, the most natural flow split would be that corresponding to zero exit pressure differentials between the subchannels.

In reference (7) Rowe and Angle reported pressure differences between the subchannel exits up to 35 mm water column. Bowring and Levy reported that, under boiling conditions, zero pressure differentials could not be established and Bestenbreur adjusted the flow splitting valves for equal pressures in the air-water separators located 0.5 m downstream of the test section exit. Therefore special attention has been paid by the present author to the natural flow split in the experiments described in this study.

A limited number of numerical computer programs has been written to predict subchannel behaviour including mixing effects. However, the only sophisticated subchannel analysis codes published, capable of handling both turbulent mixing and cross flow during boiling are COBRA (6, 14) and HAMBO (15). Both one-dimensional models have been written as a calculation tool for reactor designers. For each subchannel, the equations formed by the laws for conservation of mass, momentum and energy are solved, including terms describing the interaction effects between the subchannels.

In the COBRA code the correlation for the rate of turbulent mass exchange per unit length between two subchannels is given by

$$w' = s \ \beta \ \tfrac{1}{2} \left(\frac{M_i}{A_i} + \frac{M_j}{A_j} \right) \quad , \tag{1.9.}$$

where β, a mixing coefficient, has to be obtained empirically.
In HAMBO the equivalent correlation reads:

$$w' = \frac{s}{S} \frac{F_m}{D} \sqrt{\frac{f_i + f_j}{80}} \left(\frac{d_{h,i} M_i}{A_i} + \frac{d_{h,j} M_j}{A_j} \right) \quad , \tag{1.10.}$$

in which F_m is an empirical parameter similar to β, and S a gap shape factor.

Time-averaged, the turbulent rate of mass transfer is zero. Enthalpy exchange between two subchannels is governed by

$$q' = w' \ (h_i - h_j). \tag{1.11.}$$

The rates of cross flow in COBRA and HAMBO are calculated from the condition that a flow redistribution in the subchannels will take place until the pressure difference between the channels equals the amount of lateral friction caused by the cross flow.

In COBRA it has been assumed that the turbulent mixing may be super-imposed upon the cross flow mixing, in HAMBO a modifying effect of the cross flow on the turbulent interchange has been incorporated.

COBRA and HAMBO are mass flow enthalpy models, i.e. the fluidum described in the conservation laws is not characterised by a split-up in vapour and liquid components with their relevant properties, but is a quasi one-phase fluidum. The weight quality is calculated from the fluid enthalpy. The unknowns for which the equations have to be solved are mainly the mass flow rates and the enthalpies.

This approach results in an average density and enthalpy exchange for the two phases in both turbulent and cross flow mixing. Furthermore, the values of the employed mixing coefficients have been suited to agree with experimental data on mixing at the exit of the test sections by lack of information at other locations. Up to now, no experimental data have been available to confirm or reject the assumptions made for calculating subchannel mixing, nor to obtain assessments of the empirical coefficients needed in expressions (1.9.) and (1.10.) or for the lateral friction in gaps.

1.3. Aim of this study

The only information that exists on experiments of mass and/or heat exchange between two-phase flow channels has been dealt with in the previous section. The very limited experimental data available are mainly those that refer to the exit conditions of the subchannels, except those regarding the void fraction, which has been measured as a function of the channel length by Rosuel and Beghin (12) and by Bestenbreur (13).

The need for more mixing data has been expressed by, among others, Rogers and Todreas (3) quoted:
"Little information is available for mixing between individual sub-channels isolated from others to permit controlled conditions and none taken for individual subchannels over a continuous parameter range to permit adequate establishment of the behaviour of mixing flow rates with individual parameters of interest. This lack of even a meager amount of systematic data has not permitted confirmation of the functional property dependencies of the models for any of the mixing processes proposed."

In order to obtain more fundamental knowledge on subchannel mixing, a series of experiments has been carried out on two-phase flow mass exchange in a translucent test section containing two adjacent simplified reactor subchannels at low pressures (See Figure 4).

Bubble generation has been simulated by air injection through a porous glass wall into either or both subchannels. At the exit of the test section the mass flow leaving each subchannel enters a separator without disturbing the subchannel mixing.

The amount of exchange of each separate component as a function of the channel length was determined by measuring void fraction, mass flow, and pressure distributions.

18

The variables during the experimental program have been the simulated channel power, the liquid mass flow density and the gap width between the subchannels. Each of these parameters was considered to effect substantially the mixing process in the system.

The knowledge gained has been used to develop correlations that describe and predict the mixing of each phase for the channel-geometry used.

Air-injection instead of heat addition to the system was chosen to generate bubbles in the liquid flow. The main reason was the accurate determination of the weight quality of the gas and the desire for visual observation of the process. The choice of channel geometry was rather arbitrary although square channels were desirable for measuring void fraction with the impedance technique (See chapter 2). The hydraulic diameter was chosen equal to that of an average value of reactor subchannels.

However, being aware of the limited range of parameters, such as pressure, weight quality, Reynolds' number, type of flow, channel and gap geometry, we do not claim that we have gained more than qualitative effects of the variables.

To the author's knowledge no systematic study on subchannel mixing of this sort, in which the amount of exchange of each phase is determined as a function of the channel height, has been published up to now.

Chapter 2.   EXPERIMENTAL EQUIPMENT

2.1.   The loop

The experimental investigation has been carried out in a test section
incorporated in a loop system which will be described in this section.
A flowsheet of the system is shown in Fig. 2.

The loop was constructed of stainless steel and designed for a pres-
sure of 20 bar. Water from a storage reservoir was forced by a centri-
fugal pump through a 9 kW electric preheater and a mass flow regulat-
ing valve to the lower end of the test section. Located just upstream
of the test section was a calming-chamber through which the mass of
water flowed at a low velocity in order to quiet down any disturbances
and extra turbulences caused by the pipe bends. From this area the
fluid accelerated towards the two separate subchannels of the test
section. Into the testsection air entered either one or both subchan-
nels through a wall surface of porous glass, and the liquid and gas
components were allowed to mix across the gap between the subchannels.
At the exit of the test section, the mixture from each subchannel was
separated and entered an air-water separator. Gravity took care of the
separation of the two phases: water returned to the reservoir, air was
dumped.

At first the separators were connected to the test section exit by
pipes of a certain length, as shown in Fig. 3, in a way similar to the
experimental apparatus of other investigators (7), (10), (11), (13).
The exit valves were adjusted to obtain equal pressure in both separa-
tors. Another condition that had to be met was equal exit pressure in
both subchannels to simulate a common header. This arrangement imposed
a boundary condition on the mixing at the exit of the subchannels. For
the two-phase mass flow division had to be such that the pressure drop
over each pipe connecting the subchannel exits with the separators,
became equal.

In order to obtain this "stable" exit condition, a relatively large
amount of cross flow could be observed over the gap near the channel
exits. Under certain channel conditions, an exit division could be ob-
tained in which all the mass flow of liquid and gas left the test sec-
tion from one subchannel exit. A large amount of cross flow could then
be observed over the final part of the gap. However, these cross flows
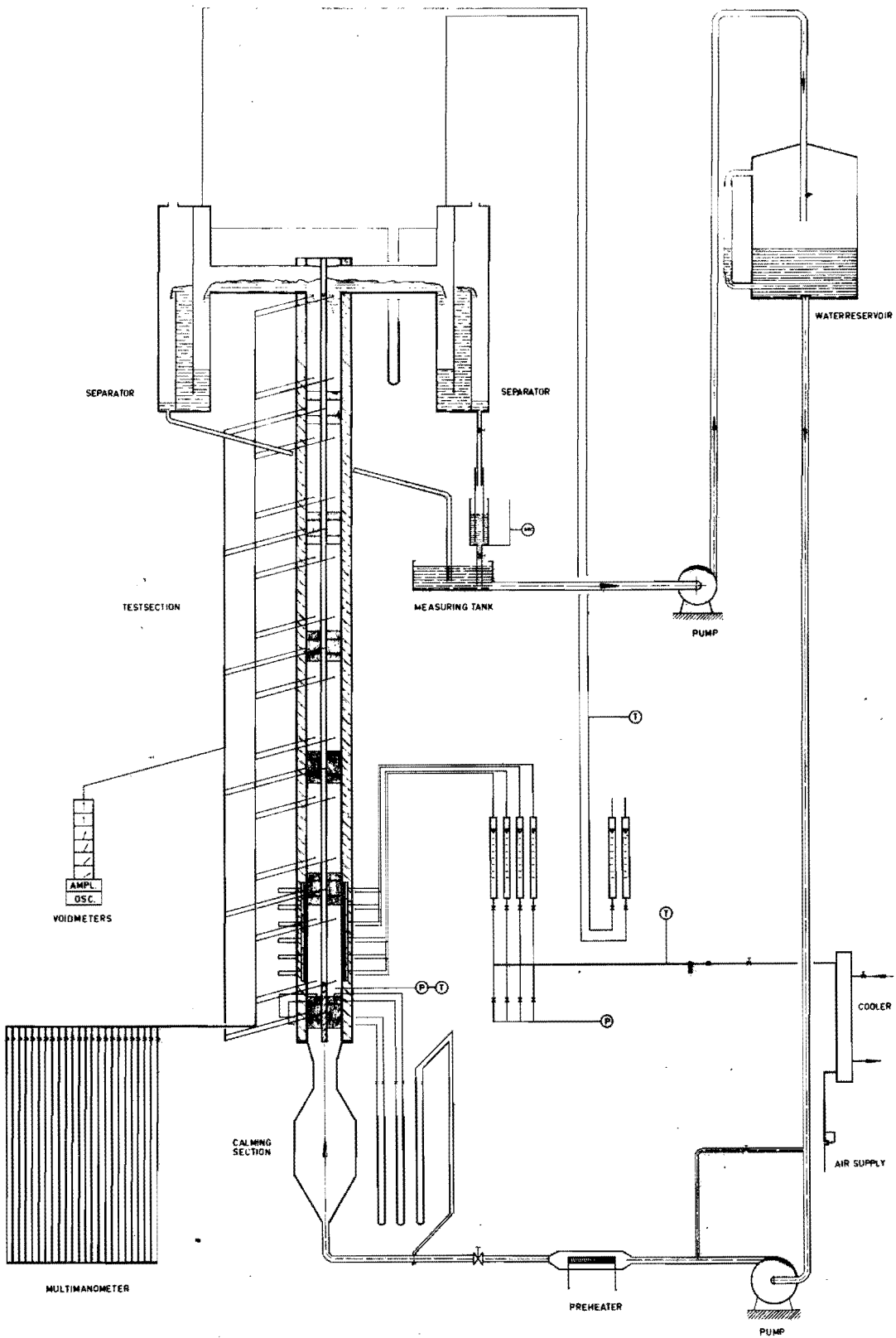did not result in a pressure difference of more than a few mm water

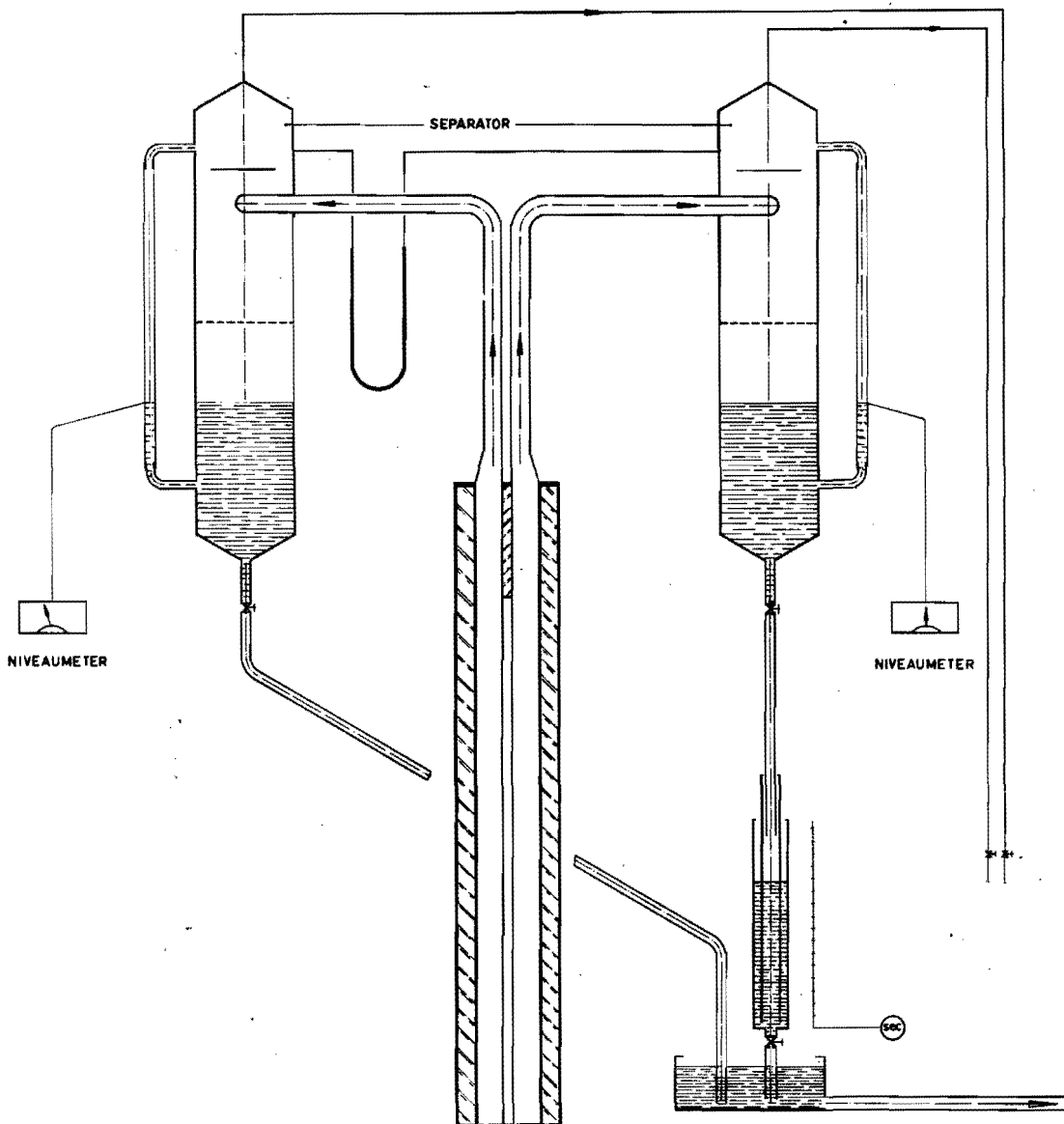Fig.2 Flowsheet of the experimental apparatus

Fig.3   Exit test section with separators

column between the subchannels. In this case the static pressure head in the non-flowing pipe equalled the sum of the static pressure head and the frictional pressure losses of the mass flow in the other pipe.

To overcome this type of "forced" mixing towards the end of the test section, the test section exit was redesigned to include large over-flow parts in the sides of each channel, just downstream of the loca-tion where the subchannels separated (See Fig. 2). Except for the very small exit pressure losses in the overflow parts, the pressures in the air dome of the separators could be made equal by adjusting the small valves in the airline to the rotameters without disturbing the exit conditions of the mixtures.

Another important requirement for proper functioning of the separators was the maintenance of a constant liquid level. Even small deviations of this level during the experiments would result in erroneous mass flow rates of air and water leaving it, because of the relatively large flow area of the separator, as compared with the flow area of the test section. Therefore, an overflow channel was incorporated in the design of the separators as shown in Fig. 2.

2.2. The test section

The test section, shown in Fig. 2. and Fig. 4. was accurately construct-ed of 3 pieces of perspex, chosen mainly to permit visual observations. A design in this material h as to be very rigid since it is a thermoplast. Owing to its low thermal conductivity, heat losses to the surroundings as well as from one channel to the other, are negligible. Disadvantages are: its large thermal expansion coefficient (if one channel is at an elevated temperature with respect to the other) and the permanent de-formation at temperatures above 70°C. These properties were important during the single-phase mixing experiments reported in (8) when heat was supplied to the channel.

The two subchannels were 10 mm square in cross-section and the distance between the channels was 4 mm. The test section inlets were separated
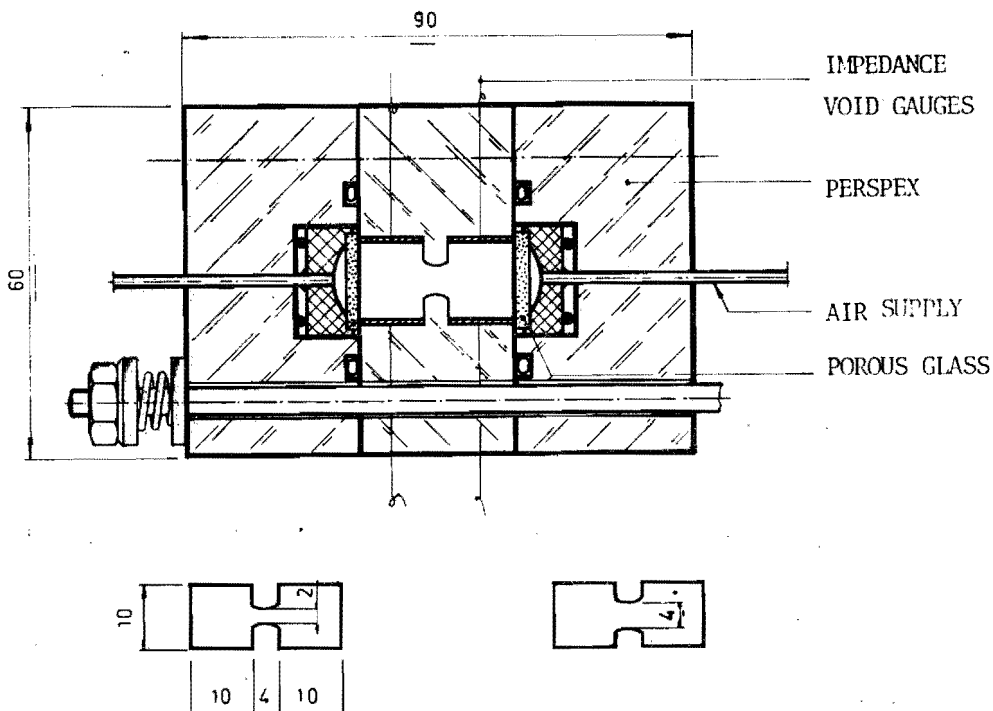

Fig.4 Test section

over 0.265 m, then connected by a gap over a length of 1.85 m or 185 hydraulic diameters. Measurements have been carried out with two different gaps of round-off shapes with minimum widths of 2 and 4 mm, as shown in Fig. 4.

Facilities for air injection to simulate bubble generation on a heated surface during boiling in saturated water were provided in each channel over a length of 0.30 m, starting at the point where the gap connected the channels. The construction is shown in the cross-section of the test section. In either of the outer parts of the test section, a groove was provided to receive a bronze supporting strip on to which pieces of porous glass were glued. Air entered the space between strip and glass from a flexible rubber tube, and was dispersed through the porous glass into the liquid flow in the form of small bubbles. Since the pressure change over the 0.30 m in the channels was not negligible compared with the pressure drop of the air over the porous glass, the air injection construction was divided into separate compartments. Thus, the air pressure for each compartment or for a set of compartments could be adjusted to the pressure in the channels. Fig. 4 also shows the embedded void gauges.

2.3.   Instrumentation

During the execution of the experimental program the following quantities were recorded:

1. total mass flow rate of water to the test section;
2. mass flow rate of air into the subchannels;
3. water temperature at the inlet of the test section;
4. mass flow rate of water at the entrance of each subchannel;
5. average liquid mass flow velocity in one subchannel at locations 0.4 and 1.12 m downstream of the connected subchannels;
6. average volumetric void fraction at several locations in each subchannel;
7. static pressure at the inlet of the test section;
8. static pressure differences in a large number of places at the wall of each subchannel;
9. mass flow rate of liquid and air at the exit of each subchannel.

The locations where the different readings have been taken are shown in Fig. 5.

The total mass flow rate of water to the test section was determined by means of a pressure drop measurement over an orifice plate located in a pipeline upstream of the test section. The instrument used was a Meriam manometer with a total uncertainty of ± 1 mm water column.

The mass flow division at the entrance of each channel was determined by subtraction of the total pressure and the static pressure on a Meriam manometer. The meters were individually calibrated against the total mass flow reading within ± 1 per cent. The total mass flow uncertainty was ± 0.5 per cent. The air flowing to the different compartments of porous glass was taken from an available 7 at. pressure line.
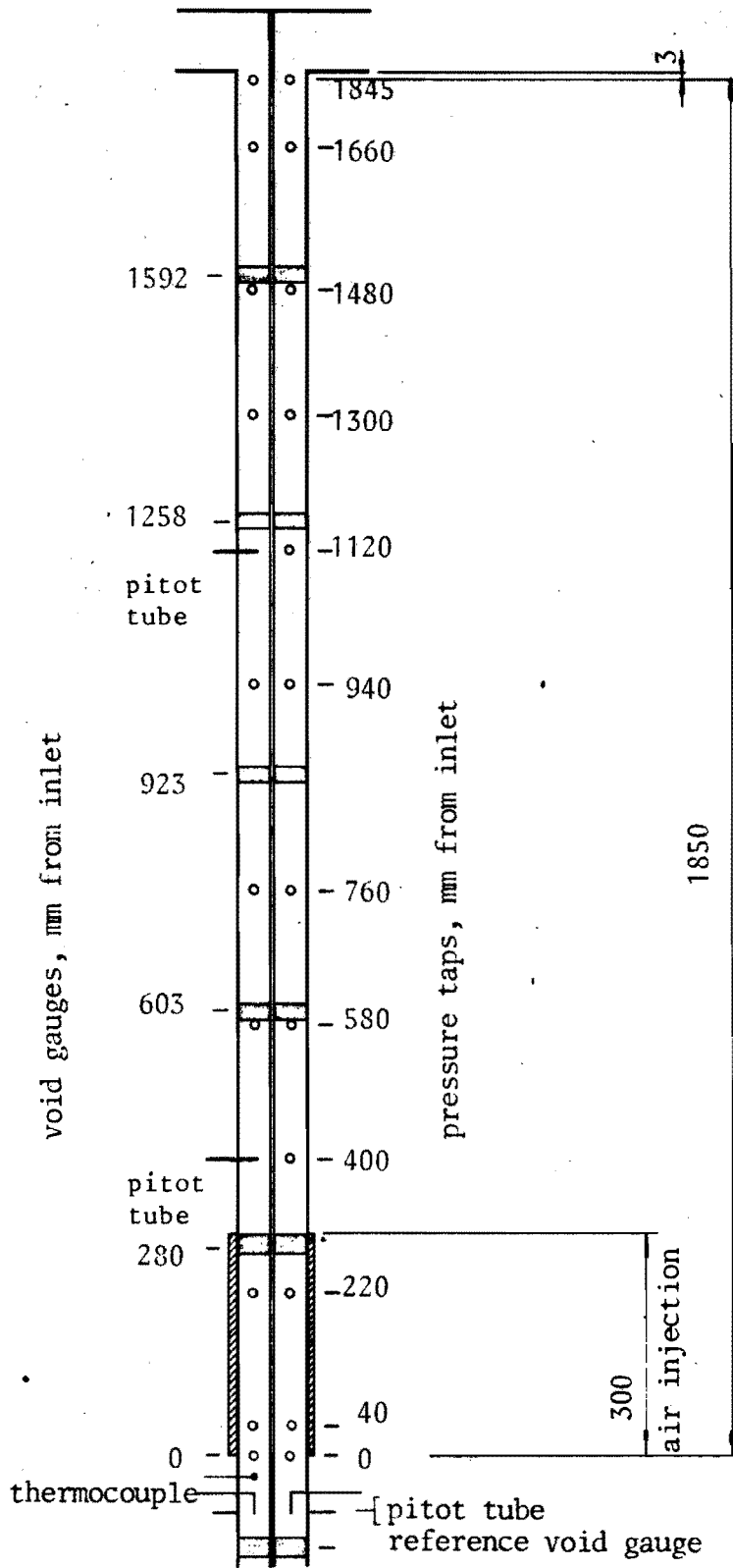
Fig.5 Location of sensors in the test section

The pressure was first reduced to about 2.5 bar and then the supply
air, after moving through a filter and a flow regulating valve, passed
a rotameter before entering the test section. The rotameters had been
calibrated by the manufacturer and were recalibrated against a wet
rotating gas meter at the Calibration Service of the University within
2% accuracy. Corrections were made for the pressure and the tempera-
ture of the air leaving the rotameters.

Temperature recordings were made with calibrated chromel-alumel thermo-
couples connected to a recorder with an accuracy of better than $1^{\circ}C$.

At two locations the dynamic pressure head of the mixture was measured
in the non-injected subchannel. The pitot tubes had an outside diameter
of 1.2 mm, a wall thickness of 0.2 mm and in the wall there was a 0.7 mm
diameter hole. The tubes, which were closed at one end, were mounted
perpendicularly to the mass stream. The holes faced upstream and their
centres coincided with the axis of the channel. The pitot tubes were
calibrated during symmetrical air injection in the subchannels when no
net mixing occurred, and the void fraction being known, the local average
liquid velocity could be calculated. An example of the calibration curves
is shown in Figure 6.

Probably the most important parameter to be determined in this two-phase
flow system is the volumetric void fraction. Its definition reads: the
ratio of that part of a volume occupied by the gas to that of the total
volume.

Of the two void fraction measuring techniques suitable to detect average
values, viz. the gamma-ray method and the impedance method, the latter
was selected. Both techniques have been described extensively in refs.
(16) and (17). Advantages of the gamma-ray method, which is based upon
the attenuation of a beam of gamma rays passing through a two-phase
flow system, where the density difference of the phases is sufficient-
ly large, are:

(1) independence of channel geometry,
(2) suitability for all regimes, and
(3) possibility to obtain a radical void fraction profile.

Disadvantages are:

(1) the long integration times required,
(2) the large interpretation uncertainty at void fractions lower than
    0.4, and
(3) indirect reading.

Advantages of the impedance method, which is based upon the change of
the impedance of the continuous water flow by the presence of gas
bubbles, are:

(1) direct reading, and
(2) if the required conditions can be met, the relatively low degree
    of uncertainty in the void fraction reading.

26

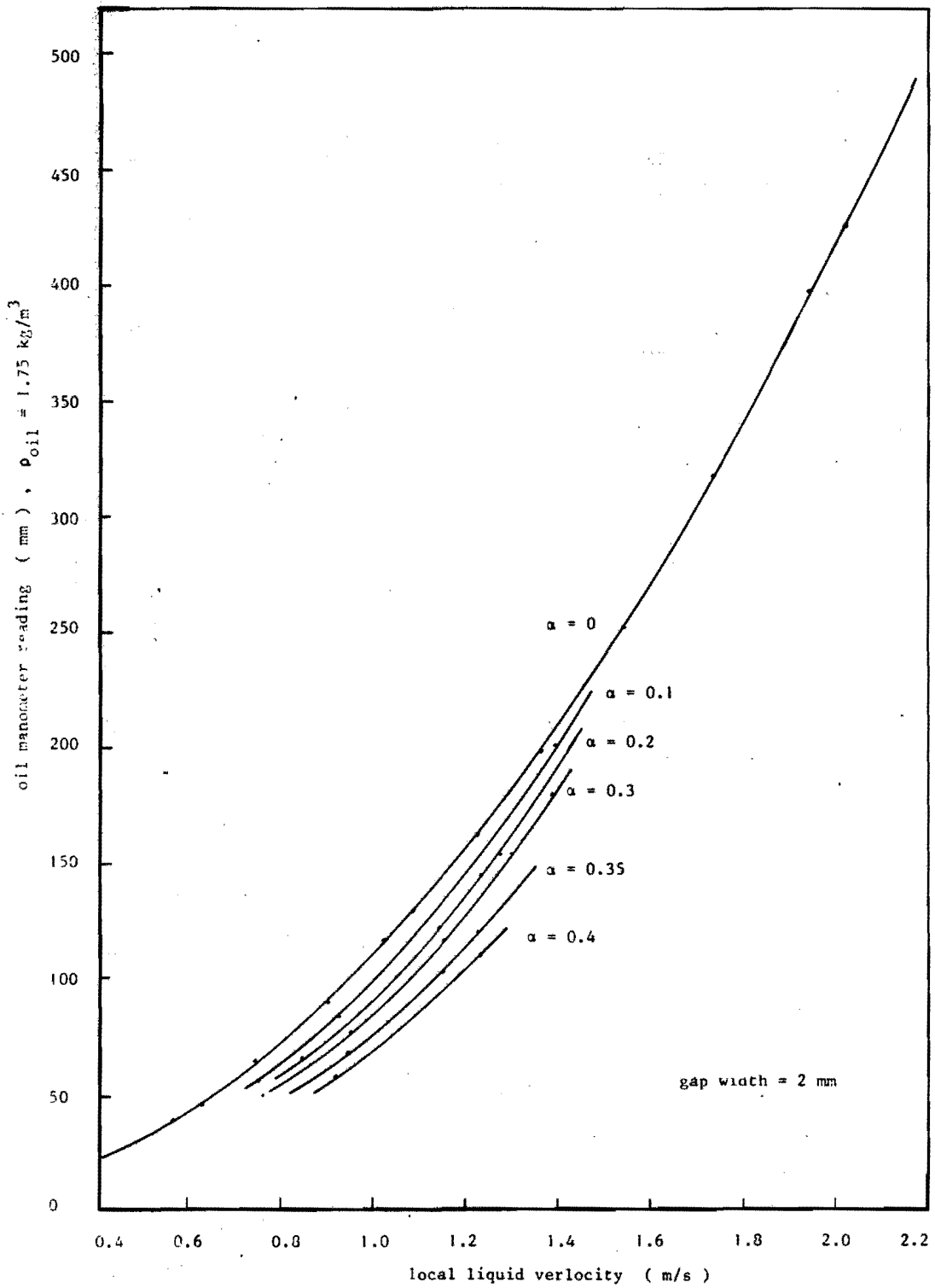Fig.6   Calibration curves for the pitot tube located 1120 mm
downstream of the test section entrance

Disadvantages are:

(1) the void gauges must be calibrated;
(2) measurements are only possible in the bubble flow and slug flow regime, and
(3) the value of the void fraction will be obtained as an average in the volume between the impedance electrodes.

The main reasons for deciding in favour of the impedance method have been the better accuracy at the lower void fraction and the avoidance of long integration times. The optimum conditions as stated in ref. (18) when using the impedance method are as follows:

(1) a homogeneous electromagnetic field between the two gauge electrodes;
(2) a non-flow obstructing design;
(3) a relatively long distance between the electrode plates in respect of the bubble diameter.

The original concept and theory of the impedance method are due to Maxwell (19), who derived a relation between the impedance of a mixture, k_α, and its void fraction, α, where the mixture was assumed to consist of a continuous fluidum with suspended gas bubbles, whose diameter were small as compared with the distance between the bubbles.

The relation reads:

$$\frac{k_\alpha - k_1}{k_\alpha + 2k_1} = \alpha \frac{k_g - k_1}{k_g + 2k_1} \; . \tag{2.1.}$$

In contrast to steam as the gaseous phase, the impedance of air at room temperature and with a relative humidity of even 100% was negligible.

This simplified the relation to:

$$k_\alpha = k_1 \; \frac{1 - \alpha}{1 + \alpha/2} \quad , \tag{2.2.}$$

graphically shown in figure 7.
The test section conditions in respect of geometry and system conditions were ideally suitable for the impedance method. The first condition as mentioned above, could be fulfilled by extending the electrode plates over the full width of two opposite sides of the square channels. The channels were made out of perspex and had non-conductive walls. Both upstream and downstream of the electrodes, guard plates were positioned. The electrical system is shown in figure 8. A sine-shaped signal is fed to the void gauge electrodes through a resistor. The guard plates are supplied from the same source, the current, however, by-passing the resistor. The electromagnetic field then created will be fairly homogeneous in the centre but will be deformed at the
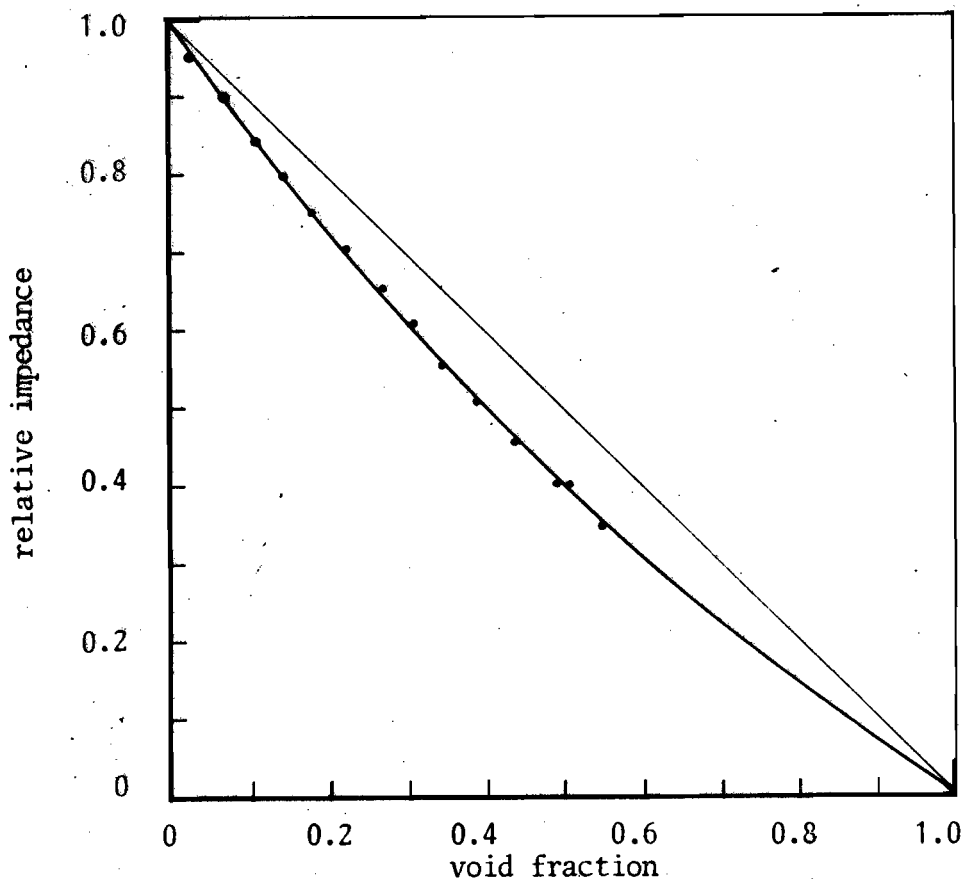
Fig.7   Maxwell curve of the relative impedance

ends of the guard plates by the conductance of the electrical current through the mixture just outside the region between the plates.
The value of the voltage drop across the resistor was small as compared with the impedance of the two-phase mixture between the plates. It was amplified and, after being rectified, measured with a milliammeter. The equipment used has been found to be linear within 2 per cent when the specific conductivity of the water was between 5.5 - 4.2 µS and with the oscillator frequency being 1500 Hz. The linearity has been checked by replacing the void plates by a decade box connected directly to the test section, thus including the wiring. A low frequency or d.c. supply appeared to polarise the fluid, a higher frequency led to problems with inductance losses between the wires connecting the plates to the measuring equipment. The plates were of silver to overcome the formation of an isolating oxyde layer. They were embedded in the channel walls in order to prevent deformation of the channel geometry which would change the slip ratio and thereby the void fraction.

Owing to the water condition and the method of air injection, the air bubble diameter was of the order of 0.5 - 1.0 mm. The distribution of
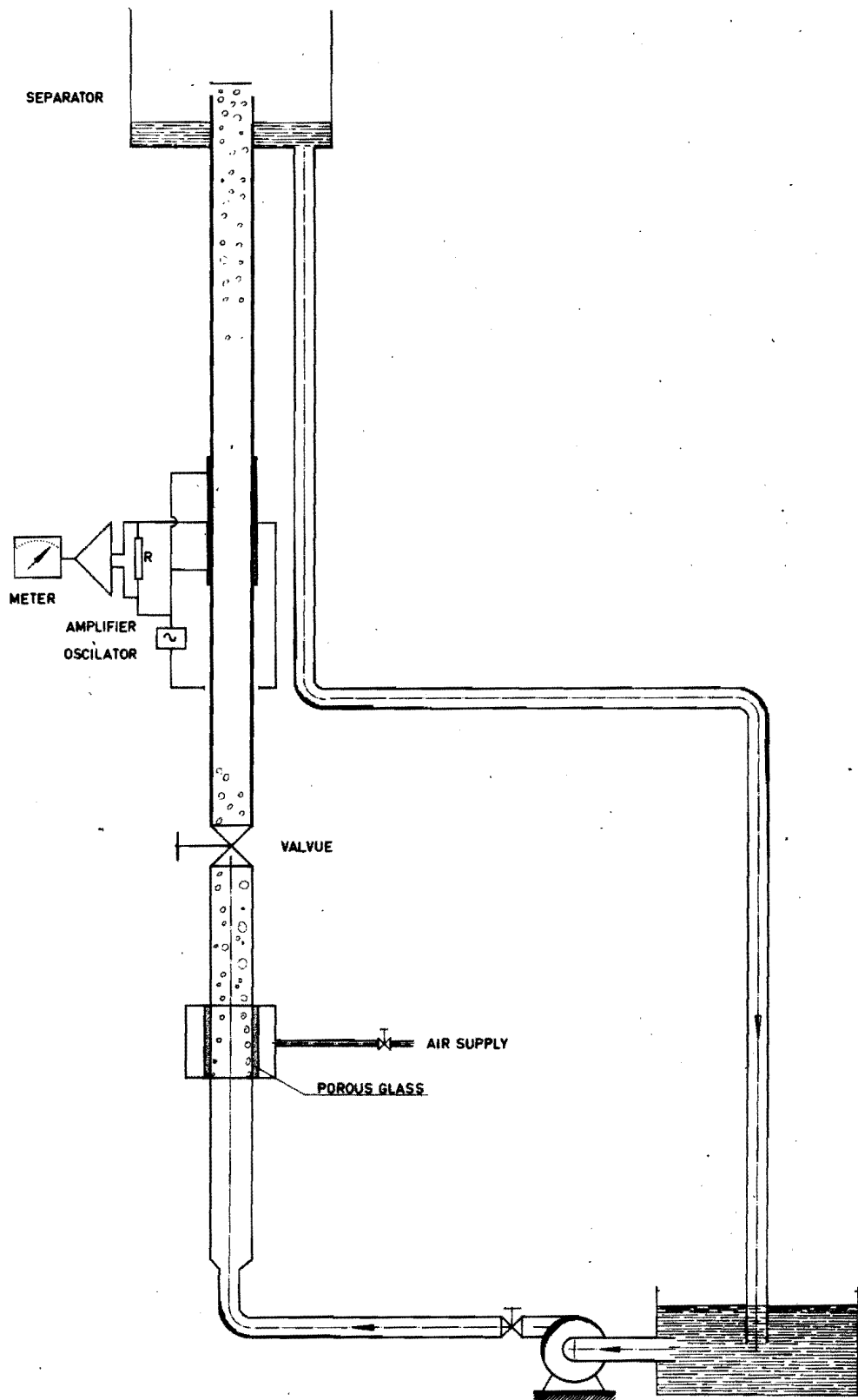
29

Fig.8 Voidgauge calibration loop

the air in the channel was fairly homogeneous up to a void fraction of
about 75 per cent, where the flow regime changed from bubble flow to
slug flow.

The void gauges were calibrated in an especially built channel having
the same cross-section as each of the subchannels. The calibration loop
is shown in figure 8. Water of equal conductance as the water being
used during the experiments was pumped through a channel of 1 m length.
At the end of the channel the water returned to the reservoir. Air was
injected into the flow some distance upstream of the channel using a
method similar to the one used in the actual experiments in order to
obtain the same bubble dimensions. After the flow profile was stabilis-
ed, the mixture entered the calibration channel. A void meter of the
same construction as in the test section was provided halfway the chan-
nel length.

The conductance of the mixture while flowing through the channel was
compared with the average void fraction in the whole channel by measur-
ing the water volume content in the channel after suddenly closing the
ball valve at the entrance. The real void fraction in the channel is
calculated as:

$$\alpha_{real} = \frac{total\ channel\ volume\ -\ collected\ water\ volume}{total\ channel\ volume}$$

This is justified by the fact that the slip and the void fraction
over the length of the channel were influenced only by the small change
in air density due to the axial pressure gradient in the mixture. As
the pressure distribution over the length of the channel was almost
linear, the void fraction in the middle at the location of the plates
was close to the average over the channel.

The calibration results are plotted in figure 7, together with the
Maxwell curve. No influence on the water velocity could be observed
as long as the bubble flow regime was maintained. All data, except the
lowest void fraction data point, were within a relative deviation of
less than 2% from the Maxwell curve. The absolute void fraction for
none of the data was in excess of 0.5% deviation from the Maxwell curve.

Although the assumption in the theory of Maxwell about the distance be-
tween the suspended bubbles being large compared with their diameter
is obviously not applicable in these experiments, the average deviation
of the data is negligible, and the Maxwell curve has been used to
translate the impedance of the mixture in the experiments into a void
fraction.

In addition to an absolute pressure measurement at the inlet of the
test section, 1 mm pressure holes have been used to determine the
axial and radial pressure distributions in the test section. The loca-
tions of these taps are shown in figure 5. The holes are connected to
a multimanometer filled with Meriam oil. The effect of the tap geometry

on the error is negligible while the manometer can be read within ± 1 mm water column.

The water flow rate from the separators has been measured by dividing a certain amount of water poured into a calibrated tank by the time needed to collect it; the air flow rate has been determined with a rotameter. Corrections on the calibration graphs for the rotameters have been made for the pressure and temperature of the air in the rotameter.

Chapter 3.   EXPERIMENTAL RESULTS

3.1. Channel correlations

In order to analyse the experimental results a data-reduction program
has been written for a numerical computer. Together with the experi-
mental data, correlations for the slip and for the two-phase friction
have to be provided as input data. Therefore, under the same conditions
as the actual mixing measurements, experiments have been performed in
which these correlations were obtained.

3.1.1. Slip

A series of experiments has been run for determining the slip ratio
between the two phases, defined by the ratio of the velocity of the
gas phase averaged over the cross-sectional area, to the average liquid
velocity. The data have been obtained by symmetrical injection of air
in each subchannel. In this case no net amount of mixing occurs and the
liquid and gas flow rate as a function of the channel length in each
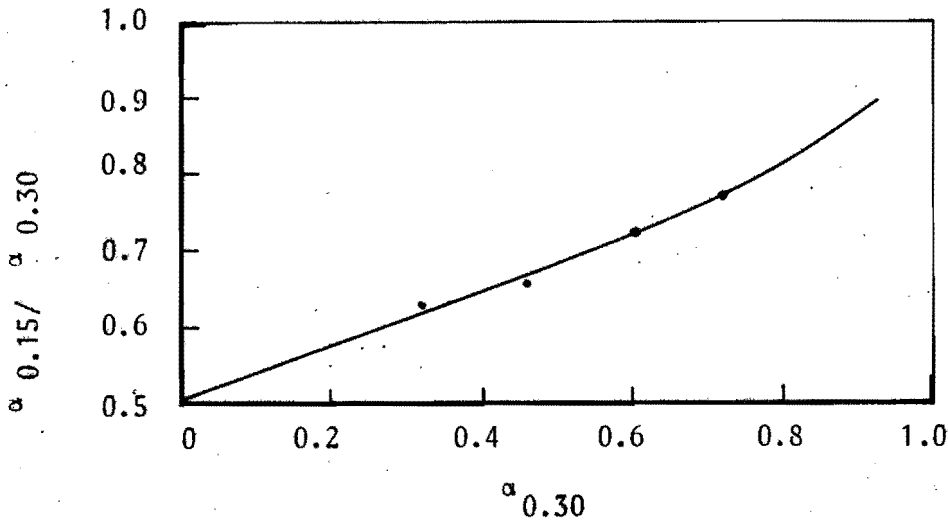
Fig.9 Void fraction halfway the injected length

subchannel is known. Injection took place over a length of 0.3 m start-
ing at the point where the gap connected the two subchannels. In this
region the void fraction increased as shown in figure 9, in which the
ratio of the void fraction halfway the injected length to that at the
end is plotted against the void fraction at the end of the injected
length. The increase in void fraction over the rest of the channel
length as a result of a decreasing air-density was between 5 and 10 per
cent. In figure 10 a graph of the average volumetric void fraction in
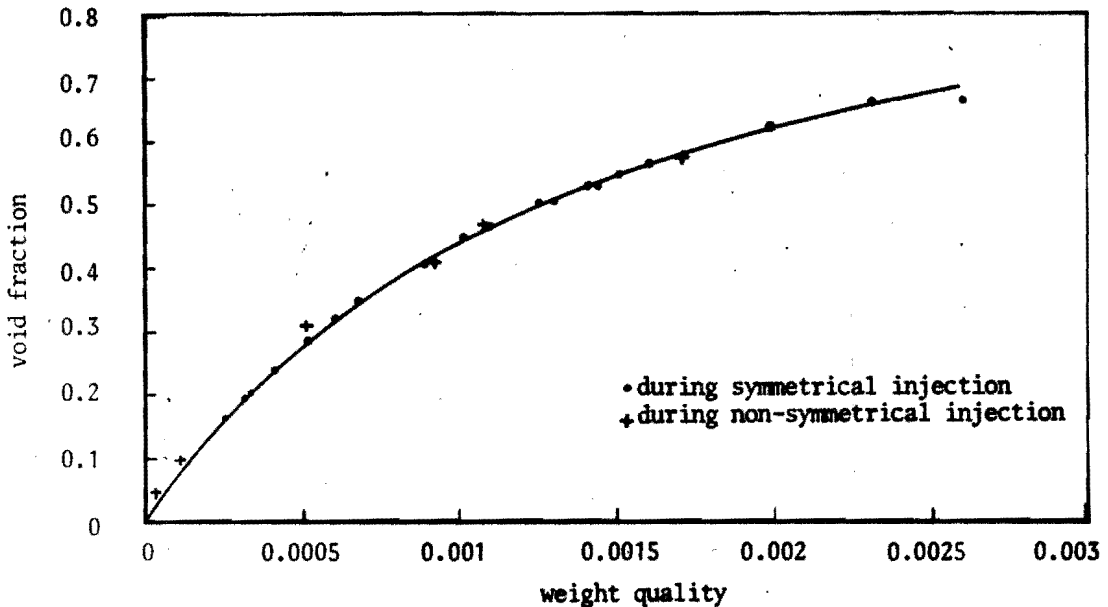the non-injected channel length against the weight quality is shown.

Fig.10 Void fraction versus quality

The mass flow of liquid has been varied between inlet velocities of 0.75
to 1.5 m/s. The curve in figure 10 has been used to calculate the slip
ratio as a function of the void fraction with the physical expression:

$$S = \frac{1-\alpha}{\alpha} \quad \frac{x}{1-x} \quad \frac{\rho_1}{\rho_g} \quad .$$

(3.1.)

In figure 11 the slip has been plotted for ρ_1/ρ_g = 750, which is in
the pressure range of the experiments.
It will be seen that for void fractions larger than 0.25 the slip ratio
becomes somewhat less than unity. In the bubble flow region this has
been observed before by Zuber et al. (20) and by Wisman (21). The slip
ratio mainly depends on the void fraction distribution over the cross-
section of the channel area.
A slip ratio in the neighbourhood of unity indicates a homogeneously
distributed bubble field over the cross-section which in the one-dimen-
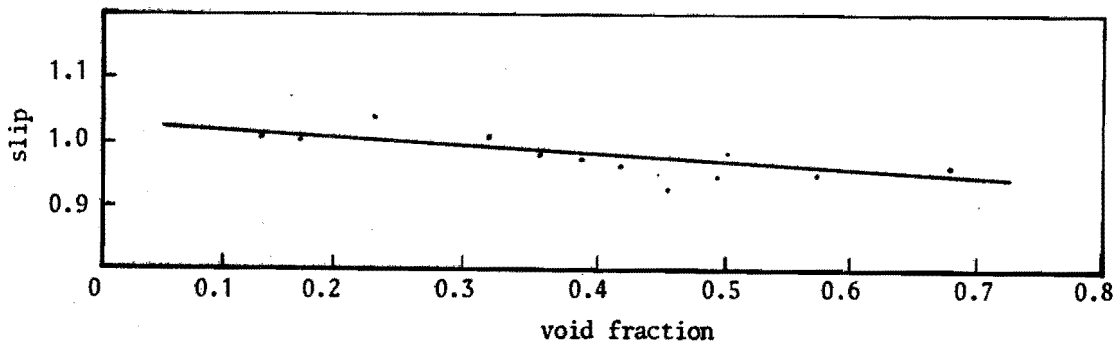sional analysis of this study may be seen as an advantage. The α-x

34

Fig.11   Slip ratio versus void fraction for $\rho_1/\rho_g = 750$

relation in figure 10 was obtained during symmetrical injection. The validity of this curve during non-symmetrical injection could only be verified for the exit condition where the weight quality was measured. Data obtained under this condition are shown in figure 10. However, data from the pitot tubes built into one subchannel indicated poor results for conditions upstream of the exit. Instead, the assumption of equal slip ratios in the two channels provided fair agreement for the exit conditions (within 10 per cent of the exchanged quantities) and was used during the data reduction.

3.1.2.   Two-phase friction multiplier

A correlation for the frictional pressure drop has been obtained from data, read on the multimanometer, during symmetrical injection.
For single-phase liquid friction the empirical relation found is:

$$f = 0.253 \ Re^{-0.24} \qquad , \qquad\qquad\qquad (3.2.)$$

where f is defined by

$$f = \frac{\Delta p_{fr}}{\frac{1}{2} \rho_1 V_1^2 \cdot \frac{\Delta z}{d_h}} \ . \qquad\qquad\qquad (3.3.)$$

The two-phase pressure drop was deduced from the local pressure losses by subtracting the pressure drop due to the hydrostatic head:

$$\Delta p_{hydr} = \left\{ \alpha \rho_g + (1-\alpha) \, \rho_1 \right\} \ g \ \Delta z \qquad ; \qquad\qquad (3.4.)$$

35

and the acceleration losses:

$$\Delta p_{acc} = \left\{ (1-\alpha)\rho_1 V_1^2 \right\}_{z + \Delta z} - \left\{ (1-\alpha)\rho_1 V_1^2 \right\}_z , \qquad (3.5.)$$

in which the contribution of the gaseous phase has been neglected. The two-phase multiplier, R, was obtained by dividing the pressure drop by the single-phase pressure loss calculated for the case when the liquid alone was flowing through the channel.
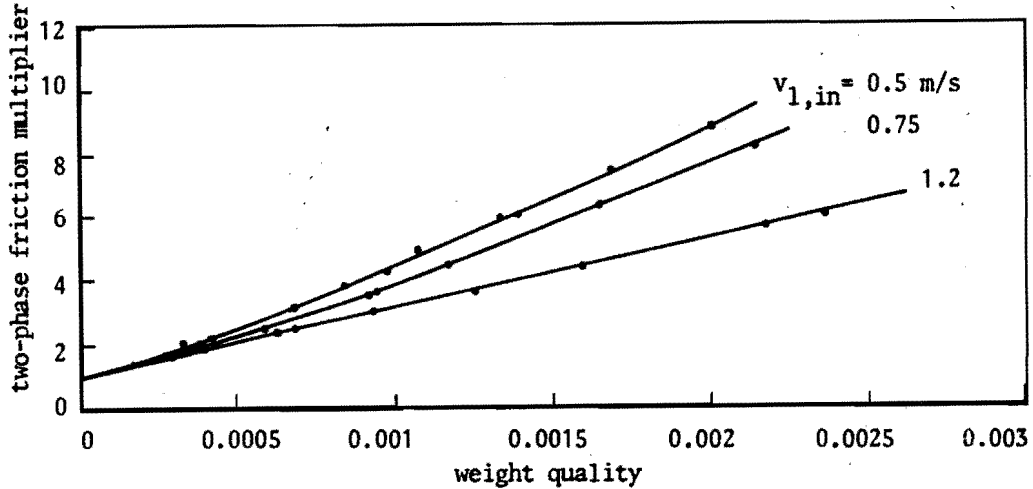

Fig.12 Local values of the two-phase friction multiplier versus quality

The experimental results for R when plotted versus the volumetric void fraction or versus the weight quality as in figure 12, revealed an effect of the mass flow rate. A similar effect of this parameter has been found before in data from CISE (Milan, Italy) as reported by Thom (22). As during mixing experiments the mass flow in each subchannel varies along the channel length, a correlation was needed as a function of the quality and the mass flow or local liquid velocity. In figure 13 the multiplier is plotted against the local liquid velocity with the weight quality as a parameter. The general expression derived from figure 13 which was used during the data reduction is

$$R = 1 + 0.16 \ (x.10^4)^{1.4}(1-0.2 \ V_1). \qquad (3.6.)$$

It is not understood why the multiplier at local liquid velocities approaching 5 m/s becomes unity. However, these high velocities were not reached during these experiments.

For a comparison of the experimental data for the two-phase friction multiplier with a well-known correlator, a graph has been made using the correlation parameters of Martinelli-Nelson, figure 14, for a definition of which reference is made to (23).
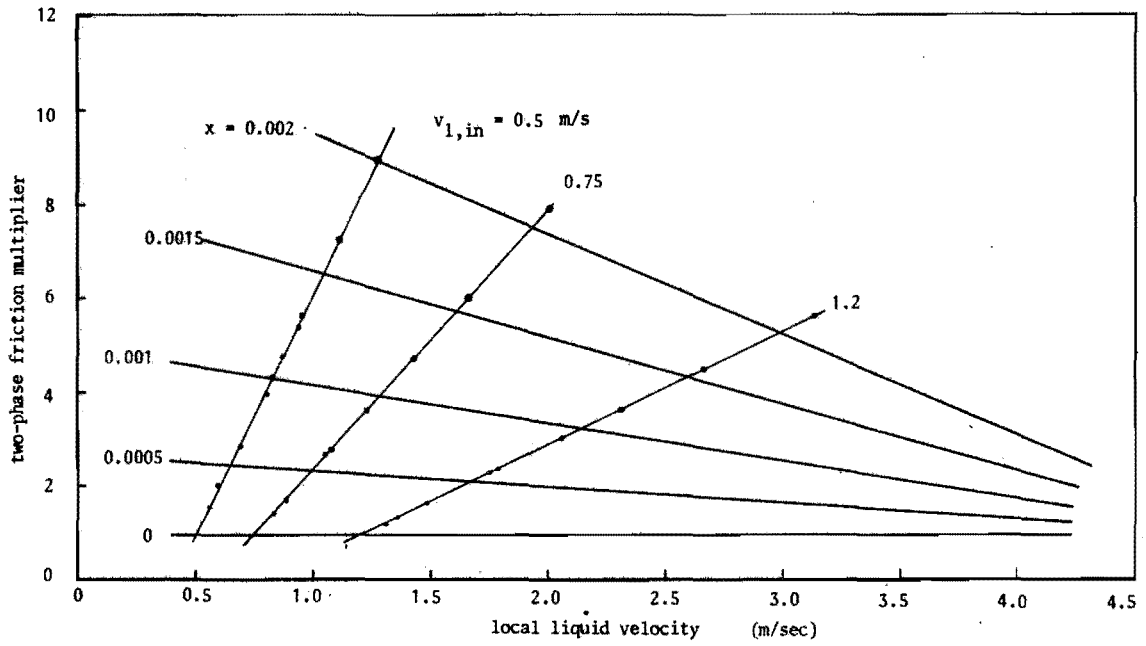
36

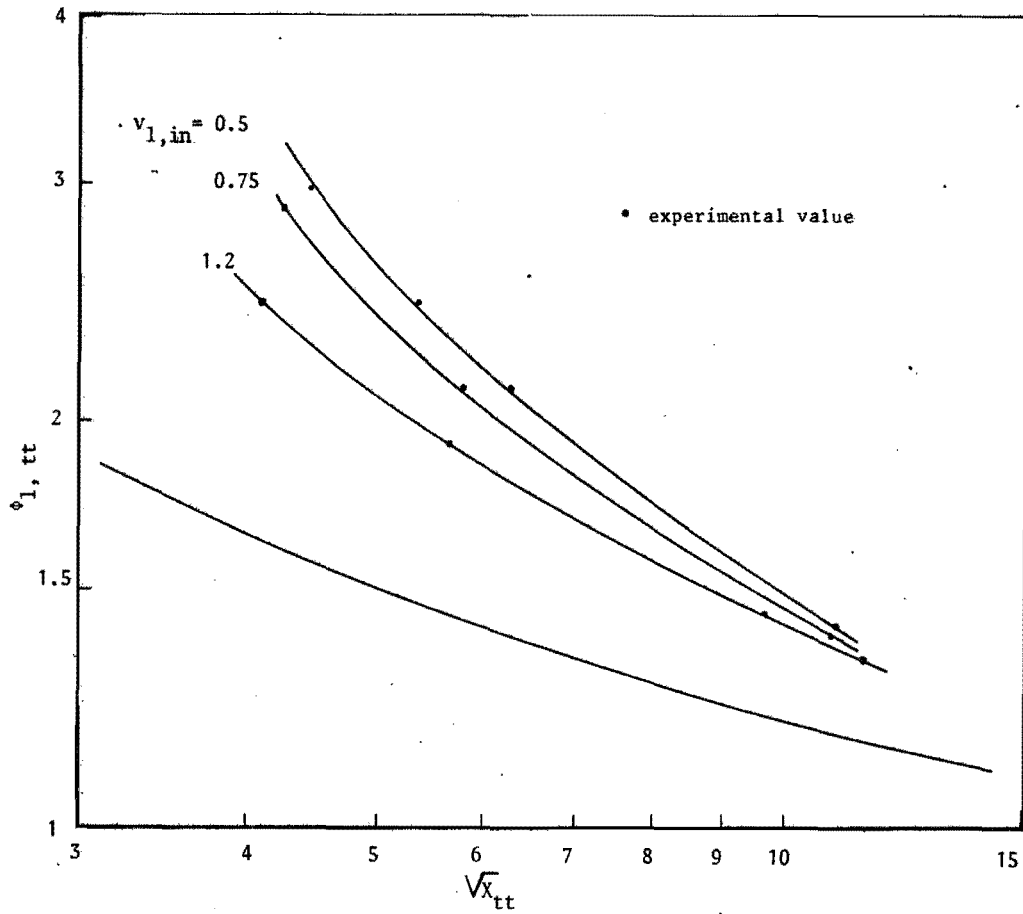Fig.13 Two-phase friction multiplier versus local liquid velocity

Fig.14 Two-phase friction parameters defined by Martinelli-Nelson

3.2. Two-channel mixing experiments

The mixing experiments were performed while injecting air into one channel over 0.30 m starting at the subchannel entrance. The increase in the injected amount of air as a function of channel length was linear. The effect of the inlet liquid velocities, 0.71, 1.05 and 1.44 m/s, was investigated at mass flow densities of 0.071, 0.106 and 0.143 $kg/sec.cm^2$. During each mass flow rate five different flow rates of air were injected in the manner shown in figure 15.
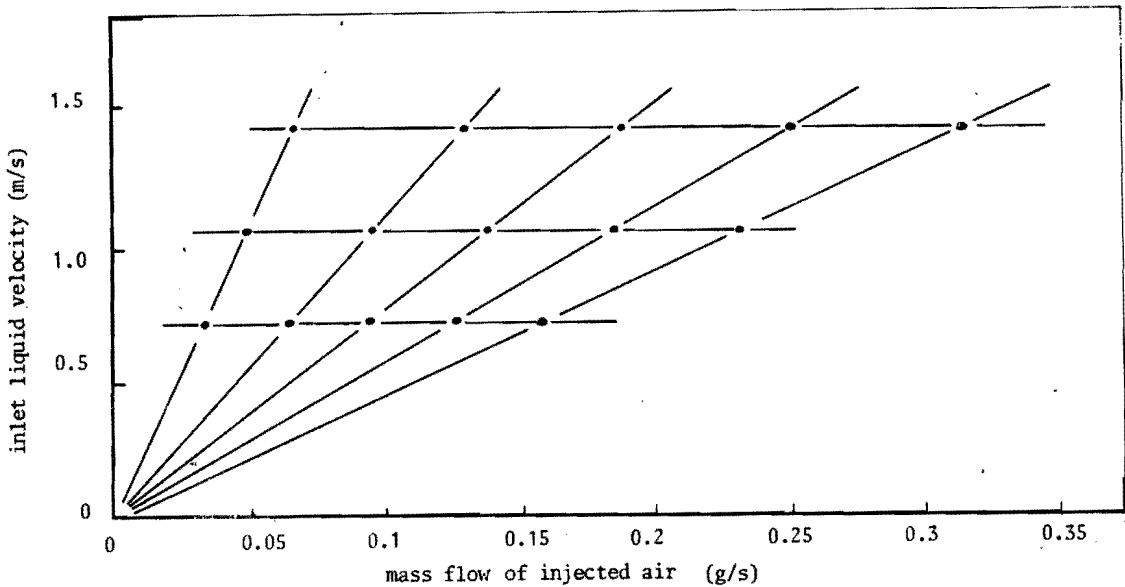

Fig.15 Experimental program

This pattern has been chosen in order to obtain about equal volumetric void fractions at each mass flow rate.

The program has been executed for the two gap sizes shown in figure 4. The two subchannels were divided by a line, drawn through the narrowest passage of the gaps. Slight corrections on the hydraulic diameter and cross-sectional area of the subchannels were applied when the 2 mm gap was widened to 4 mm; the mass flow rates of liquid and gas were increased proportionally to the change in cross-sectional area.

In figures 16 and 17, curves have been drawn through the void gauge readings for the different gaps. The void fraction and quality were completely or almost completely mixed at the exit of the channels at the lower and middle mass flow rates while using the 4 mm gap.
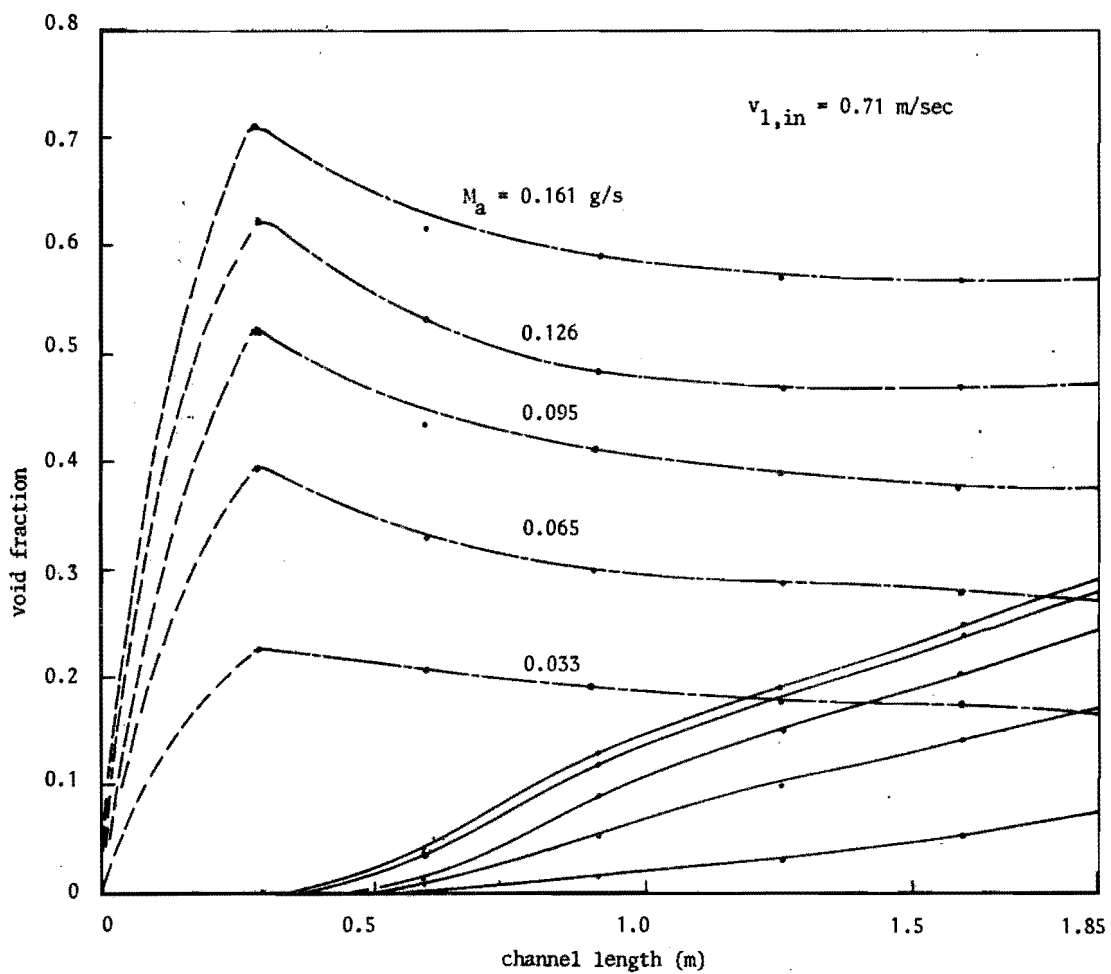
Fig.16a   Void fraction distribution in the case of a 2 mm gap
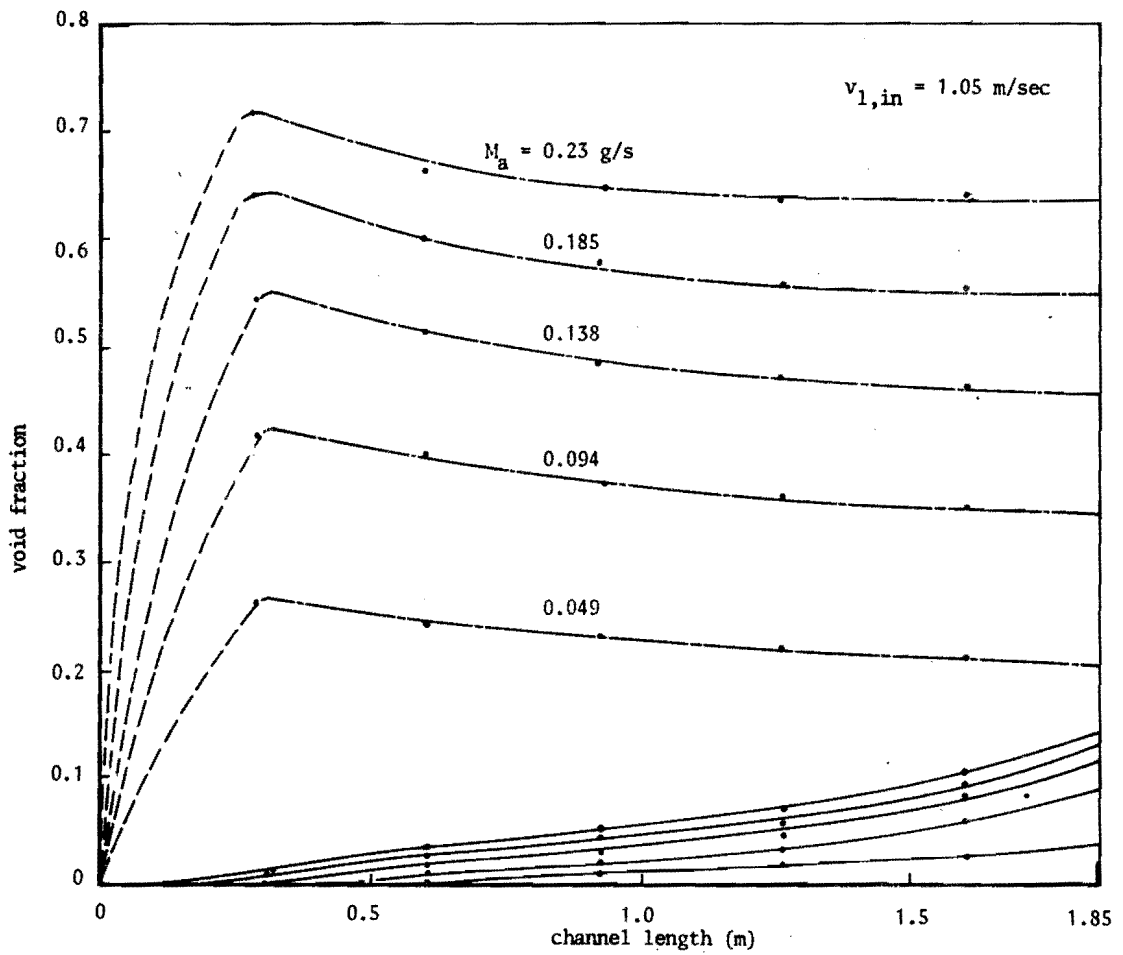and an inlet liquid mass velocity of 0.71 m/s

Fig.16b   Void fraction distribution in the case of a 2 mm gap
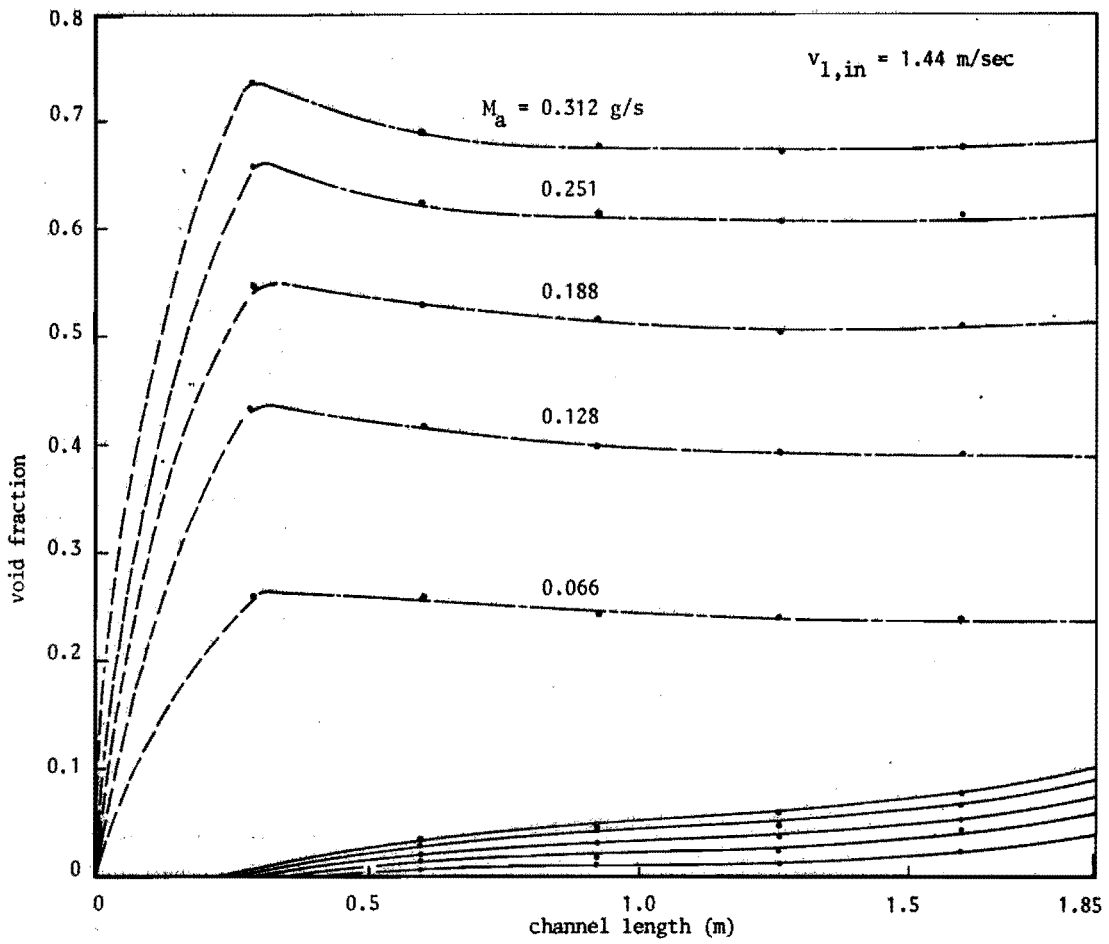   and an inlet liquid mass velocity of 1.05 m/s

Fig.16c Void fraction distribution in the case of a 2 mm gap
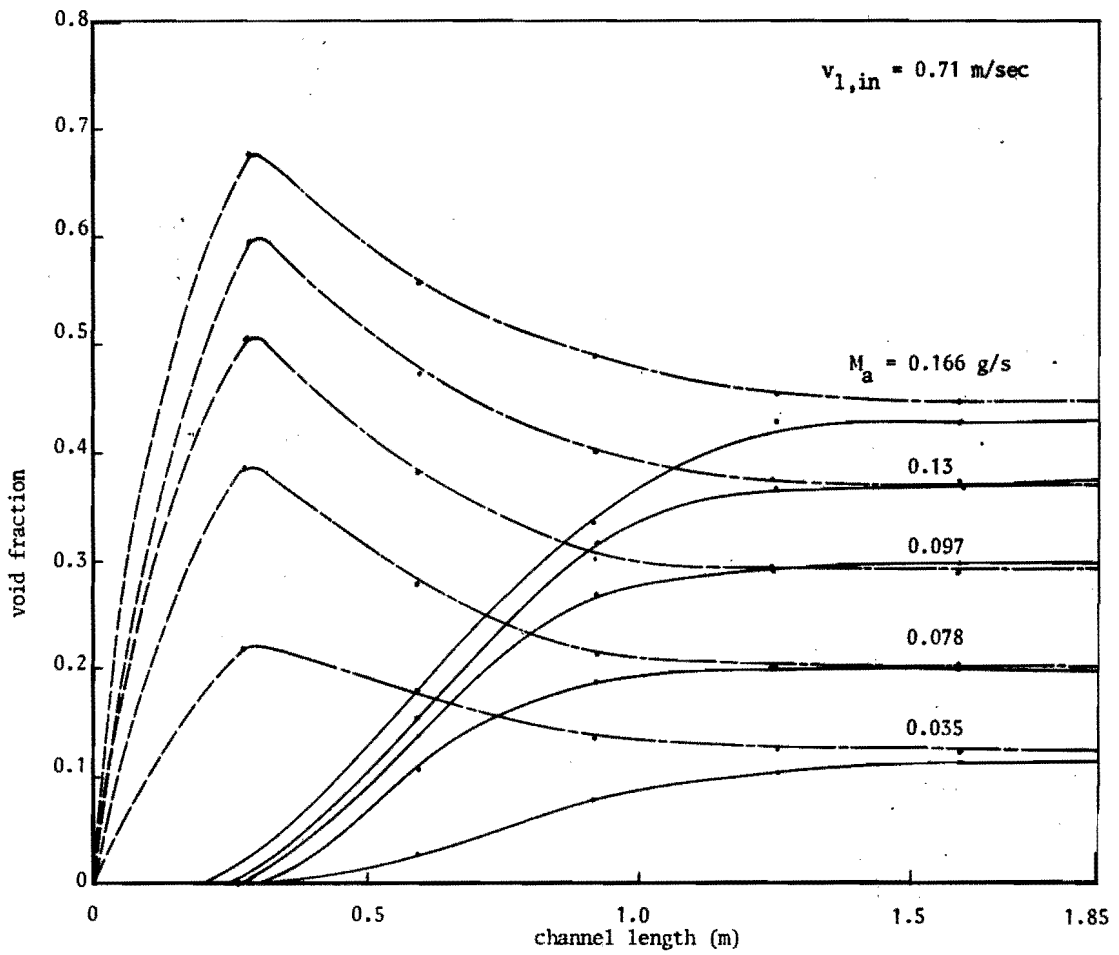   and an inlet liquid mass velocity of 1.44 m/s

Fig.17a· Void fraction distribution in the case of a 4 mm gap
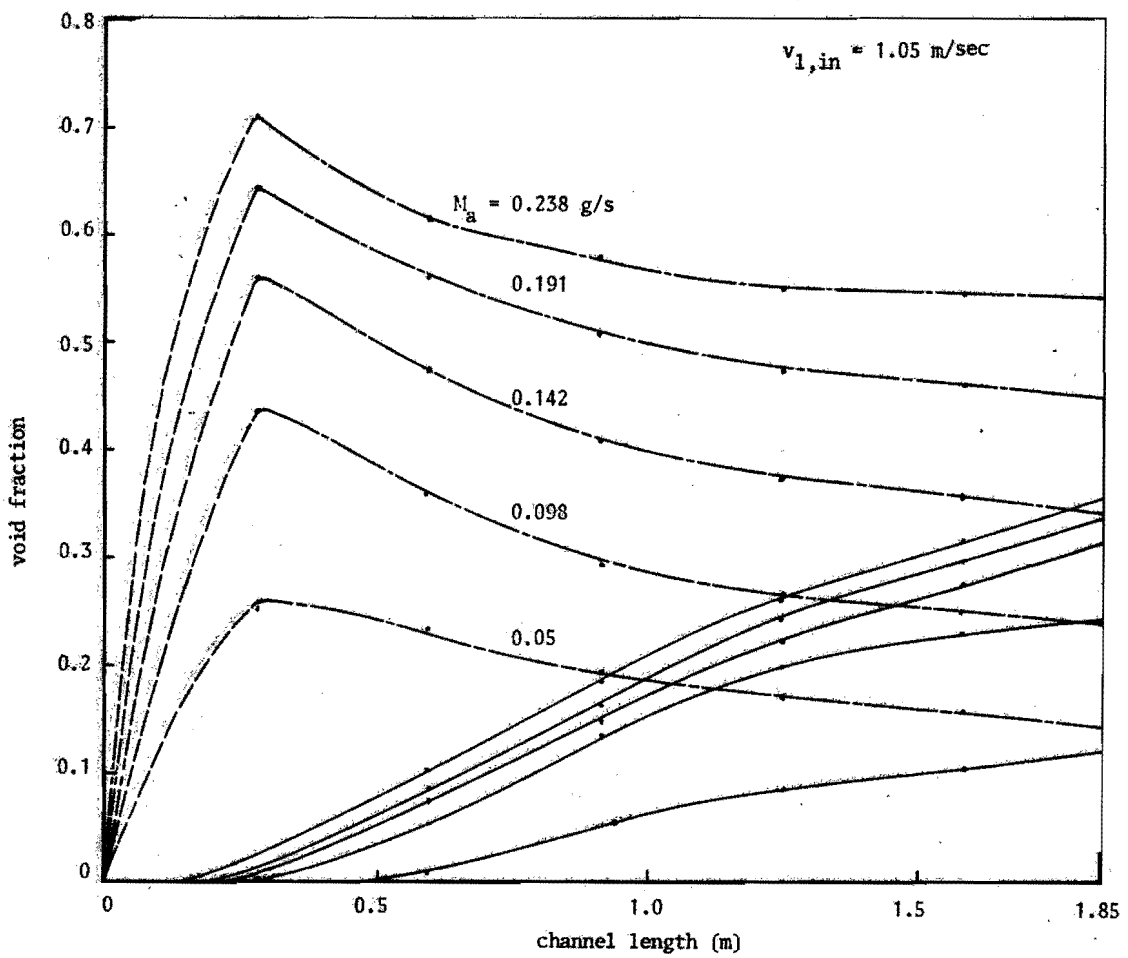and an inlet liquid mass velocity of 0.71 m/s

Fig.17b Void fraction distribution in the case of a 4 mm gap
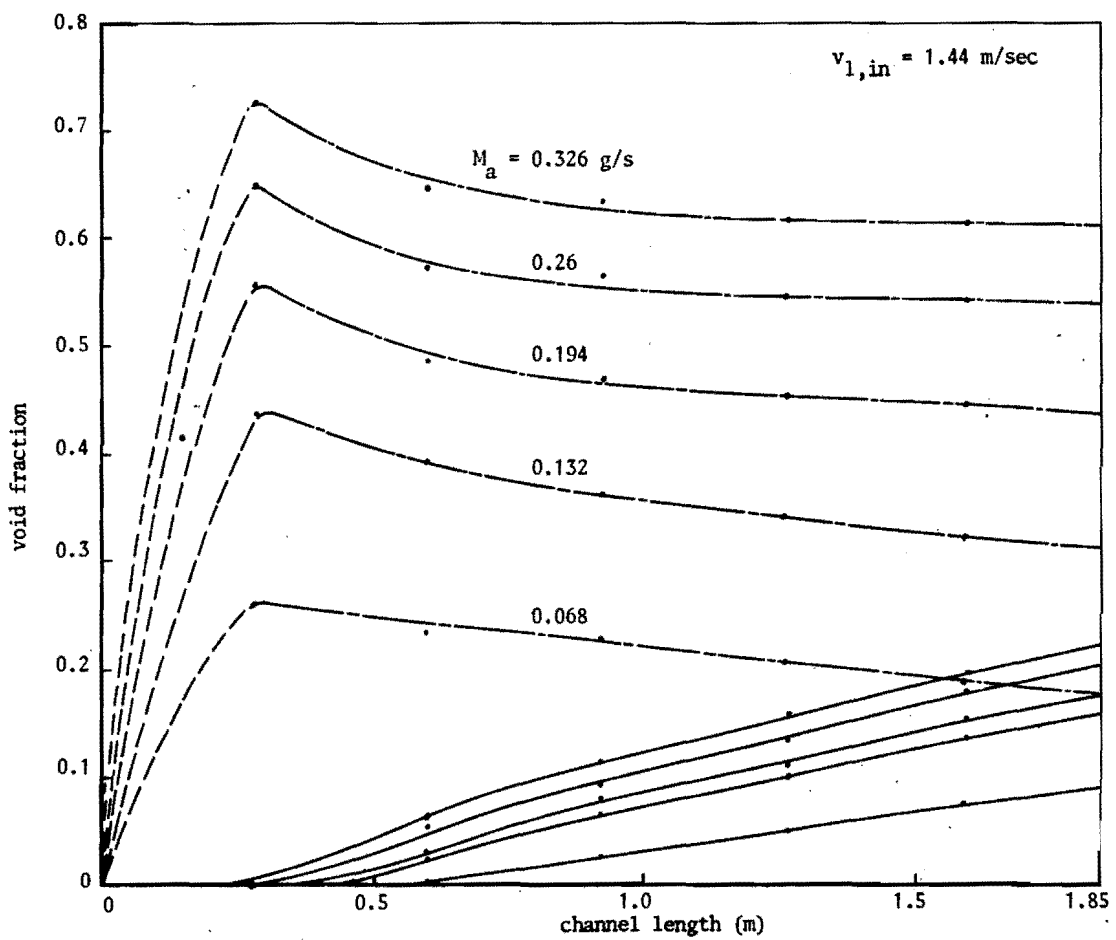and an inlet liquid mass velocity of 1.05 m/s

Fig 17c Void fraction distribution in the case of a 4 mm gap
and an inlet liquid mass velocity of 1.44 m/s

44

In figures 18 and 19 a continuous line has been drawn connecting the measured liquid velocities in the non-injected subchannel. At the end of the injected path, a sharp change in liquid velocity has been allowed. Note that the mass flow division at the entrance of the subchannel was even during all conditions. The data of figures 16 and 17 and the liquid velocities in the non-injected channel made possible the computations of the liquid velocities in the injected subchannel at intervals of 0.1 m as a function of the channel length. They were carried out with the help of the expression:

$$M_{1\ tot} = \left\{ (1-\alpha)\rho_1 V_1 A \right\}_i + \left\{ (1-\alpha)\rho_1 V_1 A \right\}_j . \qquad (3.7.)$$
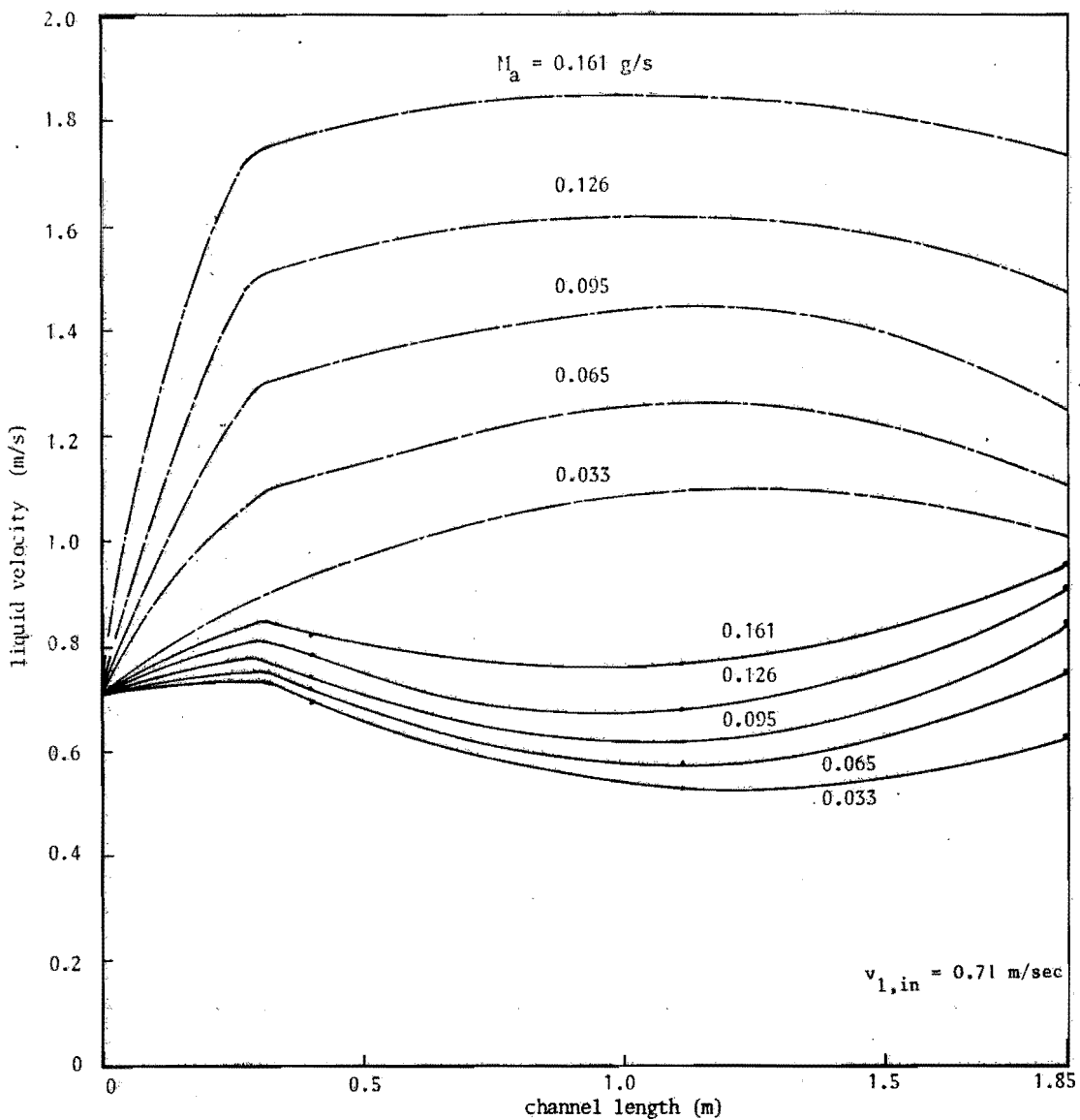

Fig.18a   Liquid mass flow velocity distribution in the case of
          a 2 mm gap and an inlet velocity of 0.71 m/s

These velocities have also been plotted in figures 18 and 19.

The void fraction and liquid velocities being known, the amount of liquid flow rate as a function of the channel length may be calculated. The changes in mass flow rate are caused by the mass exchange through the gap of the liquid phase. The total amount of liquid exchange through the gap versus the channel length has been plotted in figures 20 and 21.

With the assumption, previously made, of equal slip ratios in the two
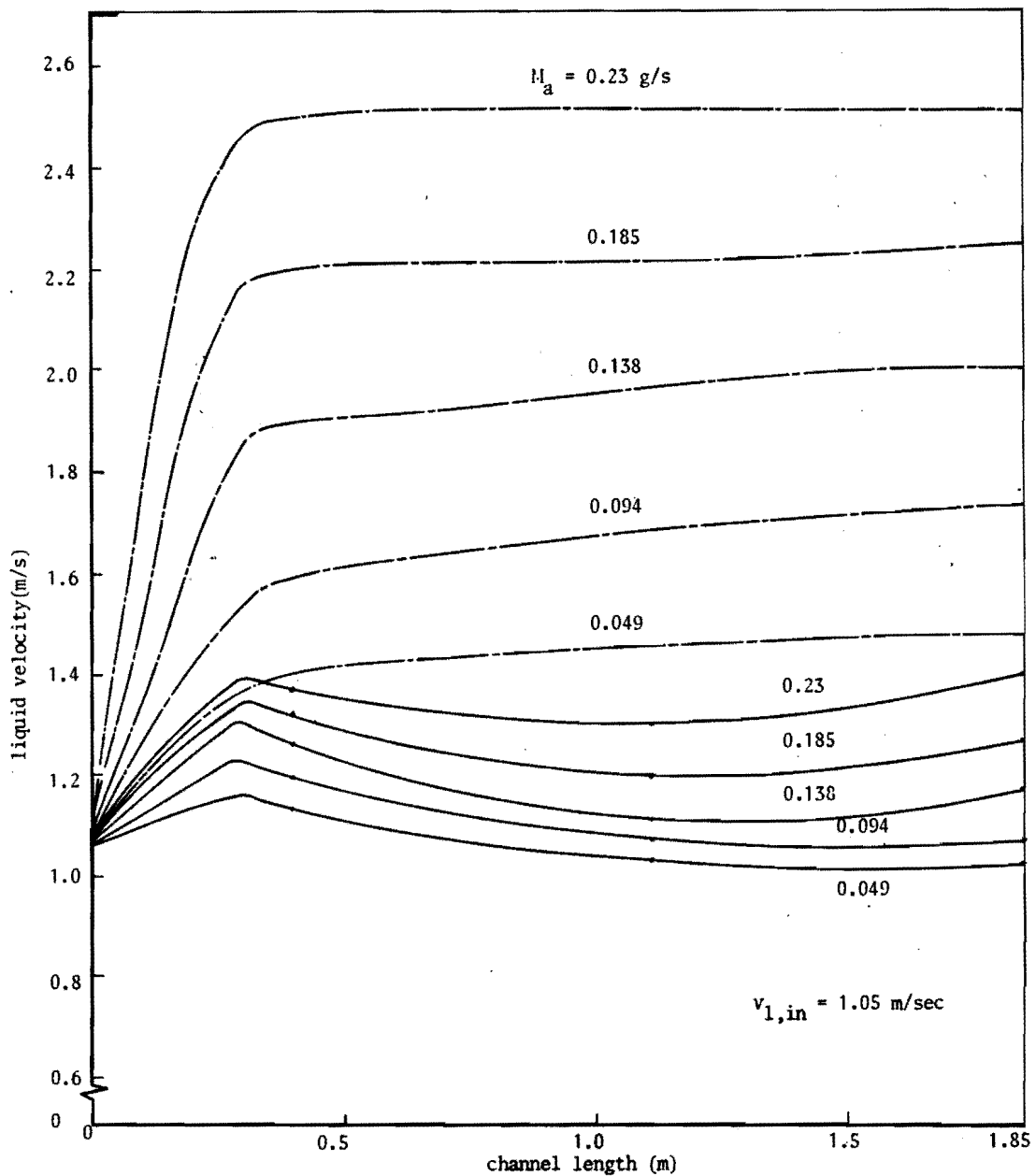
Fig.18b   Liquid mass flow velocity distribution in the case of
          a 2 mm gap and an inlet velocity of 1.05 m/s
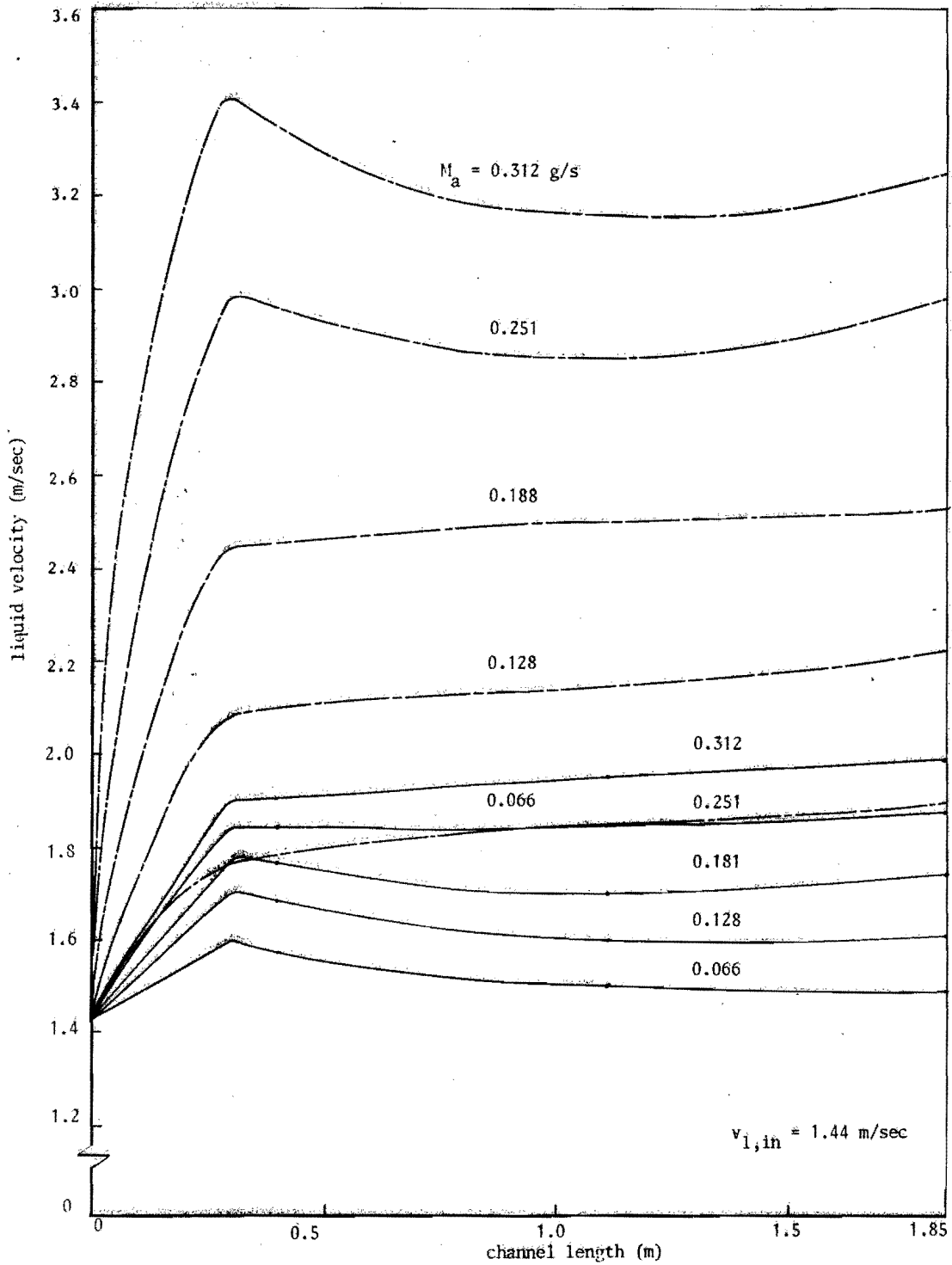
Fig.18c Liquid mass flow velocity distribution in the case of
a 2 mm gap and an inlet velocity of 1.44 m/s

subchannels, the local flow rate of the gas component in the sub-channels can now easily be determined from

$$M_{a\ tot} = \left\{ \alpha\ \rho_a S\ V_l\ A \right\}_i + \left\{ \alpha\ \rho_a S\ V_l\ A \right\}_j . \tag{3.8.}$$

The air density could be calculated from the measured pressure distribution in the channels. The total amount of gas exchange through the gap along the channel length has been plotted in figures 22 and 23.

Fig.19a   Liquid mass flow velocity distribution in the case of
          a 4 mm gap and an inlet velocity of 0.71 m/s

48

Fig.19b   Liquid mass flow velocity distribution in the case of
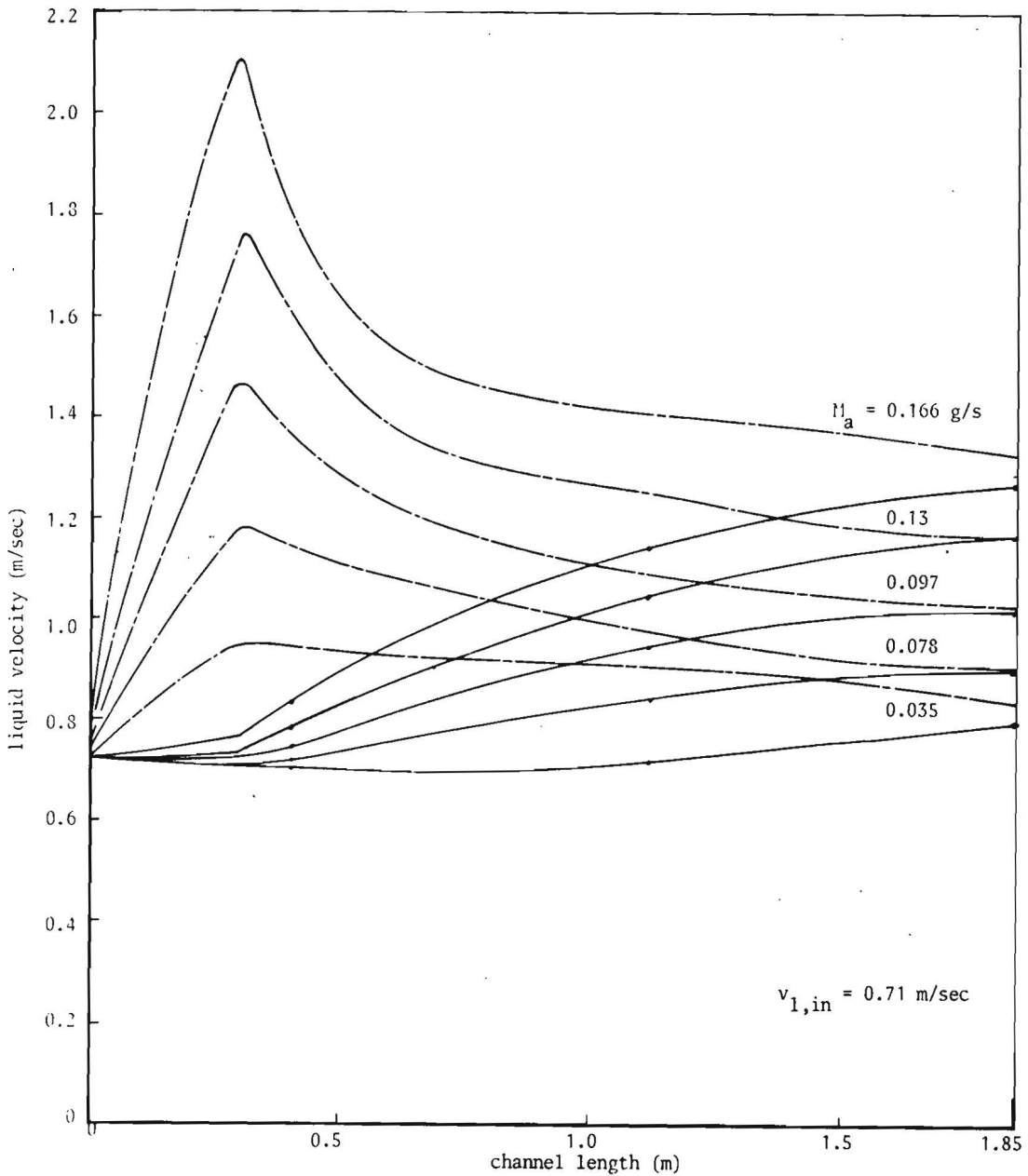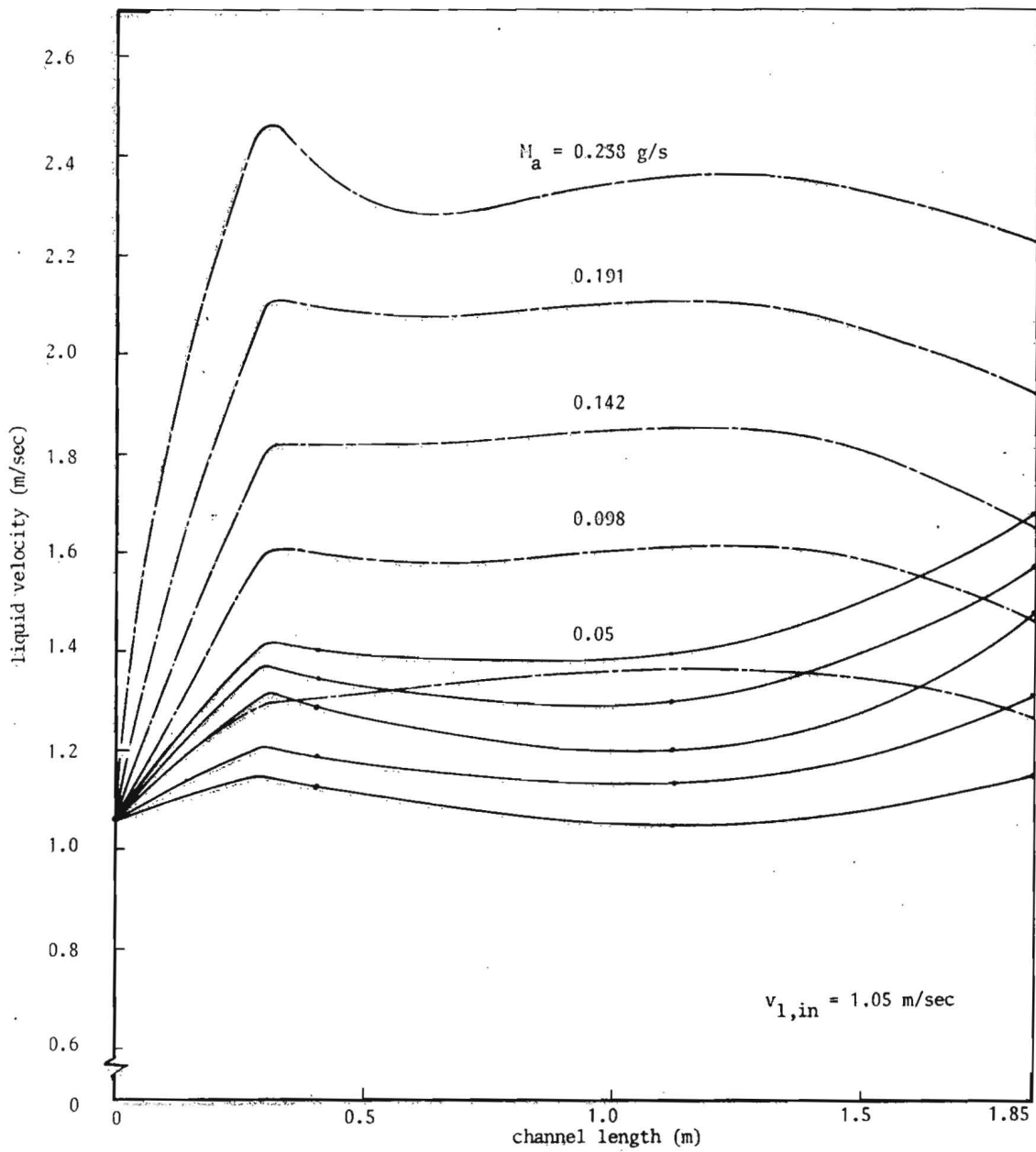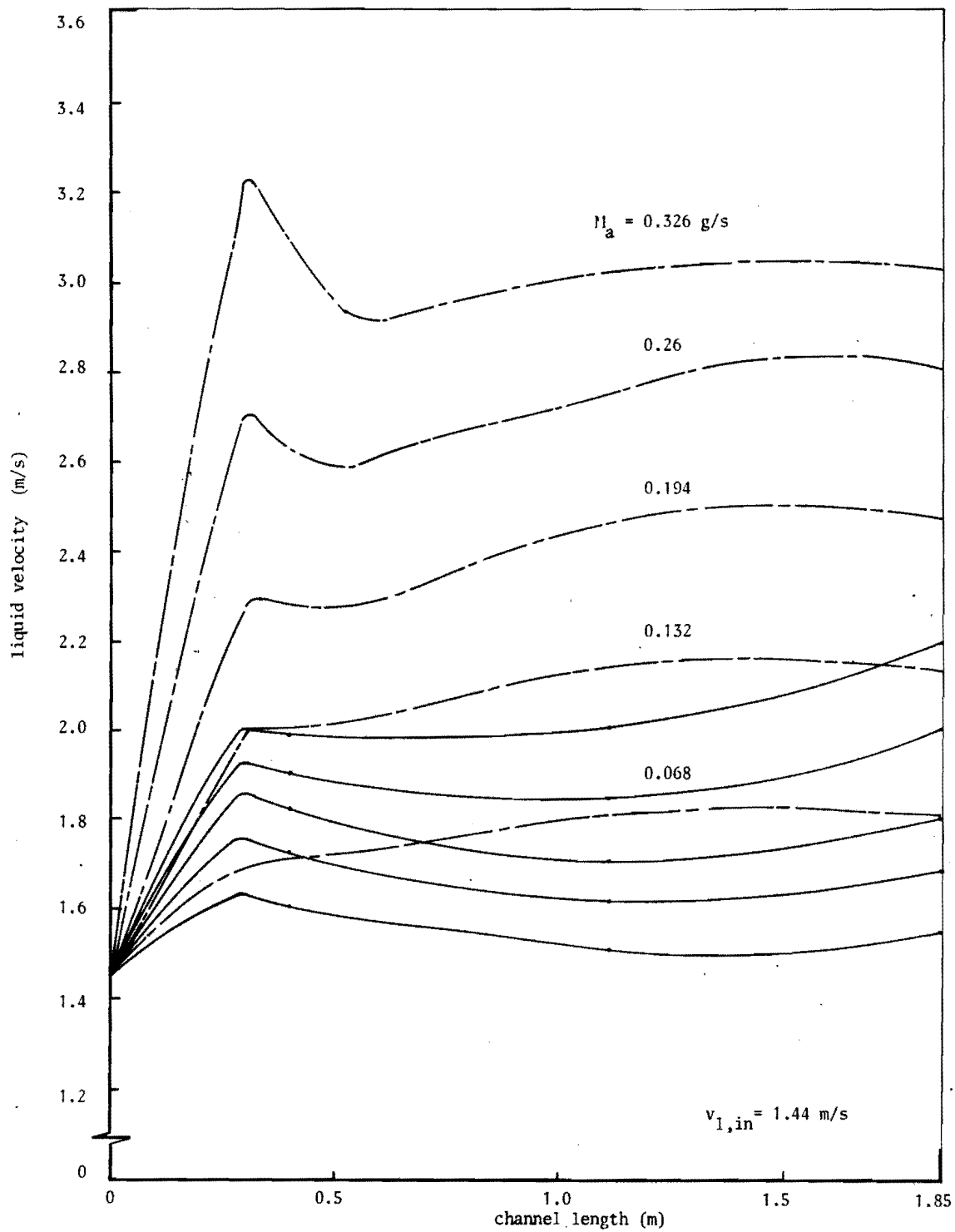   a 4 mm gap and an inlet velocity of 1.05 m/s

Fig.19c Liquid mass flow velocity distribution in the case of
a 4 mm gap and an inlet velocity of 1.44 m/s

Chapter 4.   ANALYSIS AND DISCUSSION

The reduced data shown in the figures 20 to 23 probably reveal the most
interesting results obtained from the experiments. In the figures 22
and 23 the direction and the mass flow rate of exchanged gases as a
function of the channel length has been plotted for the three inlet li-
quid mass velocities and for the different mass flow rates of injected
air by the 2 and 4 mm gap widths. The direction of exchange is similar
in all cases, air going from the higher into the lower concentration
channel. Furthermore, the curves are approximately straight lines ex-
cept in the cases where complete mixing occurred before the end of the
channel length; see figure 23a. In the figures 20 and 21 the mass flow
rate of mixed liquid has been plotted as a function of the same para-
meters. Apart from four of the five cases plotted in figure 21a (large
mass flow rates of mixing), liquid left the injected channel over the
whole of the injected section. In this section the penetration of air
into the non-injected channel was negligible. Downstream, the direction
of exchange changed to an extent depending on the liquid mass velocity.
In some cases the direction changed once more before the end of the
channel. This meant that during most of the channel length the direction
of exchange for each component was opposite to that of the other one.
From these facts the conclusion can be drawn that during the described
experiments the exchange process of each component appeared to result
from a different mechanism. Gas mixing behaved as a diffusion mechanism,
whereas the exchange of liquid rather resulted from the balancing of the
axial pressure drops in the two interacting channels. No interference
effects of the mixing liquid could be found in the data of the mixing
gas. An explanation of the behaviour of the liquid will be given in
section 4.4 of this chapter.
The experimental apparatus was not suited to detect turbulent liquid
mixing as its net mass exchange will be zero, but it may exist.
The effect of the variables in the experiments on the mixing will be
discussed in the following sections.

4.1.   The effect of the channel power

In figures 24 and 25 the total mass flow of mixed air versus the mass
flow rate of injected air has been plotted for the 2 and 4 mm gap width.
In general, it can be seen that the relative rate of mixed air decreases
with increasing mass flow rate of injected gas, and that gas mixing in-
creases largely with the gap width. A more sharply defined picture is

obtained when plotting the ratio between the air mixed into the non-in-
jected channel and the total mass flow rate of injected air. See figures
26 and 27. It can be seen that the mixing varied with the amount of si-
mulated channel power. The rate of gas mixing increased with the mass
flow rate of injected air to a peak value and decreased at larger mass
flow rates of air. The peak is more pronounced at higher gas mixing per-
centages.
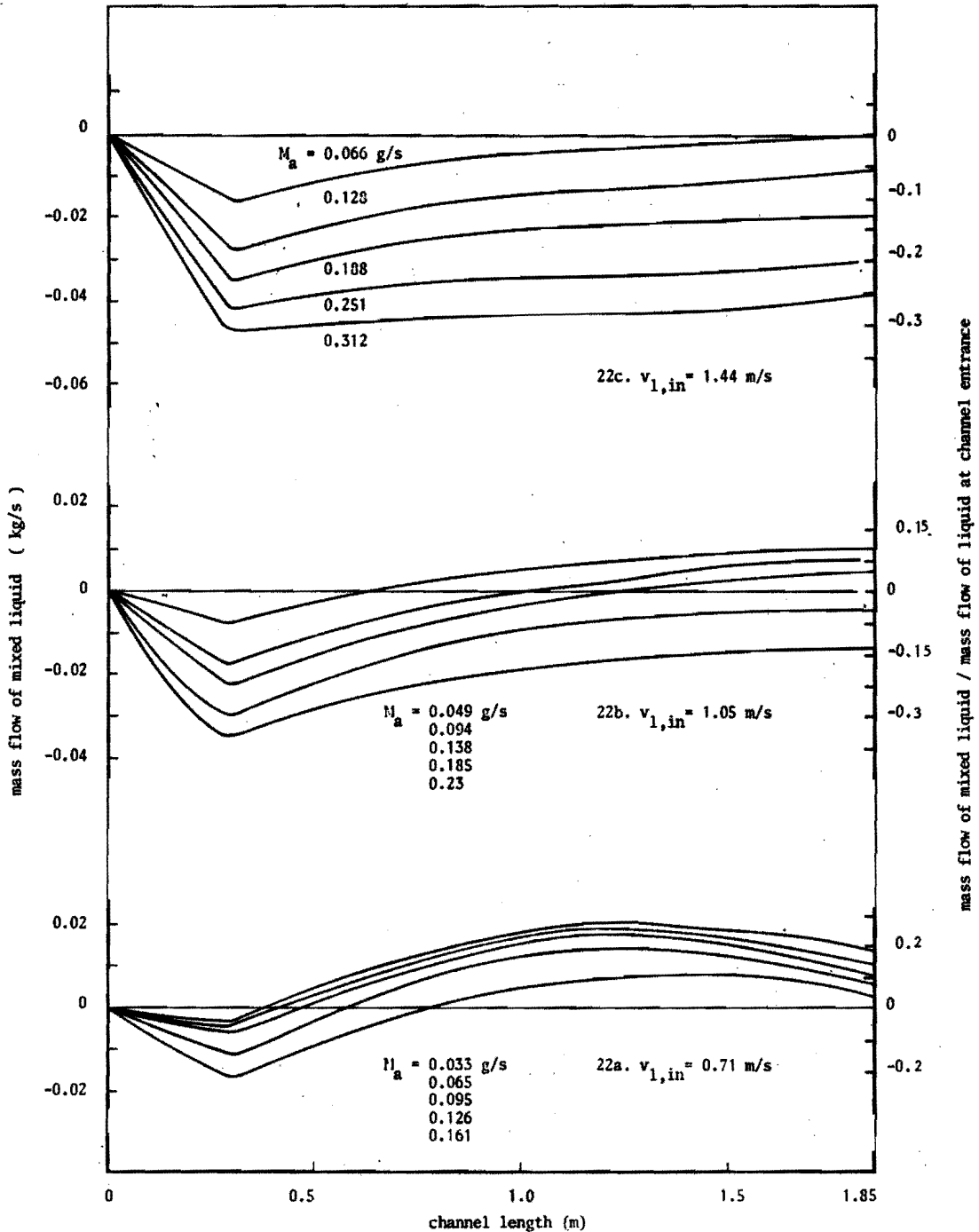
Fig.20 Mixed liquid distribution in the case of a 2 mm gap

The effect of the channel power on the gas exchange can be explained by the behaviour of the mechanism of gas diffusion. In general, the rate of diffusion increases with larger concentration gradients; furthermore, diffusion takes time and this can be of importance in a flowing system. With very little air injection the concentration difference, which is the driving force of the gas diffusion, is small and will lead to a low percentage of air penetrating into the non-injected channel. When larger mass flow rates of gas are injected, the concentration difference and thus the gas diffusion increases. However, at the same time the liquid and the gas velocity increases greatly in the injected channel, decreasing the transit time of the gas in the channels. This effected the dif-
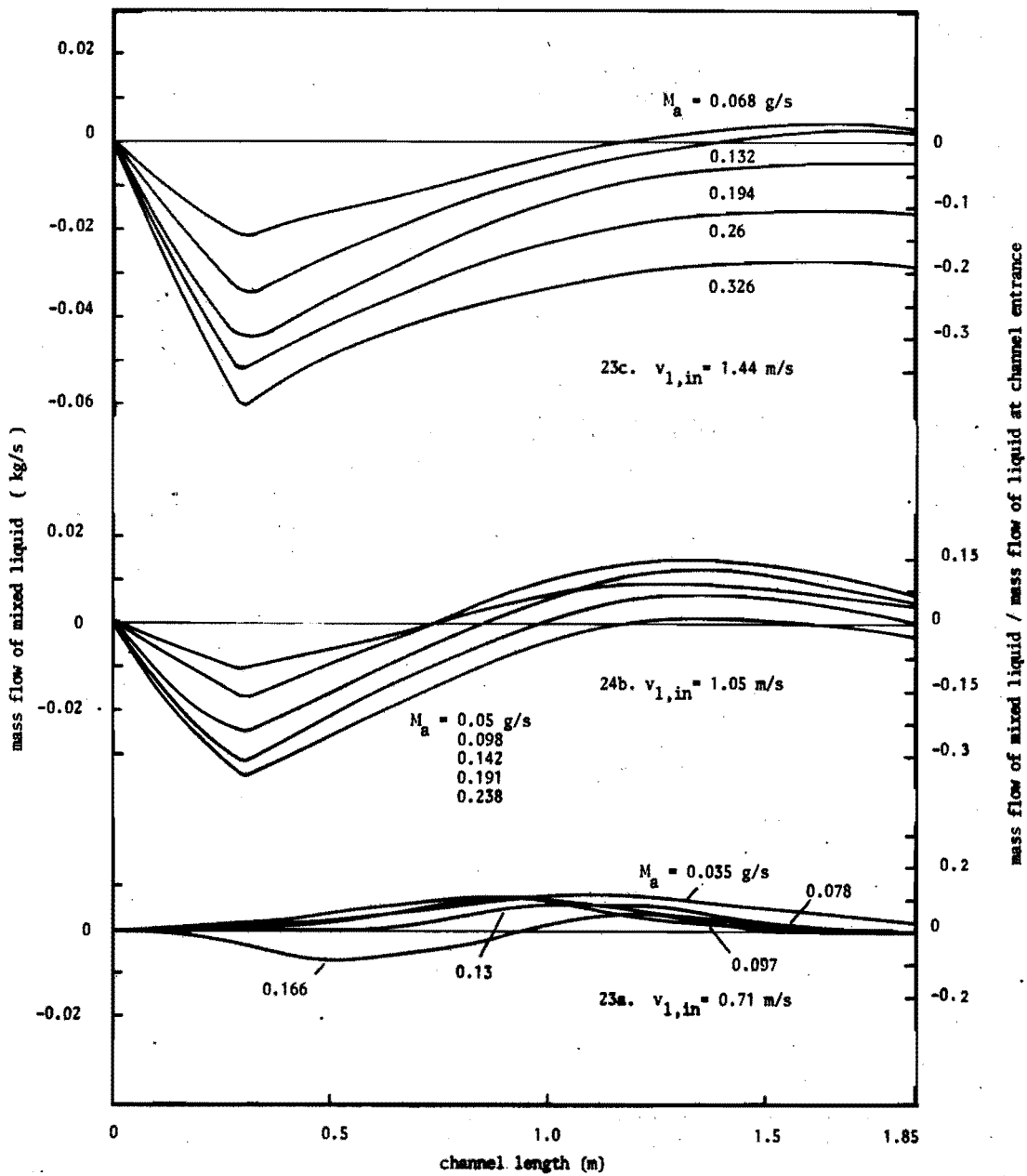
Fig.21 Mixed liquid distribution in the case of a 4 mm gap

fusion in the experiments in the negative sense, and after having reached an optimum value in relative gas exchange the transit time effect dominated.

The different rates of decrease in the percentage of mixed air, after the maximum value has been reached, can at least partly be explained by the smaller difference in gas concentration between the subchannels at higher gas exchange percentages. Hence, the transit time effect may have a greater pull. For the same reason the diffusion opposing transit time effect, its value being a function of the gas velocity, will extend its influence at lower local gas velocities during conditions of higher
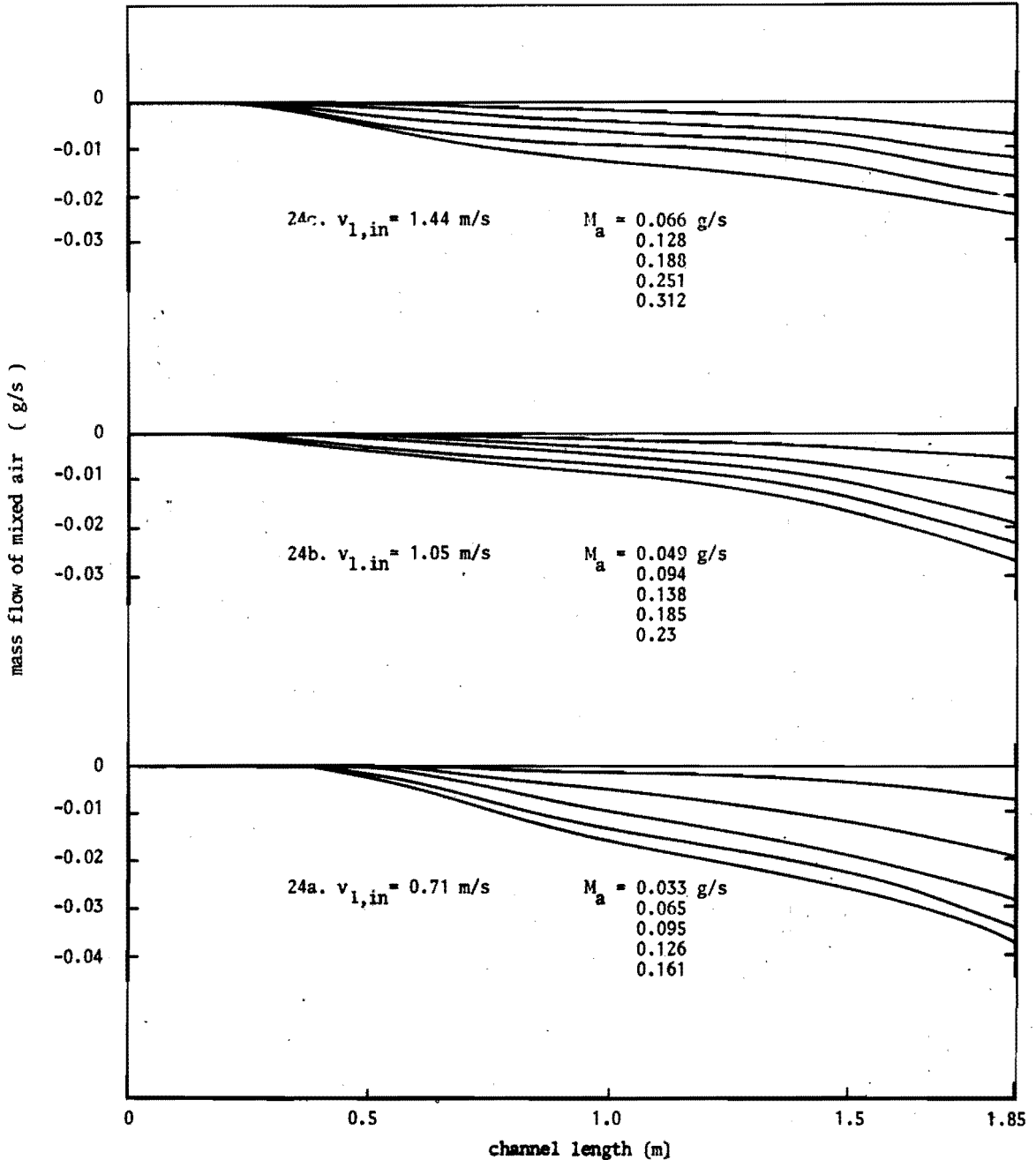
Fig.22 Mixed air distribution in the case of a 2 mm gap

Fig.23 Mixed air distribution in the case of a 4 mm gap

The y-axis is labeled "mass flow of mixed air (g/s)" and the x-axis is labeled "channel length (m)".

Panel 25c. $v_{1,in} = 1.44$ m/s, with curves labeled $M_a = 0.068$ g/s, 0.132, 0.194, 0.26, 0.326.

Panel 25b. $v_{1,in} = 1.05$ m/s, with curves labeled $M_a = 0.05$ g/s, 0.098, 0.142, 0.191, 0.238.

Panel 25a. $v_{1,in} = 0.71$ m/s, with curves labeled $M_a = 0.035$ g/s, 0.078, 0.097, 0.13, 0.166.
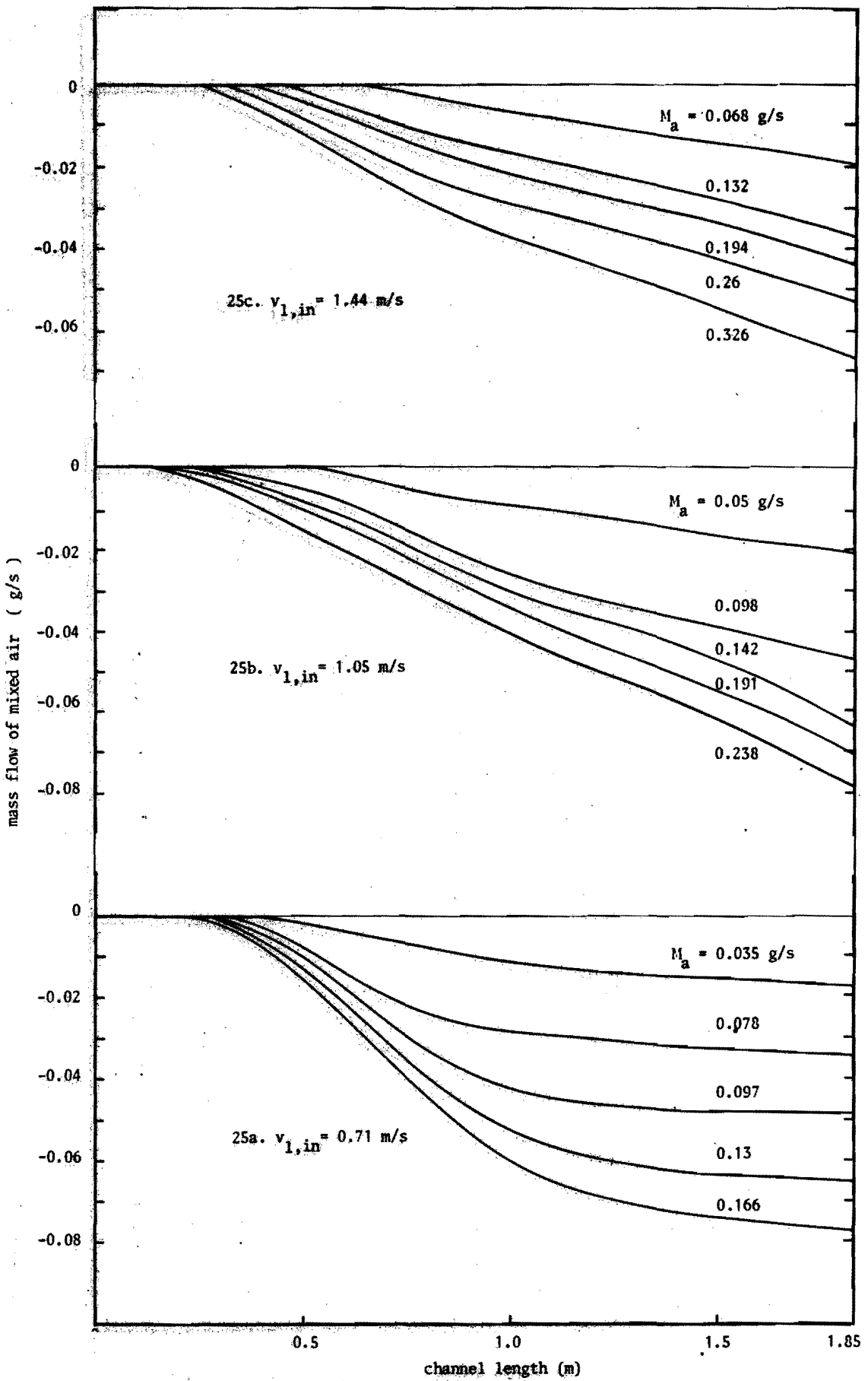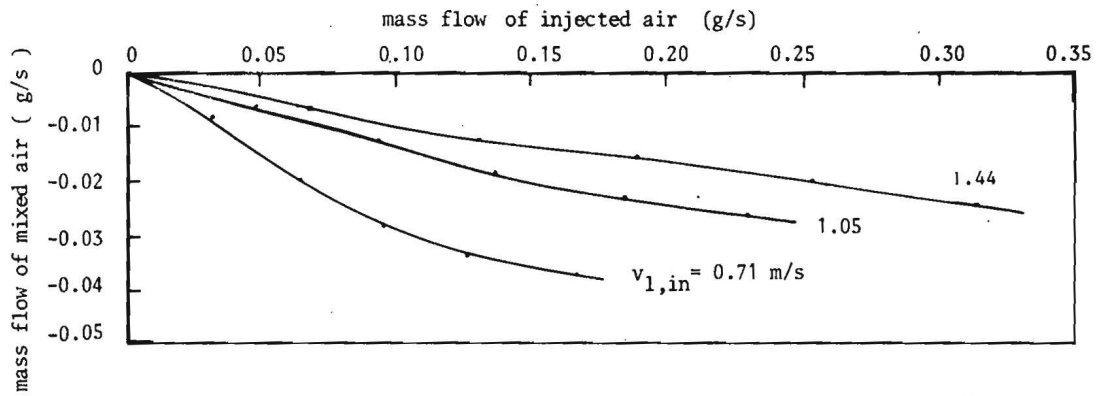
Fig.24   Total mass flow of mixed air versus injected air
in the case of a 2 mm gap

gas mixing percentages. The average local gas velocities in the injected
channel at the maximum gas mixing values are approx. 1.90, 1.60 and 1.20
m/s for the curves of the inlet liquid velocities of 1.44, 1.05 and 0.71
m/s respectively at both gapwidths. This might help to explain why the
peak value in gas mixing during all experiments was obtained at appro-
ximately the same mass flow rate of injected air.

Fig.25   Total mass flow of mixed air versus injected air
in the case of a 4 mm gap

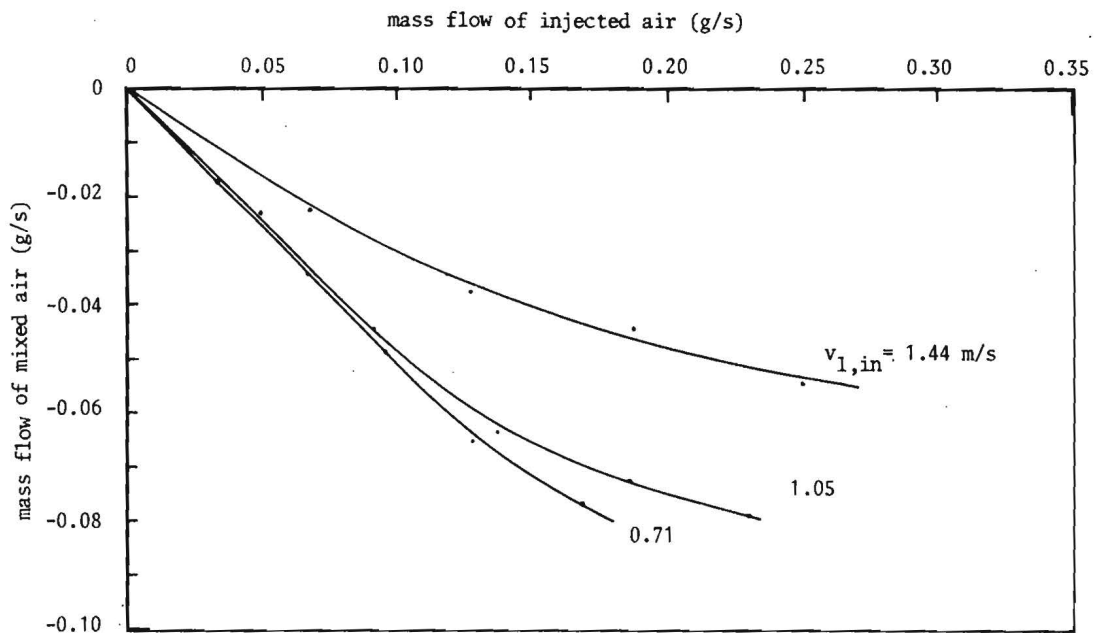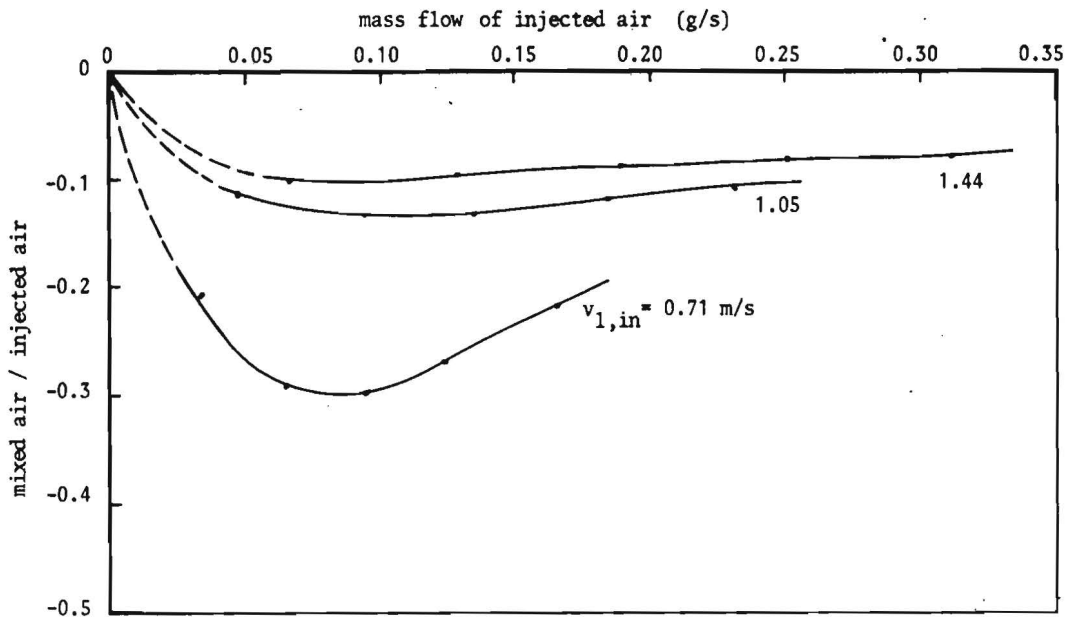Fig.26 Percentage of mixed air versus injected air
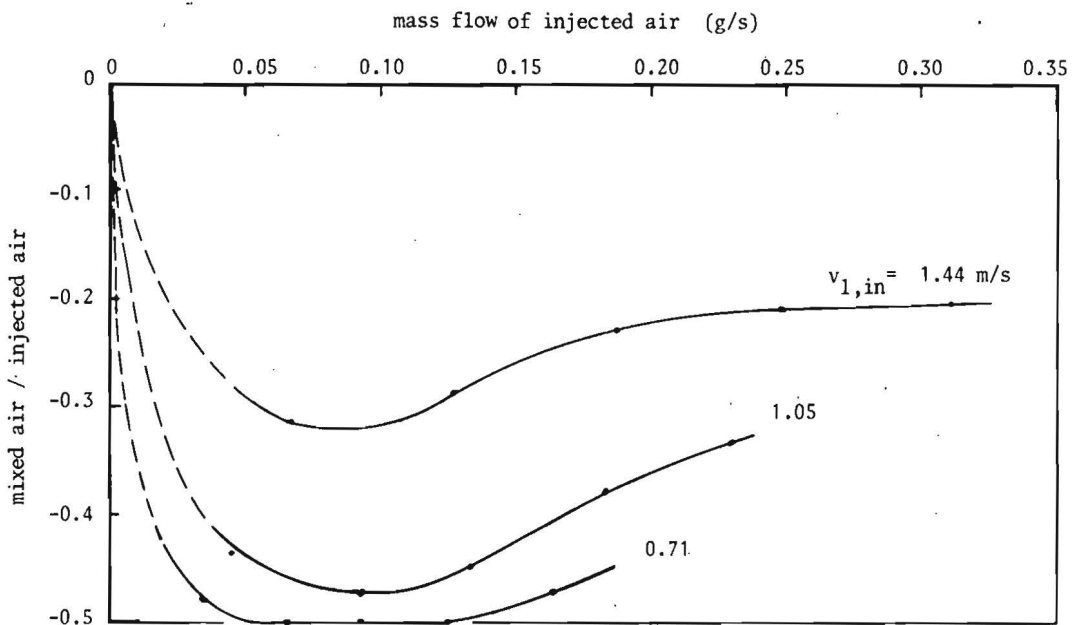   in the case of a 2 mm gap

Fig.27 Percentage of mixed air versus injected air
        in the case of a 4 mm gap

The liquid mass flow division over the channels taken from the average value as a function of the amount of injected air has been plotted in figures 28, 29 and 30. The curves in figure 28 have been calculated numerically from the laws of conservation of mass and momentum for the case of parallel channels, only connected at the inlet and outlet. The empirical correlations regarding slip and two-phase friction described in chapter 3, have been provided as input. An iteration for the inlet liquid mass division over the two channels was used to obtain equal pressure drops over the length of the channels. The curves in figures 29 and 30 refer to the 2 and 4 mm gap width respectively. In general, it can be said that at small mass flow rates of injected gas more than the average mass flow rate of liquid passes through the injected channel; at higher mass flow rates of gas most liquid went into the non-injected channel. The change of curve with gap width appears also to be a function of the liquid mass flow and is most pronounced at the lowest mass flow velocity.

In figures 31 and 32 the combined picture of gas and liquid exchange is visible in the curves of the weight quality at the exit of the subchannels versus the mass flow rate of injected air. Note the change in slope in all curves between 0.10 and 0.15 g/s of injected air. At higher mass flow rates of gas, the dependability of the outlet weight quality in the non-injected channel on the mass flow rate of injected gas is small.

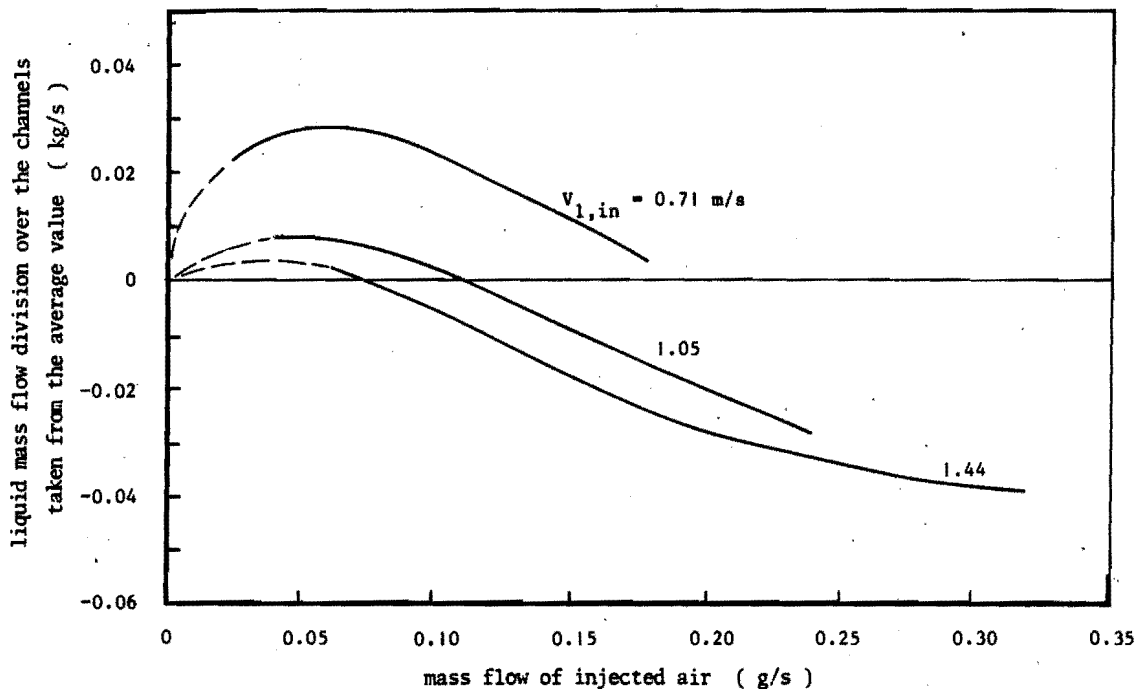Fig.28   Liquid mass flow division versus mass flow of injected air
in the case of parallel channels
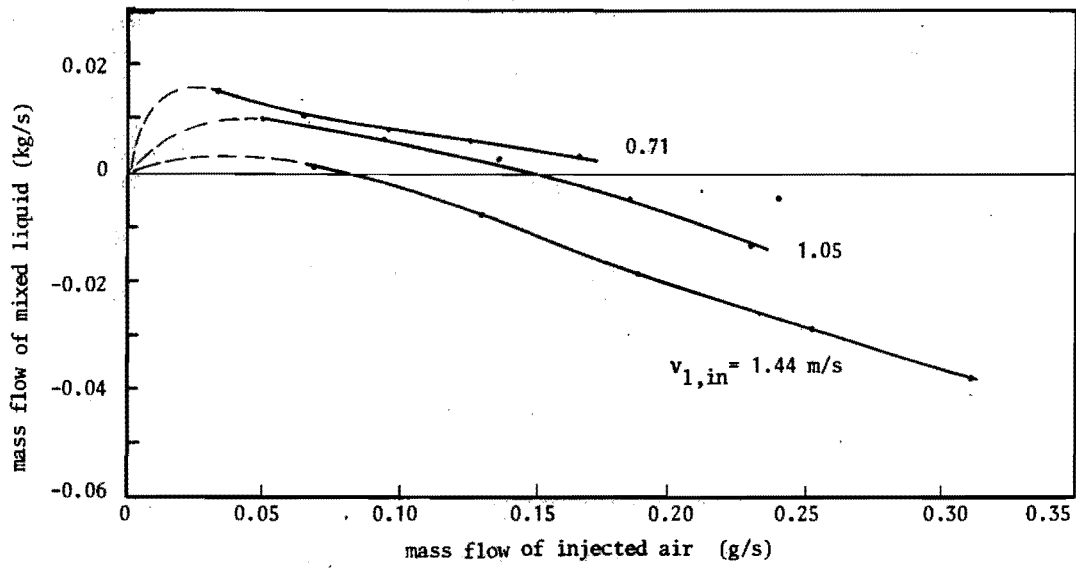
Fig.29   Mass flow of mixed liquid versus injected air
          in the case of a 2 mm gap
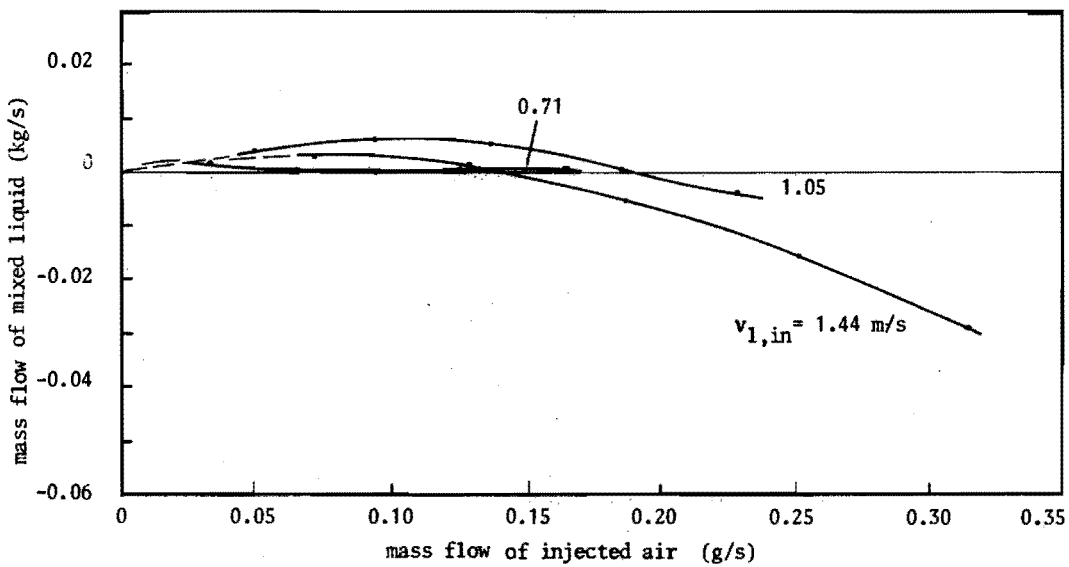

Fig.30   Mass flow of mixed liquid versus injected air
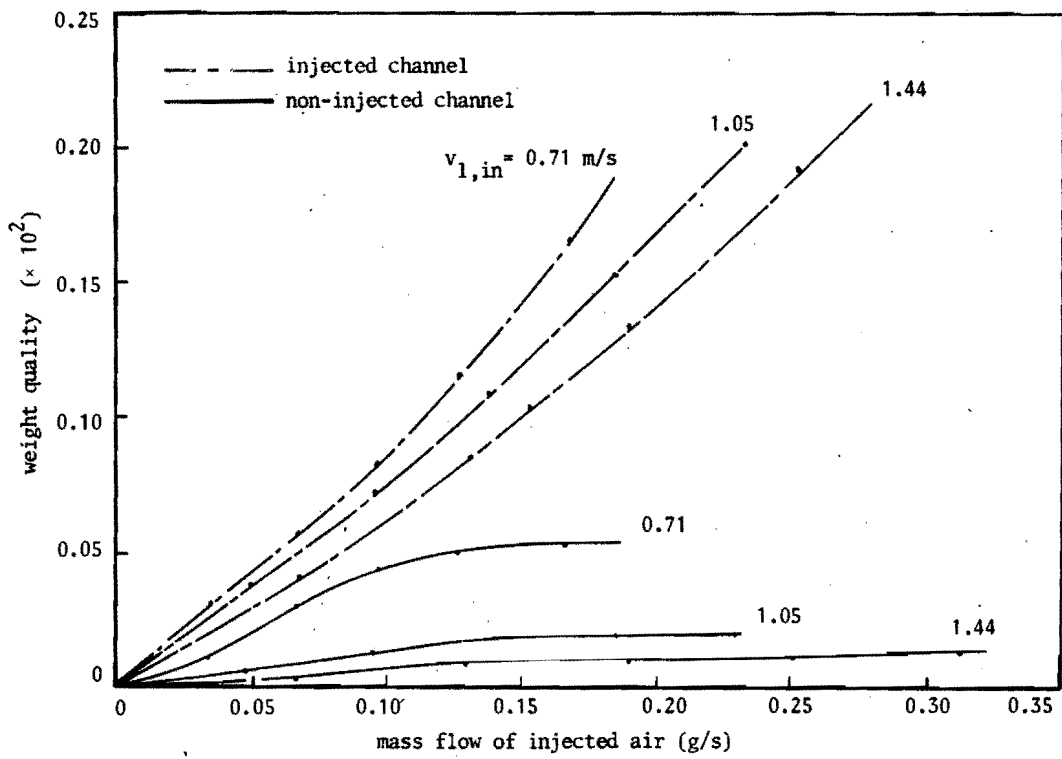   in the case of a 4 mm gap

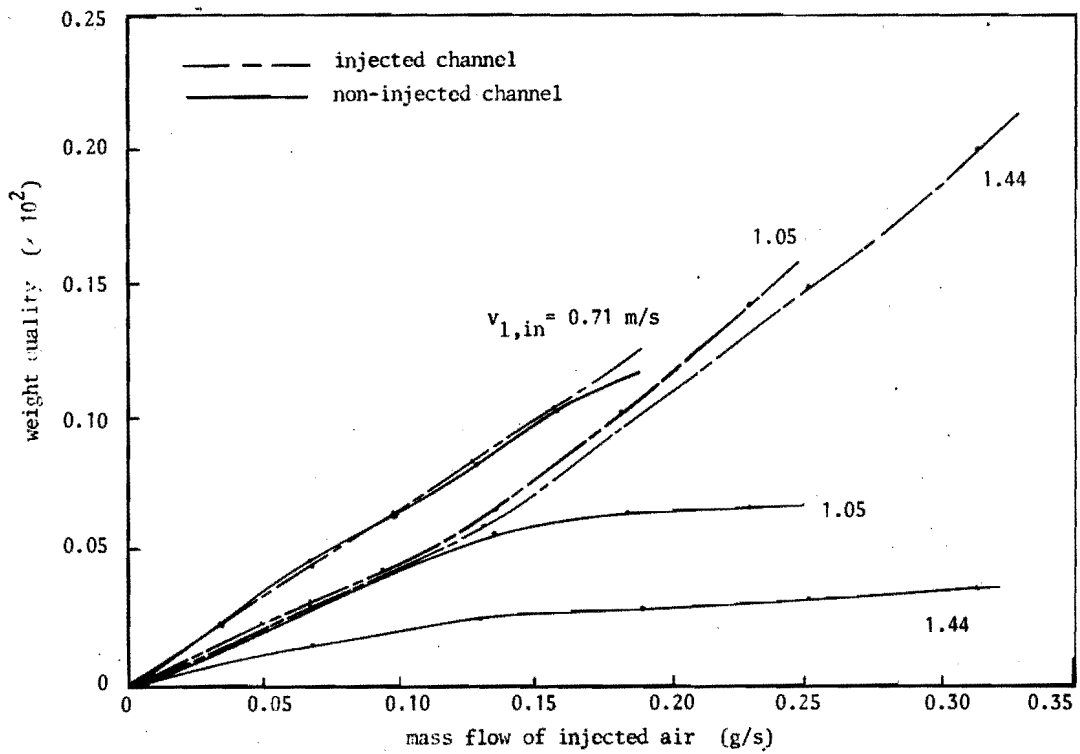Fig.31 Weight quality versus injected air in the case of a 2 mm gap

Fig.32 Weight quality versus injected air in the case of a 4 mm gap

4.2.   The effect of the mass flow velocity

The inlet liquid velocity had a great effect on the two-phase mixing
as it has on single-phase mixing. However, the over-all effect is
opposite in the two cases. In figures 33 and 34 the ratio of the mass
flow rate of mixed air to the mass flow rate of injected air has been
plotted versus the inlet velocity for three flow rates of injected air.
The general trend is decreasing gas mixing with increasing liquid mass
velocity. This effect could be expected from a diffusion mechanism in
view of the shorter transit time.
In the 2 mm gap data, the decrease in gas mixing is roughly proportional
to an inlet velocity of about 1.0 m/s, at higher inlet velocities the
decrease in mixing is moderate. The curves of the 4 mm gap width look
similar except for a 'delayed' effect of the inlet liquid velocity.

4.3.   The effect of gap width

The gap width had also a great effect on the two-phase mixing. In figure
35 the ratio of the mass flow rate of mixed air and of the injected air
has been plotted versus the gap width for the three different mass flow
rates. The effect is an about linear increase in gas mixing with gap
width. This result is in agreement with an exchange mechanism by diffus-
ion, where the rate of exchange is proportional to the cross sectional
area between the areas with different concentrations.

The required average channel length for 0.95 mixing in gas flow rates
has been plotted in figure 36 as a function of the gap width with the
liquid inlet velocity as a parameter. The data, through which arbitrary
straight lines were drawn, have been obtained by extrapolation of the
mass flow rate of gas in the injected channel as a function of the chan-
nel length as far as half the value of the injected mass flow rate on
semi-logarithmic paper.

4.4.   Pressure distribution

The pressure distribution in both subchannels along the channel length
has been measured with an oil-filled multimanometer. When plotting these
data no lateral pressure differences larger than the experimental uncer-
tainty of $\pm$ 1 mm water column, were found between the channels at any
level, at any mass flow rate of liquid or gas, nor at any gap width.
This result was not improbable, considering that the maximum mass flow
rate of liquid exchange per unit gap width during the experiments was
about 0.05 kg/s at the highest mass flow rate of gas injection and the
highest inlet liquid velocity using the 2 mm gap width. At this maximum
mass flow rate of liquid exchange the average transverse liquid velocity
in the gap was 0.083 m/s. The frictional pressure drop over the radial
direction of the gap due to this liquid velocity is 0.2 mm water column
if a horizontal mass flow direction and laminar flow are assumed.
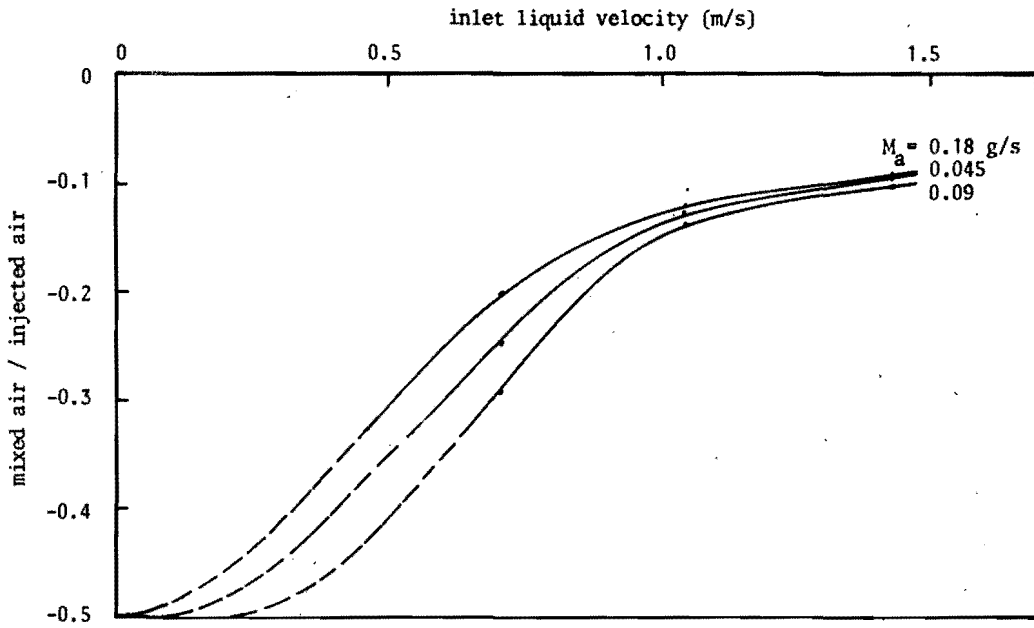
Fig.33   Percentage of mixed air versus liquid inlet mass flow velocity
in the case of a 2 mm gap
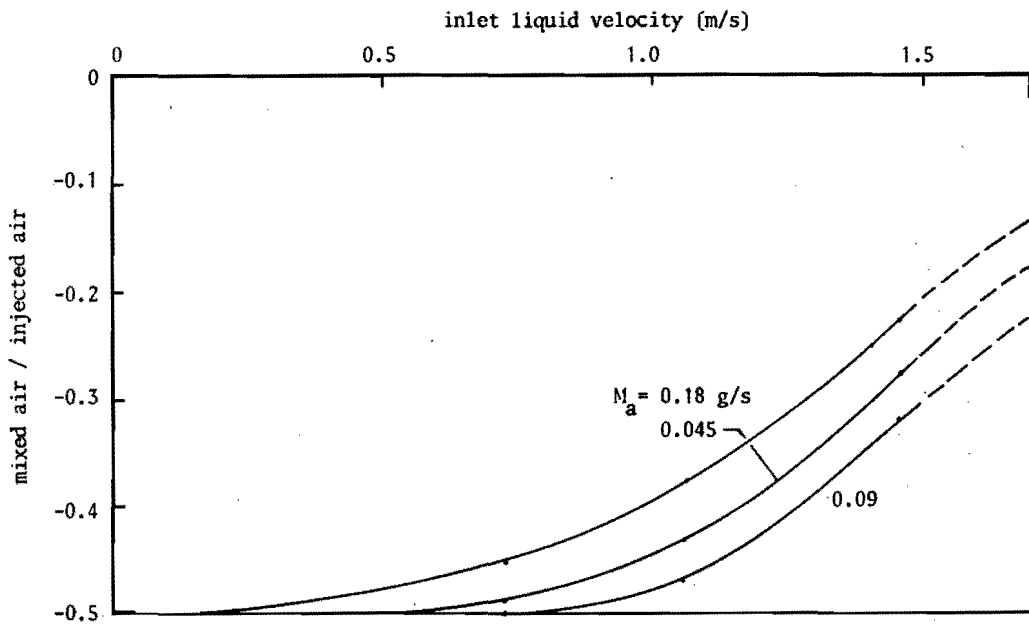
Fig.34   Percentage of mixed air versus liquid inlet mass flow velocity
in the case of a 4 mm gap
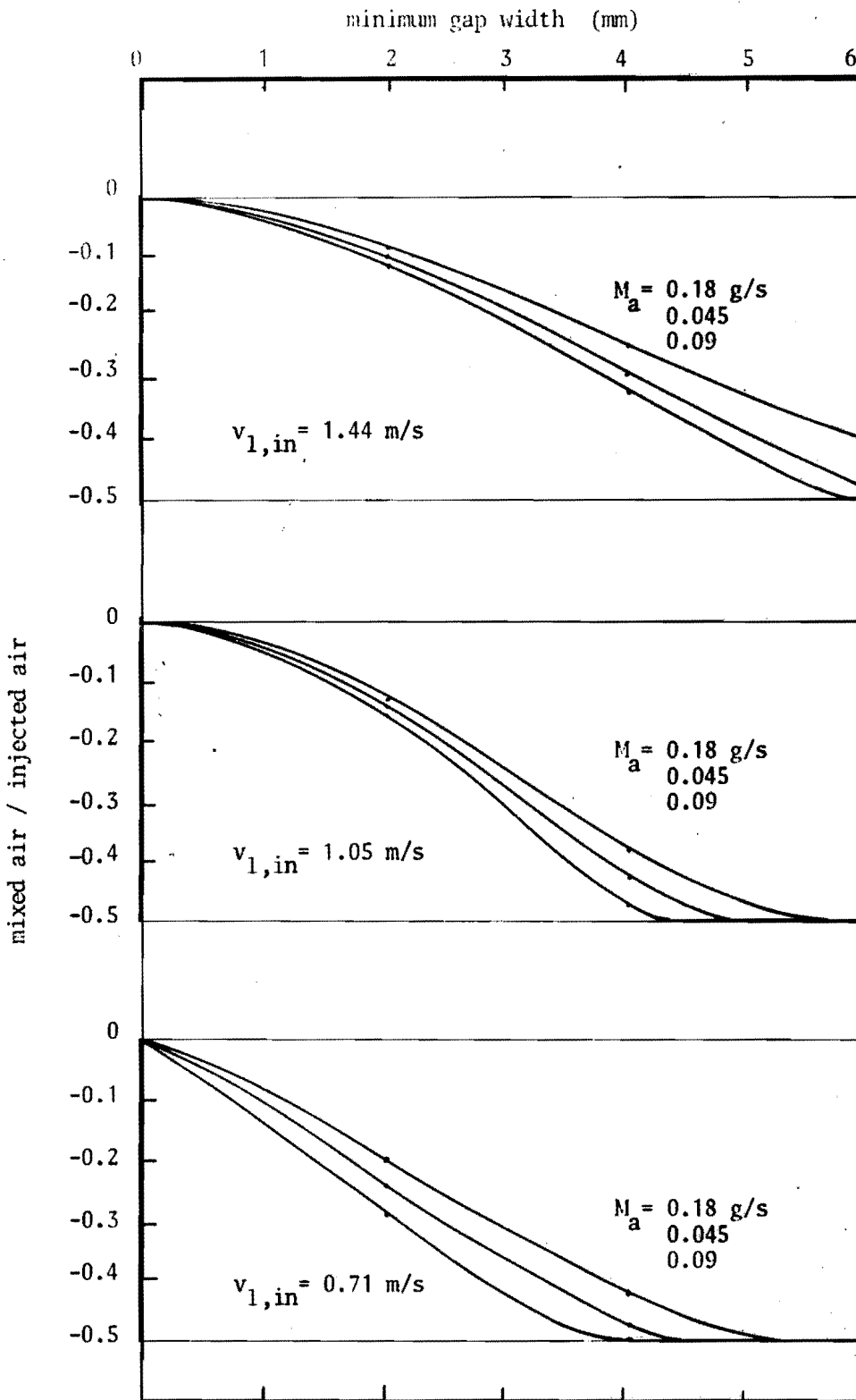
Fig.35   Percentage of mixed air versus gap width
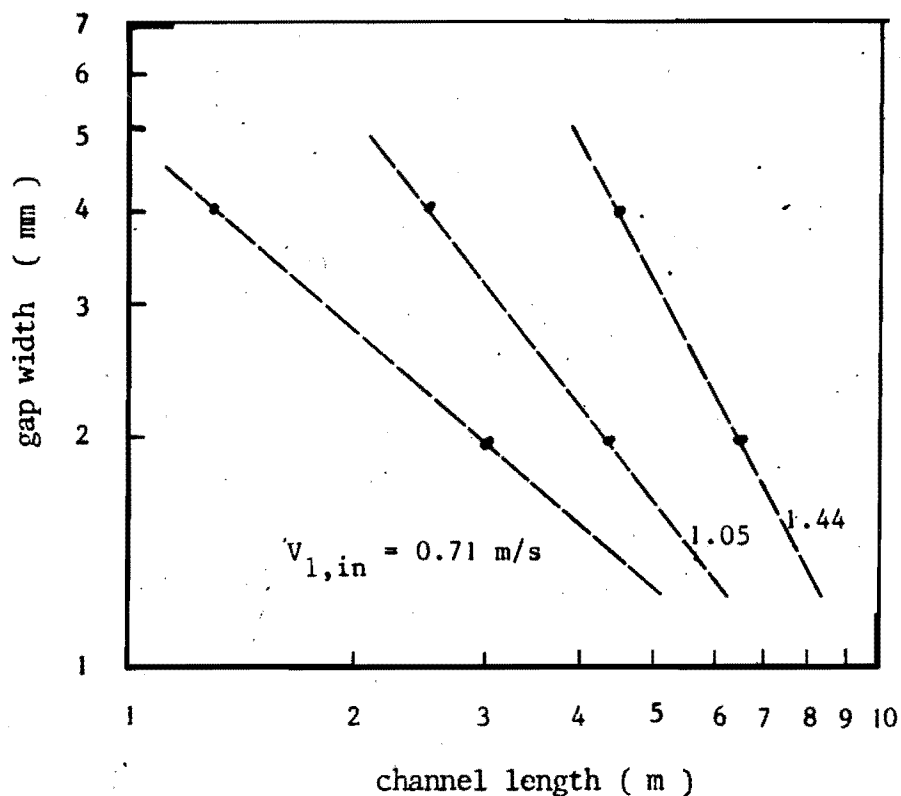
Fig.36   Channel length required for 0.95 mixing

In a data reduction program the pressure distribution has been analysed
for possible momentum exchange between the subchannels. Therefore, the
liquid velocity and void fraction distribution of both channels, together
with the empirical correlations regarding slip and two-phase friction
(chapter 3) have been read in at intervals of 0.10 m, to compute the
pressure losses due to friction, static head, and acceleration over axial
parts of the channel.
Subtraction of these three terms from the measured pressure drop would
have revealed any momentum exchange between the channels. If it had,
the value of these momentum terms must have been equally large but
opposite in sign. In the reduced data, shown in tables 4.1 and 4.2, the
terms left over after subtraction were within ± 2% of the measured
pressure drop. The cases in which the signs of these terms were opposite
to each other were rare. The conclusion drawn is that when during the
experiments momentum exchange between the subchannels took place, the
values of the corresponding transverse pressure differences were negli-
gibly small.

The axial pressure drop over a vertical hydraulic channel consists of
two parts, first a hydraulic pressure head, being a function of the
average density of the medium, and secondly, a friction term, being
mainly dependent on the liquid velocity. During bubble generation in
such a channel both these pressure terms obtain new values. The hydraulic
head decreases and since the average velocity increases the frictional

term will increase. Also, the friction coefficient increases with in-
creasing void fraction or quality. At low inlet velocities and with a
low degree of bubble generation the decrease in hydraulic head may over-
balance the increase in friction, the total pressure drop growing smal-
ler, despite the additional acceleration pressure loss that arises. At
larger values of the void fraction, the frictional term may increase ra-
pidly so that the total pressure drop increases. At high inlet veloci-
ties, the increase in friction will be larger than the decrease in
static hydraulic head right from the first bubble entering the channel.

All these phenomena are demonstrated in the total pressure drop over the
test section as a function of the injected mass flow of air which has
been plotted in figure 37. In this graph, curves have been drawn repre-
senting the measured pressure drop for the 2 and 4 mm gaps. The pressure
drop appeared to be a function of the gap width between the subchannels.
The pressure drop in the 4 mm gap experiments were lower than for the 2
mm gap at all mass flow rates. From the pressure terms, tabulated in tables
4.1 and 4.2, it can be derived that in general both the friction loss
and the hydrostatic head were smaller at the larger gap width. The largest.
contribution in the difference between the pressure drop curves was made
by the friction terms. This may be explained by the fact that the average
liquid velocity in the test section was lower during comparable experi-
ments with the 4 mm gap than with the 2 mm gap, owing to the different
void distribution over the subchannels. The contribution of the hydro-
static head grew with the mass flow rate of injected gas.
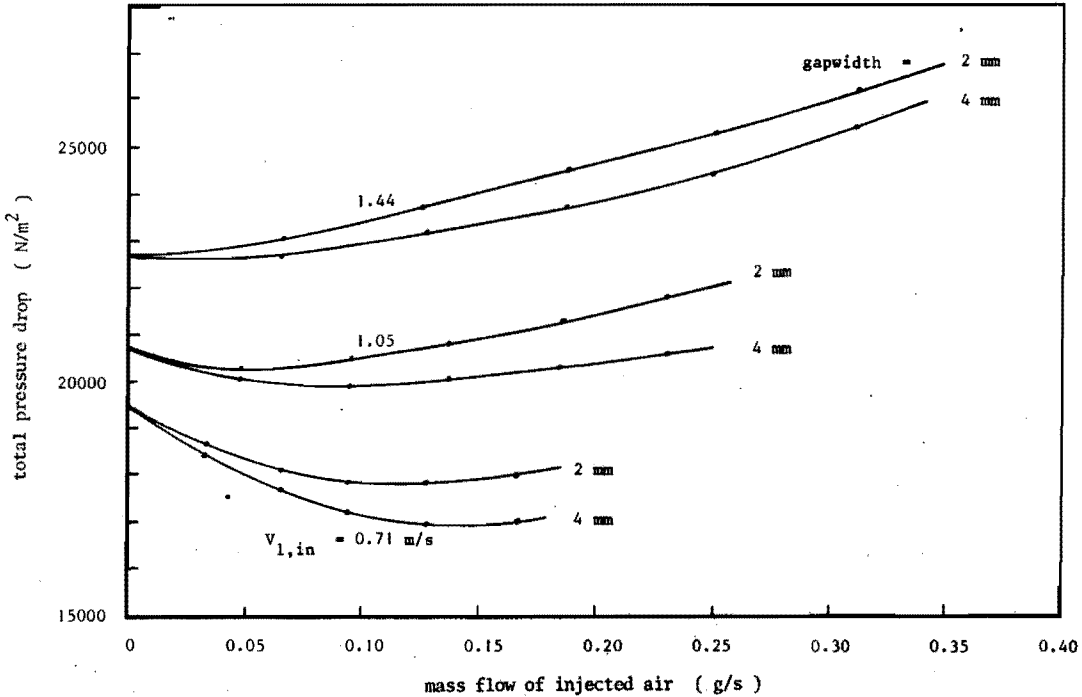
Fig.37   Total pressure drop versus mass flow of injected air

Table 4.1   Pressure drop in the case of a 2 mm gap

$V_{1,in}$ (m/s)	M_1 (g/s)	Δp_{tot} (N/m^2)	Δp_{fr}	Δp_{hydr}	Δp_{acc}	Δp_{exch}
0.71	0	19440	1340	18100	-	-
			1340	18100	-	-
	0.033	18690	3230	14840	350	270
			997	17770	-147	70
	0.065	18215	4814	12740	390	271
			1170	17000	- 50	95
	0.095	17895	6300	10930	495	170
			1370	16415	12	98
	0.126	17925	7776	9365	630	154
			1585	16130	71	149
	0.161	18050	9610	7720	790	- 70
			1840	15970	135	105
1.05	0	20700	2600	18100	-	-
			2600	18100	-	-
	0.049	20206	5300	13980	560	366
			2578	17805	-160	- 17
	0.094	20617	7825	11700	880	212
			2850	17520	- 85	352
	0.138	20880	10035	9740	1065	40
			2990	17325	71	494
	0.185	21445	12320	8138	1145	-158
			3487	17280	275	403
	0.231	21840	13748	6765	1192	135
			3825	17080	542	393
1.44	0	22620	4520	18100	-	-
			4520	18100	-	-
	0.066	23060	8330	13866	658	206
			4973	17790	60	237
	0.128	23800	11468	11245	975	112
			5529	17740	361	170
	0.188	24615	14195	9230	1110	80
			6053	17593	755	214
	0.251	25412	16294	7510	1395	213
			6675	17410	1158	169
	0.312	26345	17962	6344	1491	548
			7410	17300	1513	122

Table 4.2   Pressure drop in the case of a 4 mm gap

$V_{1,in}$ (m/s)	M_1 (g/s)	Δp_{tot} (N/m^2)	Δp_{fr}	Δp_{hydr}	Δp_{acc}	Δp_{exch}
0.71	0	19440	1340	18100	–	–
			1340	18100	–	–
	0.035	18425	2653	15508	93	171
			1350	16975	46	54
	0.078	17704	3529	13823	126	226
			1883	15678	138	5
	0.097	17248	4527	12157	234	330
			2364	14607	197	80
	0.13	16990	5773	10658	304	255
			2874	13790	319	7
	0.166	17042	7024	9185	437	396
			3330	13247	383	82
1.05	0	20700	2600	18100	–	–
			2600	18100	–	–
	0.05	20191	4518	14969	280	424
			2598	17181	63	149
	0.098	19933	6374	12812	511	235
			3384	16284	203	62
	0.142	20103	8174	10987	722	223
			3847	15647	378	231
	0.191	20316	10111	9207	945	53
			4291	15206	538	281
	0.238	20603	11937	7790	1170	-294
			4770	14879	719	235
1.44	0	22620	4520	18100	–	–
			4520	18100	–	–
	0.068	22678	7482	14361	536	299
			4829	17522	126	201
	0.132	23244	9935	11922	1060	327
			5577	17133	313	221
	0.194	23781	12269	10034	1312	96
			6089	16751	612	330
	0.26	24480	14539	8431	1551	– 41
			6721	16455	1099	205
	0.326	25518	16576	7150	1496	296
			7486	16370	1665	– 3

The behaviour of the different pressure terms in a boiling channel, described above, proved to be the driving force for the liquid exchange during the experiments, called cross flow. In figure 38 a typical example is given of the partial pressure terms resulting in the total pressure drop. When injecting gas into one channel, the diffusion process distributes the bubbles over the two subchannels, resulting in a given different hydrostatic head for each subchannel. In order to obtain equal axial pressure gradients, the liquid will redistribute itself in such a way that the friction and acceleration terms compensate the difference in the respective hydrostatic heads.

The curves for the lowest mass velocity in figure 37 shows a decreasing pressure drop at low mass flow rate of injected gas. The liquid velocity is too low for increased friction loss to compensate completely for the decreased static pressure loss. The static pressure loss in the injected channel being smaller than in the non-injected channel, liquid will move into the injected channel until pressure balance is obtained. This is in agreement with the curve for the lowest mass flow rate in figure 29. At the highest mass flow rate the increase in two-phase friction is larger than the decrease in static head, and the net amount of liquid exchange between the channels is reversed.

As the subchannels proved to have equal axial pressure gradients, the process of liquid redistribution due to different static heads is a continuous one over the length of the test section. The relatively large mass flow rate of liquid leaving the injected subchannel during the injected length are due to the large acceleration and friction pressure drop, that would occur if no liquid redistribution took place. Downstream of the injected length, acceleration forces are almost negligible compared with the static and friction losses, so that in some cases another redistribution must occur.

4.5.   Mixing correlation

The experimental data have been used to develop a correlation for the gas mixing in the described experiments. As a general form, Fick's diffusion law has been used rather than a turbulent diffusion expression. The gas exchange, apparently, did not behave as a turbulent mechanism for the mixing did not correlate with the level of turbulance. Also, the scale of gas bubble exchange is of a different order than the microscopic turbulence.

No attempt has been made to include all effects in the correlation quantitatively, since the exact influence will quite certainly depend upon the physical conditions of the two-component mixture such as bubble diameter and void fraction distribution over the cross section of the channel, as well as on the geometry of the test section.

According to Fick the basic law of diffusion, stating the rate of mass transfer N of the diffusing component P is:

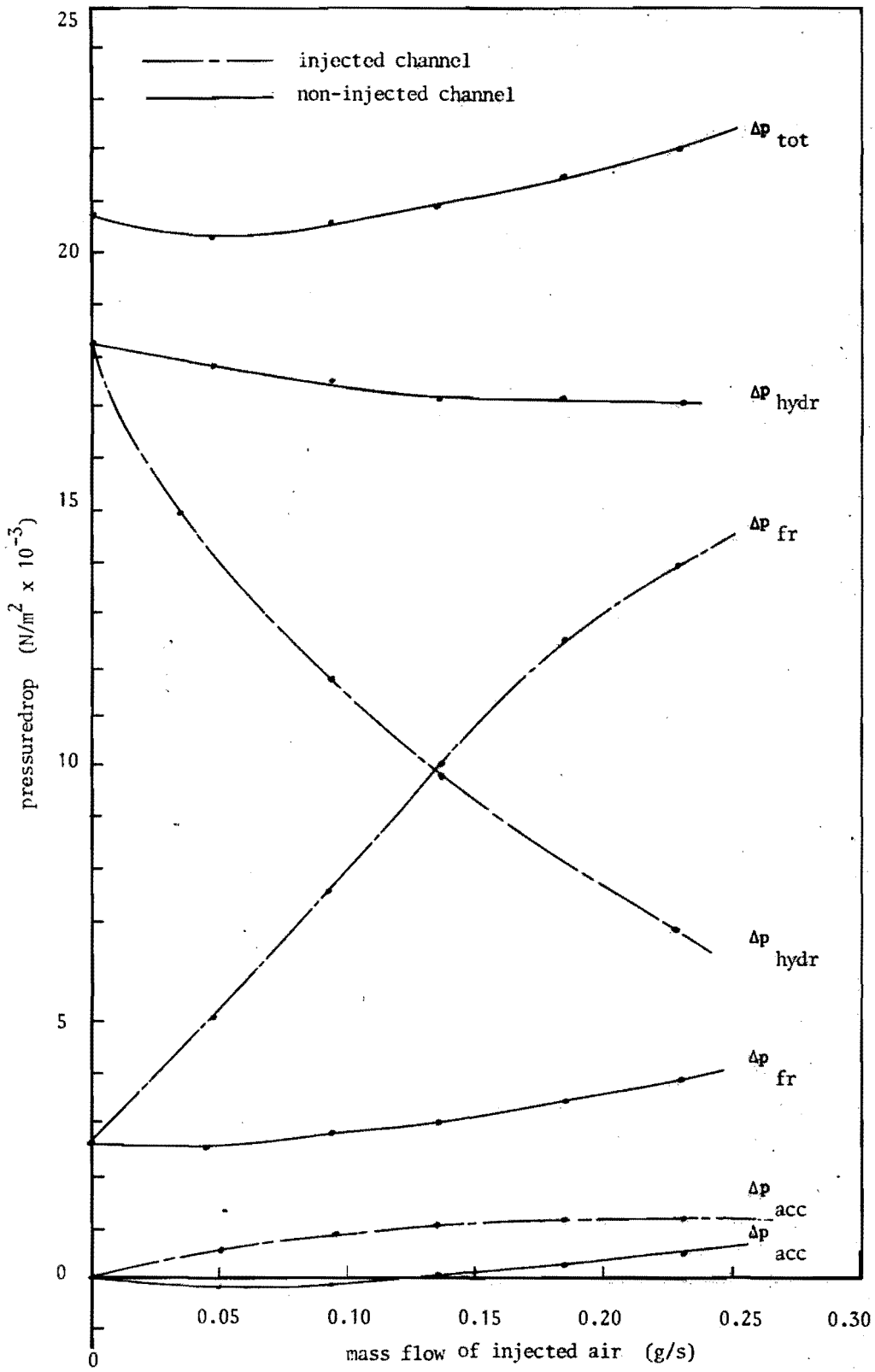$$N = - D \, A \, \frac{dP}{dy} \quad , \qquad\qquad\qquad (4.1.)$$

Fig.38 Pressure balance for an inlet liquid velocity of 1.05 m/s
in the case of a 2 mm gap

where D is the coefficient of diffusion.

Various quantities may be selected for the exchanged property P, such as the amount of gas per unit channel length or the weight quality. As the equations describing the thermohydraulic behaviour of subchannels during mixing (to be discussed in chapter 5) are solved for the void fraction, this quantity has been selected as the diffusing property. The rate of gas diffusion may depend on a large number of parameters: the gas velocity, the rate of bubble generation, the liquid velocity profile in the subchannel, the void fraction distribution in the sub-channel, the system pressure, the condensation rate during subcooled boiling, the type of flow pattern, the hydraulic channel diameter, the distance between the channels, the minimum gap width, the gap form, and others.

However, only the average gas flow velocity and the gap width have been correlated.

The rate of gas exchange per unit gap length may be written as:

$$M_{ij} = - \frac{s}{y} \, D \, \rho_g (\alpha_i - \alpha_j) \, , \qquad\qquad (4.2.)$$

in which $D = D(V_g)$, has been determined empirically utilising a digital computer program described in the next chapter.

The final correlation regarding the gas diffusion obtained from the air-water experiments is the simple relation:

$$M_{ij} = - d \, \frac{s}{y} \, \frac{\rho_g}{V_{g,i}} \, (\alpha_i - \alpha_j) \, , \qquad\qquad (4.3.)$$

in which d is a coefficient; its empirical value is given in section 5.2.

The liquid exchange, due to cross flow, is governed by a combined set of conservation equations for mass and for momentum, in which a mixing term is added in the continuity equation for mass, and by a boundary condition for the lateral pressure difference.

Chapter 5.   THEORETICAL STUDY

An attempt has been made to describe the steady-state process of gas and liquid exchange between vertical hydraulically interconnected subchannels and its effect on some channel parameters by means of a digital computer code. The model is built around the basic equations expressing the laws of conservation of mass, momentum and energy. The mixing terms describing the interaction effects between the subchannels, are inserted in the basic equations. The set of one-dimensional equations can be solved if one considers the equation of state, correlation functions for gas mixing, the slip, the two-phase friction and the heat division parameter (that is, the parameter describing the distribution of the heat input to the two-phase mixture over the two phases) and the boundary conditions.
In addition to the difference in the mixing terms, which are based upon the experimental findings on two-phase flow mixing, the model differs from the existing models, refs. (14) and (15) in the manner in which the equations for a two-phase flow are written and solved (See also section 1.2.).

5.1.   The digital computer code

The division of a multirod assembly into subchannels is more or less arbitrary. In a one-dimensional model the choice should be so made that the various properties and values over the cross-section are as homogeneous as possible. This is usually accomplished by taking the shortest distance between the rods as a division line. However, in certain conditions such as dry-out, a subchannel is sometimes considered to centre around a heating element and to have wide boundaries. The channels are divided in the axial direction into a number of nodes and the equations are formulated for one such short node. The basic equations are given in the literature (25). The general three-dimensional equations are commonly simplified to a one-dimensional form by accepting sectional average quantities of the physical variables. The two-phase character of the system is introduced by the definition of the volumetric void fraction.
The simplified equations read:

conservation of mass

$$\frac{\partial}{\partial z} \left\{ (1-\alpha)\rho_l V_l + \alpha \rho_g V_g \right\} A = 0 , \qquad\qquad (5.1.)$$

conservation of momentum

$$\frac{\partial}{\partial z} \left\{ (1-\alpha)\rho_1 V_1^2 + \alpha\rho_g V_g^2 \right\} A + \frac{\partial p}{\partial z} A = - FA - g \left\{ (1-\alpha)\rho_1 + \alpha\rho_g \right\} A ,$$

$$(5.2.)$$

conservation of energy

$$\frac{\partial}{\partial z} \left\{ (1-\alpha)\rho_1 V_1 h_1 + \alpha\rho_g V_g h_g \right\} A = q''' A \qquad (5.3.)$$

Furthermore, we need a fourth equation which depends on the boiling region.
For the non-boiling and the subcooled boiling region, defined by $T_1 < T_{sat}$, we add:

$$\frac{\partial}{\partial z} \left(\alpha\rho_g V_g h_e \right) A = \varkappa q''' A \qquad (5.4a.)$$

and for the region of bulk boiling, $T_1 \geq T_{sat}$, equation (5.4a.) is replaced by:

$$\frac{\partial}{\partial z} \left(T_1 - T_{sat} \right) A = - F_1 \left(T_1 - T_{sat} \right) A. \qquad (5.4b.)$$

By means of the heat division parameter $\varkappa$, equation (5.4a.) regulates the amount of energy that goes into the formation of vapour while equation (5.4b.) makes it possible to superheat the liquid phase in the bulk boiling region to an extent given by the value F_1.
In the equations above, h represents specific enthalpies:

$$h_1 = c T_1 , \quad h_g = c T_{sat} + e, \quad h_e = e .$$

The equations describing the process of exchange between the subchannels obtained from the experimental results, have been added to the right hand side of equations (5.1.), (5.2.), (5.3.) and (5.4a.).
The mass exchange term for gas diffusion and for cross-flow yields:

$$Mc_{ij} = - \left\{ d \frac{s}{y} \frac{\rho_g}{V_{g,i}} (\alpha_i - \alpha_j) + s \rho_1 V_{g,ij} \right\} \cdot \qquad (5.5.)$$

72

Because of lack of experimental evidence no term allowing for turbulent liquid mixing has been added to the momentum equations.

Two exchange terms have been added to the equation of conservation of energy, first the term describing the enthalpy carried across by the gaseous phase through diffusion, and secondly the liquid enthalpy exchange by cross-flow:

$$Me_{ij} = - \left\{ d \; \frac{s}{y} \frac{\rho_g}{V_{g,i}} (cT_{sat} + e)(\alpha_i - \alpha_j) + s \; \rho_l V_{c,ij} cT_l \right\} . \qquad (5.6.)$$

The first part of expression (5.6.) has also been added to equation (5.4a.) in which the amount of boiling is expressed:

$$Mg_{ij} = - d \; \frac{s}{y} \frac{\rho_g}{V_{g,i}} (cT_{sat} + e)(\alpha_i - \alpha_j) . \qquad (5.7.)$$

Furthermore, a boundary condition is needed in which the pressure difference between the subchannels is made equal to the lateral cross-flow frictional pressure drop:

$$P_i - P_j = C_{ij} \; \tfrac{1}{2} \rho_l V^2_{c,ij} , \qquad (5.8.)$$

in which C is a pressure loss coefficient of the transverse cross-flow in the gap, the value of which has to be determined experimentally.

In order to solve the equations, we further need equations of state for ρ_l, ρ_g, c, e and T_{sat} as functions of the temperature, pressure or both, and correlation functions regarding the slip ratio S, the two-phase friction multiplier R and the heat division parameter $\varkappa$.
With the introduction of slip ratio, the gas velocity can be eliminated from the equations. In the model has been programmed (25) a choice of existing empirical or semi-empirical slip correlations, such as found by Bankoff-Jones (26), Zuber-Findlay (27) and Marchaterre-Hoglund (28). Furthermore, especially derived experimental correlations can be added as subroutines. The two-phase friction multiplier is used in the frictional pressure drop term:

$$F = R \; f \; \tfrac{1}{2} \rho_l V_l^2 / d_h . \qquad (5.9.)$$

The friction correlations of Bankoff (26) and Martinelli-Nelson (23) have been programmed in the model, and correlations derived for the

present study may be added as subroutines. The definition of R and the liquid velocity in expression (5.9.) varies for the several correlations used (25).

A heat division parameter has to be defined for the subcooled boiling region. In the single-phase region all the power dissipated in a channel serves to increase the enthalpy of the liquid. In the subcooled region, a significant portion of the power is used to evaporate liquid, the remainder providing the enthalpy increase of the liquid until the average liquid temperature reaches the saturation value. Next, all energy is used to evaporate liquid except for a small portion that provides the slight superheat to the liquid phase. The liquid temperature at the onset of subcooled boiling is calculated from the criterion of Jens and Lottes (29). A choice can be made between the heat division parameter by Bowring (30), being a constant, or as used in (16), where kappa is defined as:

$$\varkappa = \frac{T_1 - T_b}{T_{sat} - T_b} \; .$$

(5.10.)

By means of these correlation functions the number of available equations, i.e. 13, is sufficient to solve the system for the unknowns: α, V_1, p, T_1, T_{sat}, ρ_1, ρ_g, V_c, S, F, $\varkappa$, c and e.

Solving the set of equations

The model has been written for a cluster consisting of n interconnected subchannels of which each one may be connected with m neighbouring channels. Each channel is divided into a number of nodes and the equations for each subchannel are solved for each node in succession. The system of n times the set of equations for each node is solved simultaneously for each identical increment in order to fulfil the boundary condition given by the cross-flow lateral pressure drop.
By differentiation of the channel equations (5.1.), (5.2.), (5.3.) and (5.4.), the following 4 differential equations can be derived for V_1, α, T_1 and T_{sat}:

$$C_1 \frac{dV_1}{dz} + C_2 \frac{d\alpha}{dz} + C_3 \frac{dT_1}{dz} + C_4 \frac{dT_{sat}}{dz} = 0$$

$$F_1 \frac{dV_1}{dz} + F_2 \frac{d\alpha}{dz} + F_3 \frac{dT_1}{dz} + F_4 \frac{dT_{sat}}{dz} = F_5$$

$$E_1 \frac{dV_1}{dz} + E_2 \frac{d\alpha}{dz} + E_3 \frac{dT_1}{dz} + E_4 \frac{dT_{sat}}{dz} = E_5 \qquad (5.11.)$$

$$G_1 \frac{dV_1}{dz} + G_2 \frac{d\alpha}{dz} + G_3 \frac{dT_1}{dz} + G_4 \frac{dT_{sat}}{dz} = G_5$$

where the matrix coefficients are given in (34).
The mixing equations (5.5.) to (5.8.) are added to these channel equations and the right hand sides of equations (5.11.) are replaced by

$$= 0 \quad + \sum_{i=1}^{m} Mc_i$$

$$= F_5$$

$$\qquad (5.12.)$$

$$= E_5 + \sum_{i=1}^{m} Me_i$$

$$= G_5 + {\sum_{i=1}^{m}}' Mg_i$$

The $\sum'$ in the last term indicates that Mg_i is only added to equation (5.4a.); it vanishes for equation (5.4b.).
The set of equations is integrated by the use of an Euler method with matrix inversions in every step of the calculation procedure.

In an early version of the code the equations were solved as an initial value problem with an iteration over the total channel length for equal total pressure drops varying the inlet mass flow distribution. This method failed because the cross-flow mixing terms from equations (5.12.) are proportional to a factor $p_i - p_j$ where p_i and p_j are variables in the left hand sides of equations (5.11.).

The stability of a numerical integration procedure has been set by the well-known Lifschitz requirements, which among other demands, stipulate that for each dependable variable of the integration procedure, the partial derivative of any term on the right hand sides of the set of equations in respect of any dependent variable has to be limited. As pointed out by Rowe (6), this means that for instance the partial derivative of the cross-flow velocity V_c, (V_c is a function of $\sqrt{p_i - p_j}$), in respect of the system pressure p has to be limited. This requirement is hard to fulfil as we are looking for a solution where $p_i - p_j$ will be small compared with p_i or p_j.

Another approach to solve the initial value problem has been a relaxation method in which the cross-flow terms were added to the equations as constants with the help of an iteration until the requirement set by equation (5.8.) was met. This relaxation method did not lead towards a stable convergent solution either.

It seems that the only practical method to solve the equations is using equation (5.8.) as a boundary condition for each integration node and adding an iteration until the parameters in all channels are in harmony with this boundary condition. In the method described here, the cross-flow velocities between the subchannels as a separate set of unknowns tend to be solved by iteration (31), similar to the method in Hambo (15). A procedure has been added which calculates a correction $\partial V_{c,ij}$ by starting from a calculated or assumed value of the cross-flow velocity $V_{c,ij}$.

Consider the expression

$$\varepsilon_{ij} = p_i - p_j - \tfrac{1}{2} C_{ij} \rho_{1,c}\, V_{c,ij}/\,V_{c,ij}/\, , \qquad (5.13.)$$

in which ε indicates to what extent equation (5.8.) has been satisfied. We now need an expression for the correction to be added to $V_{c,ij}$ in order to minimise ε.
This may be written as:

$$0 = (p_i + \frac{dp_i}{dV_{1,i}}\, \partial V_{1,i}) - (p_j + \frac{dp_j}{dV_{1,i}}\, \partial V_{1,i}) +$$

$$- C_{ij}\rho_{1,c}(V_{c,ij} + \partial V_{c,ij})/V_{c,ij} + \partial V_{c,ij}/. \qquad (5.14.)$$

Subtracting equation (5.14.) from (5.13.) and neglecting $(\partial V_c)^2$ terms we have

$$\varepsilon_{ij} = -\lambda_i\, \partial V_{1,i} + \lambda_j\, \partial V_{1,j} + C_{ij}\, \rho_{1,c}/V_{c,ij}/\partial V_{c,ij} ,$$

76

where $\lambda = \dfrac{dp}{dV_1}$

After some reduction it may be shown (31) that

$$\partial V_{1,i} = -\frac{\Delta z}{\rho_{1,i}} \sum_i s_{ij} \rho_{1,c} \partial V_{c,ij} \cdot \tag{5.15.}$$

Substitution of eq. (5.15.) in (5.14.) finally gives:

$$\varepsilon_{ij} = \lambda_i \frac{\Delta z}{\rho_{1,i}} \sum_i s_{ij} \rho_{1,c} \partial V_{c,ij} +$$

$$- \lambda_j \frac{\Delta z}{\rho_{1,j}} \sum_j s_{ji} \rho_{1,c} \partial V_{c,ji} +$$

$$+ C_{ij} \rho_{1,c} /V_{c,ij}/ \partial V_{c,ij} \cdot \tag{5.16.}$$

In the set of n equations of the form of eq. (5.16.)

ε_{ij} equals ε_{ji} ;

s_{ij} equals s_{ji} ;

$V_{c,ij}$ equals $- V_{c,ji}$; and

$\partial V_{c,ij}$ equals $- \partial V_{c,ji}$.

The set of equations (5.16.), although consistent in itself, is for most practical applications ill-conditioned, because the pressure loss coefficient $C \ll 1$. This can be overcome by replacement of the nth equation in the set of equations (5.16.), for the first node by

$$0 = \sum_i^i \rho_{1,c} \partial V_{c,ij} \quad , \tag{5.17.}$$

and for all other nodes by

$$0 = \sum_i^i \rho_{1,c} / V_{c,ij} / (V_{c,ij} + \partial V_{c,ij}) \quad , \tag{5.18.}$$

77

where $\displaystyle\sum_{i}^{i}$ denotes the sum of these terms for all subchannels, which to-
gether with the gaps form a "closed loop".
Equation (5.18.) has been obtained by varying expression (5.13.) with
$\partial V_{c,ij}$ for each subchannel and adding all the expressions. The system
equations are integrated twice as a start, each time with a differ-
ent starting value for the cross-flow velocities in order to obtain
numerical values for λ, which are then re-evaluated during the next ite-
rations.

5.2. Comparison with experimental data

The digital mixing program described in the previous section has been
used to compute channel parameters for a number of cases in which the
input data fed into the computer was taken from the experimental program.
To simulate the adiabatic air-water experiments with the model written
for two-phase, boiling channels the heat division parameter was set to
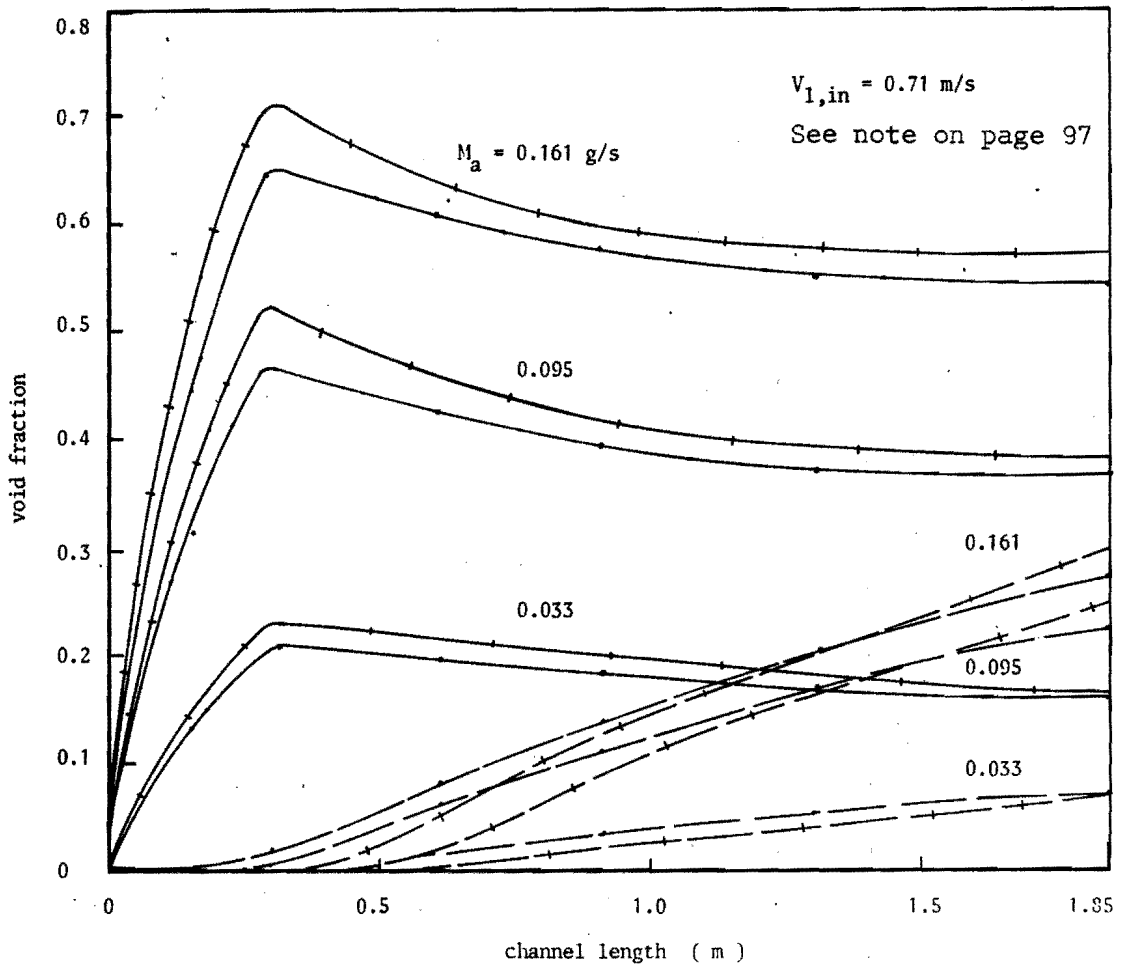
Fig.39 Comparison of the calculated and observed void fraction
distribution in the case of a 2 mm gap

unity and the channel power was calculated by multiplying the mass flow
rate of injected air by the latent heat of evaporation. Provided as input
data were the subchannel and gap geometry, and the heated channel length;
physical quantities as the mass flow rate, the inlet temperature and
pressure, the single-phase friction coefficient and the channel power;
properties of matter of the gas and of the liquid with the equations of
state; and numerical values such as the length of an integration step and
a value indicating to what extent the boundary condition for the cross-
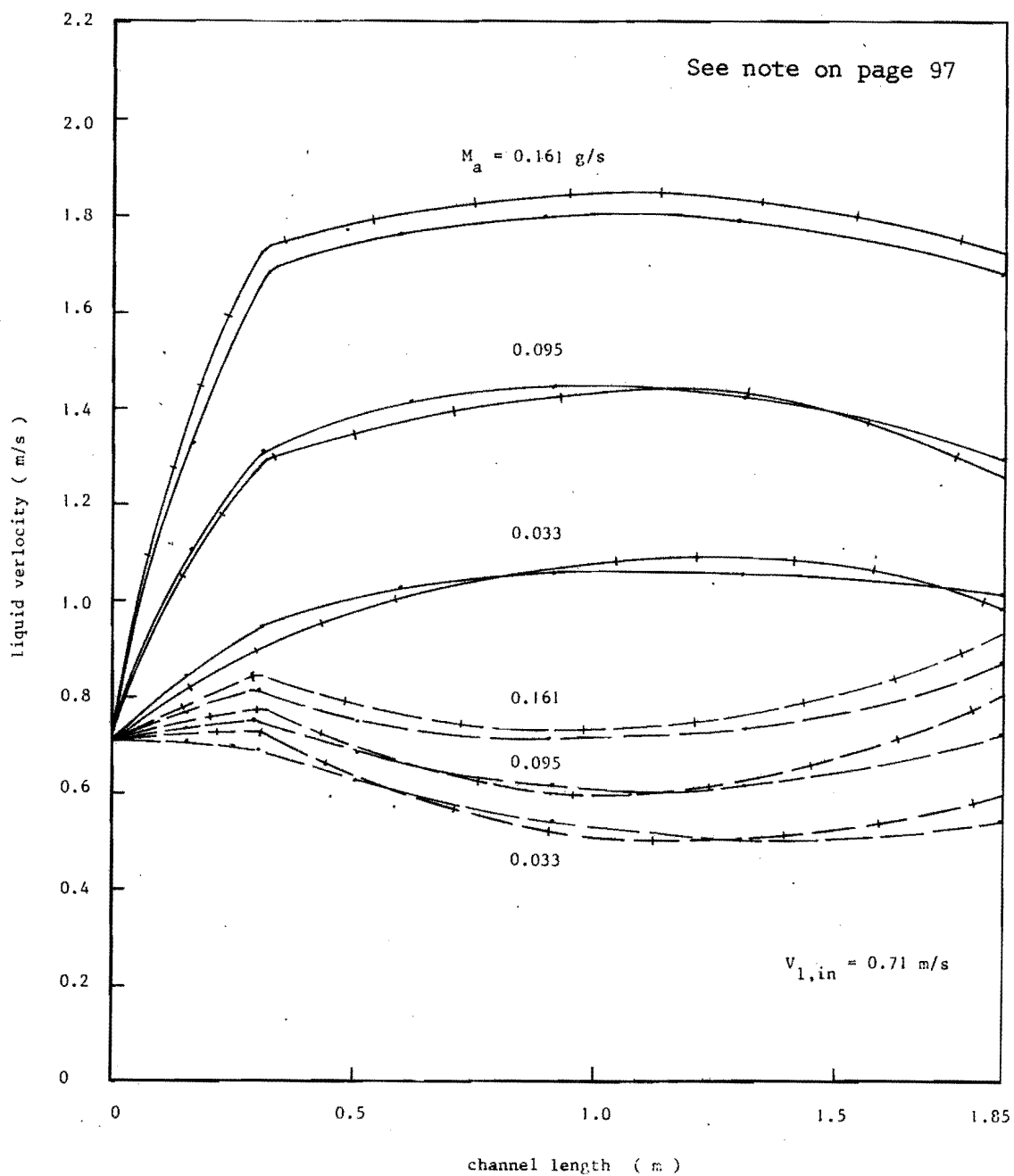
Fig.40   Comparison of the calculated and observed mass flow velocity
distribution in the case of a 2 mm gap

flow had to be satisfied. Furthermore, the two-phase friction correlation
obtained from the experiments was programmed as a subroutine. The slip-
ratios during the experiments were close to unity and this value was taken
as a constant. The lateral pressure loss coefficient was given such a
value that the pressure drop over the gap due to cross flow was in all
cases less than the experimental value of 1 mm water-column. In an at-
tempt to simulate the observed effect of the channel power, the sub-
channel parameters were computed for the case of an inlet liquid velo-
city of 0.71 m/s and a gapwidth of 2 mm for three different amounts of
power, corresponding with the lowest, the middle and the highest mass
flow rates of injected air during the experimental program.
The diffusion coefficient d in the mixing terms for the gaseous phase
has been fitted for the best result compared to the experimental data.
In figure 39 the computed curves have been plotted for the void fraction
distribution in the subchannels as a function of the channel length to-
gether with the experimental data. The value of d in these runs was
0.15×10^{-3} m^3/sec^2. In figure 40 the liquid velocities were plotted in
the same manner. The results are very satisfactory, considering the
simple diffusion expression. A comparison of the computed and experimen-
tally observed percentage of air penetrated into the non-injected sub-
channel is plotted in figure 41.
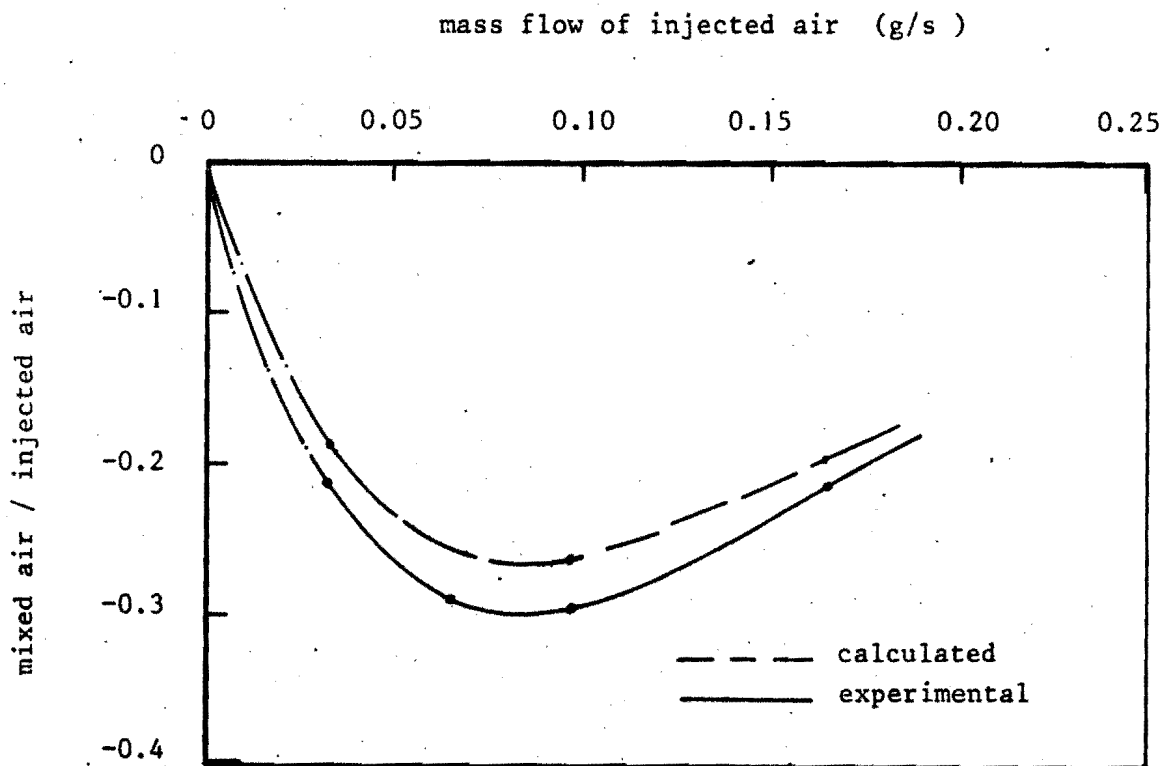
Fig. 41 Comparison of the computed and experimentally
observed percentage of mixed air

Although the quantitative results obtained from the model deviate some-what from the experimental values, it has been shown that the qualitative effects of the diffusion mechanism can reasonably well be calculated using the proper mixing expressions. Computed curves for the void fraction and the liquid velocity as functions of the channel length were plotted for the case of a higher mass flow velocity in figures 42 and 43 together with the comparable experimental data. Again, the best fit was obtained with $d = 0.15 \times 10^{-3}$ m³/sec2.

The effect of the gap width on the mixing, calculated by the mathematical model, is shown in the figures 44 and 45, in which the usual parameters were plotted for two identical cases except for the gap width, together with the experimental data. The best fit in this case was obtained with a somewhat larger value of the diffusion coefficient d, viz. 0.4×10^{-3} m³/sec2.
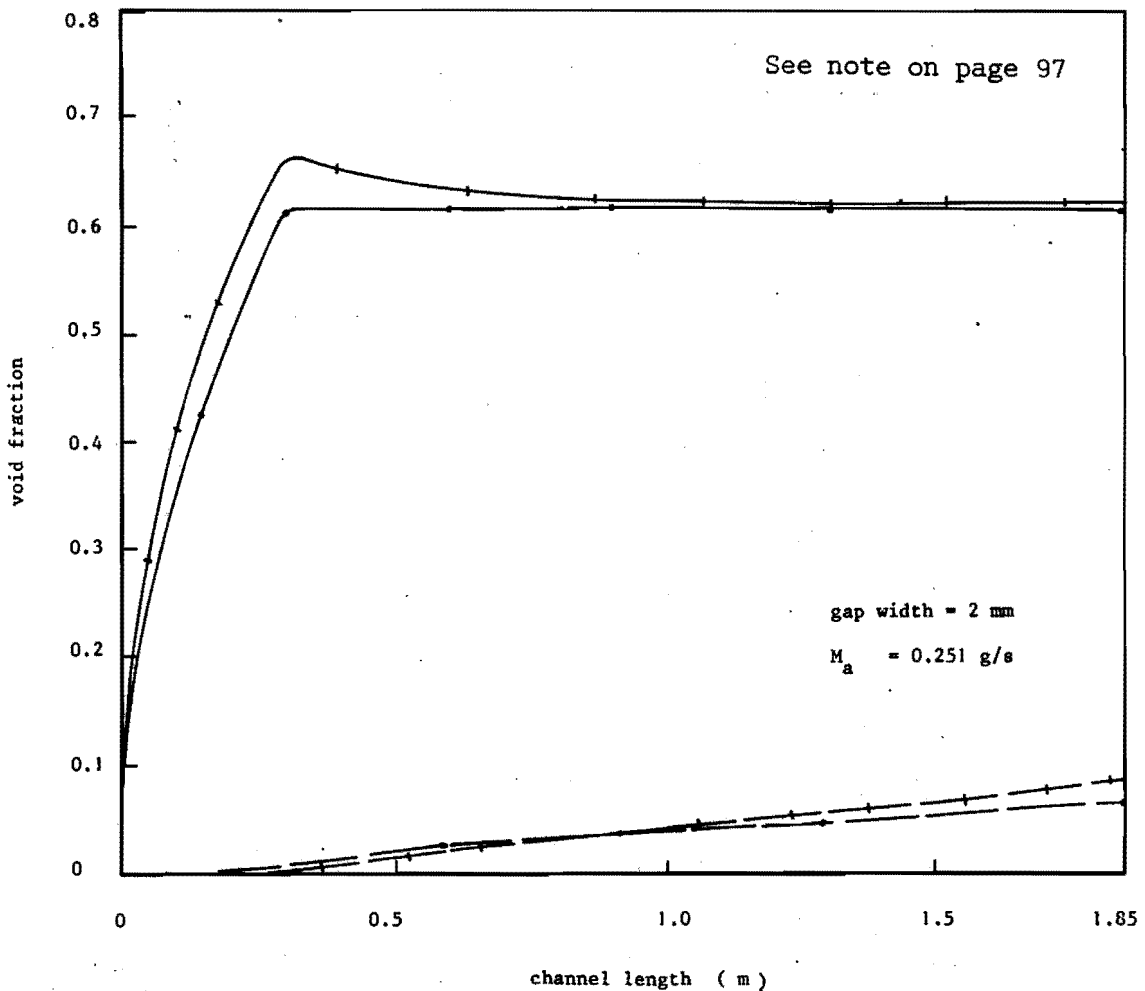
Fig.42 . Comparison of the calculated and observed void fraction distribution in the case of an inlet liquid velocity of 1.44 m/s
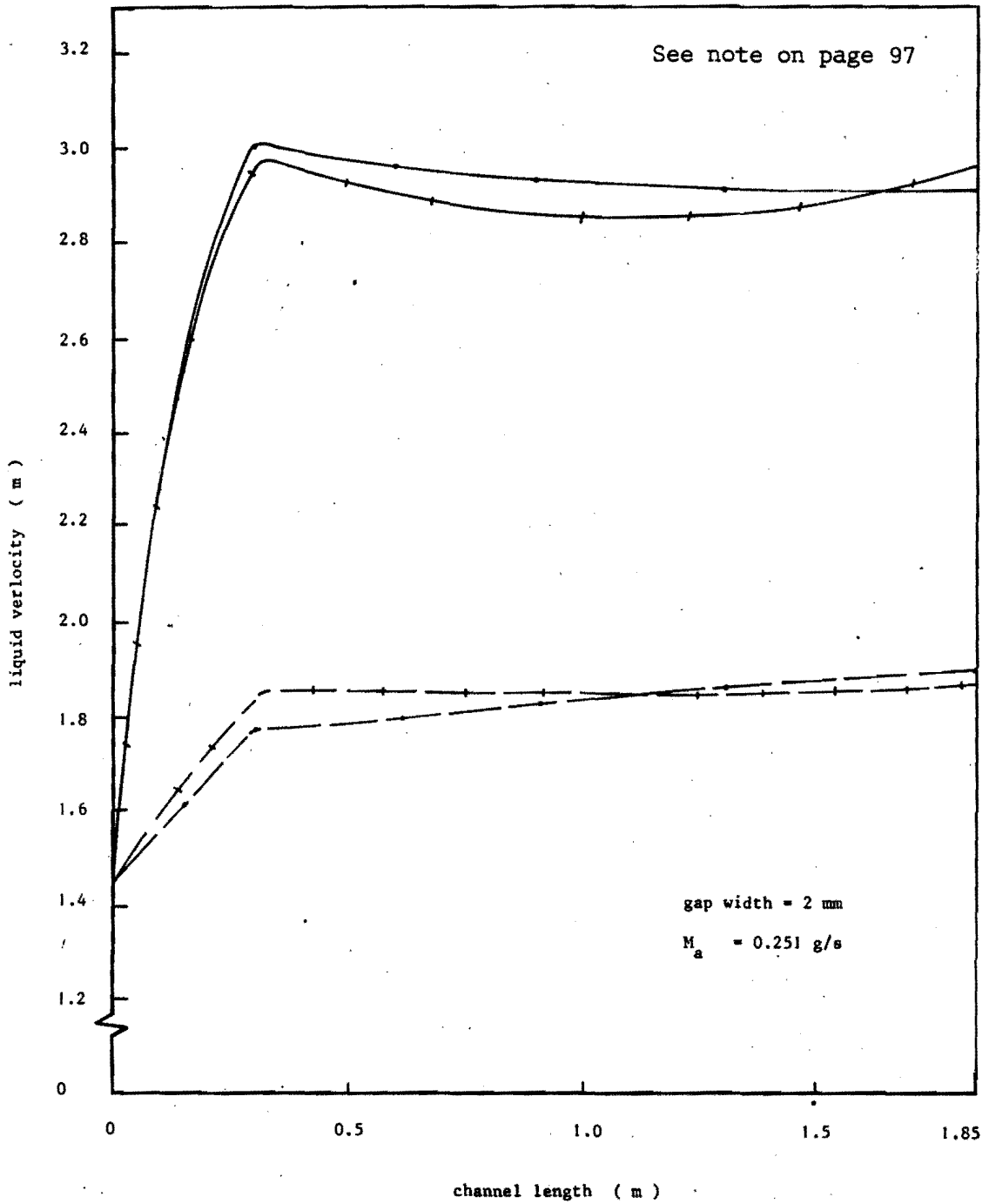
Fig.43 Comparison of the calculated and observed liquid velocity distribution in the case of an inlet liquid velocity of 1.44 m/s

82

No attempt to refine the diffusion expression (4.3.) has been undertaken, as the model only served to prove that the effects of the different variables during the experiments could be simulated by a mathematical code in which expressions were added, describing the observed mixing mechanism.

Furthermore, it is anticipated that the diffusion expression as well as the value of the coefficient d will not be universally valid and will depend on various parameters and conditions not investigated in this study.
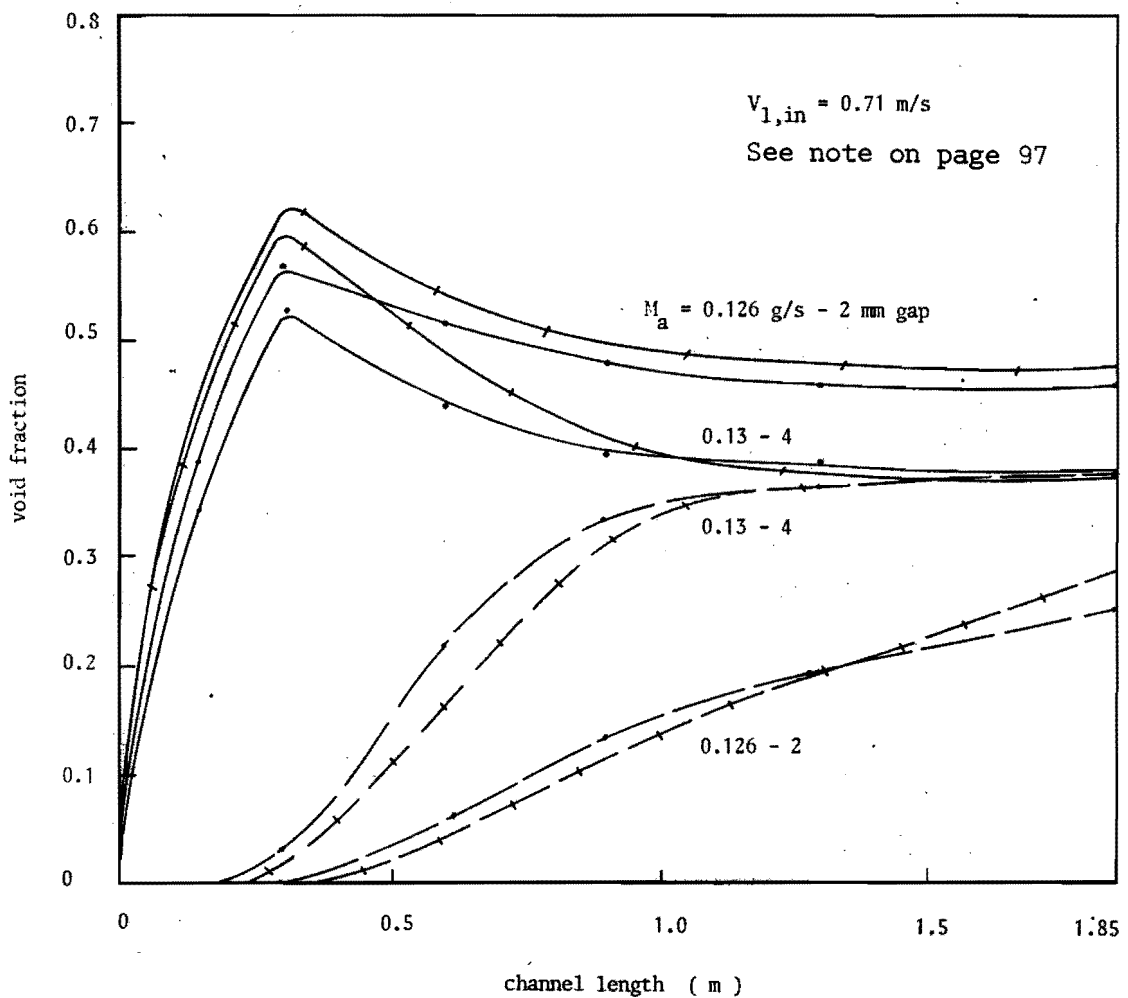
Fig.44 Comparison of the calculated and observed effect of the gap width on the void fraction distribution

83

See note on page 97
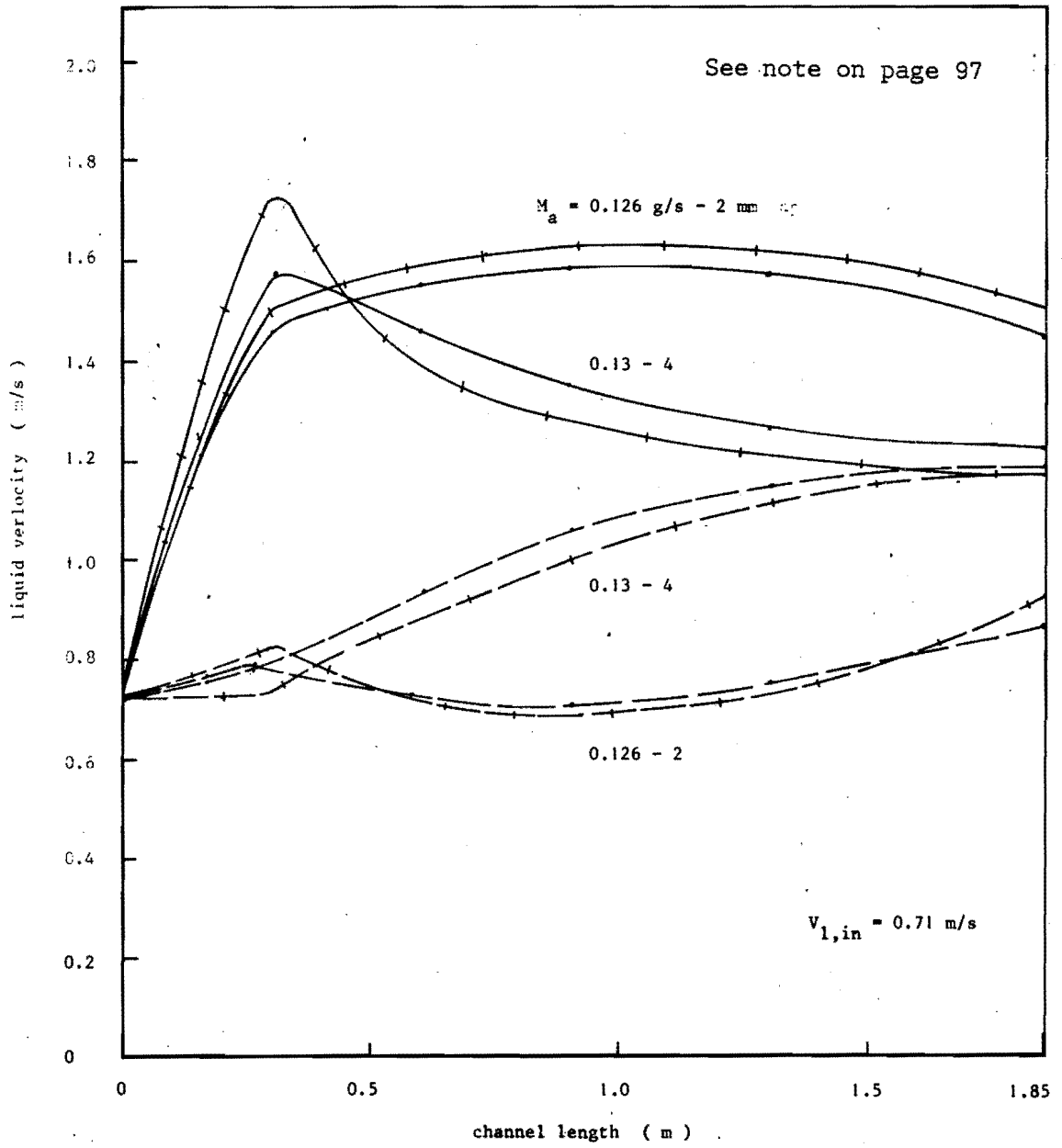
Fig.45. Comparison of the calculated and observed effect of the gap width on the liquid velocity distribution

Chapter 6.   CONCLUSIONS

The results obtained from the observations on two-phase (two-component) mixing are subject to a number of conditions. The experiments have been carried out in an adiabatic air-water mixture simulating steam-water at saturation condition; the density ratio of the liquid and gas at 1 bar, which is about 750, equals that of steam-water at approximately 2.3 bar. Naturally, the quality in this pressure range is low. All data were gathered in the bubble flow regime of the mixture, the average bubble diameter varied from 0.5 to 1 mm, the void distribution over the cross-section of the subchannels was rather homogeneous, the slip ratio in the channels close to unity. Furthermore, the results were to a somewhat lesser extent subject to the test section geometry.
Nevertheless the following conclusions are suggested:

(1) The exchange between the two channels of each phase in the two-phase flow structure appeared to result from different phenomina. Gas mixing behaved as a diffusion mechanism; the exchange of liquid by cross-flow followed of necessity the redistribution of the void, governed by the condition of equal axial pressure gradients. The liquid cross flow was superimposed on the gas diffusion without interference effects, although the direction of exchange was often opposite.

This conclusion was based on the data shown in the figures 20 to 23, and tables 4.1. and 4.2., part of which has been plotted in figure 38. The mechanism observed is different from the description in existing mixing models (See Chapter 1), where the average density of the mixture is assumed to take part in turbulent mixing as well as in cross-flow exchange between the subchannels, and in which no gas exchange by diffusion is taken into account.

The experimental apparatus was not suited to detect turbulent liquid mixing as its net exchange will be zero, but it might exist. It goes without saying that the different types of mass exchange will affect the enthalpy exchange between the subchannels in the case of power supply to the channels.

It is felt that the mechanism described is also the predominant mixing phenomenon in the bubble flow region of a steam-water mixture. This probably holds even under subcooled conditions in the colder subchannels, where condensation may take place, and independently of the geometrical conditions.

(2) The relative rate of gas mixing increased with the amount of simulat-
ed channel power to a peak value and decreased at larger mass flow
rates of injected air. The effect is more pronounced at higher gas
mixing percentages.

This effect of the channel power on the gas exchange, shown in figures
26 and 27, can be explained by the behaviour of the mechanism of gas
diffusion. The rate of diffusion increased with the concentration gradient
between the subchannels but decreased with shorter transit time of the
gas in the channels. At larger mass flow rates of injected air the gas
velocity in the donating channel increased rapidly and the transit
time effect preponderated. The transit time effect had greater impact
at higher percentages of mixed gas when the concentration gradient was
small. The properties of the gas diffusion mechanism described in chap-
ter 4 may serve to explain the observations by Rowe and Angle, as
quoted in chapter 1. They observed a peak in enthalpy mixing with exit
steam quality, its value decreasing with increasing mass flow rates.

(3) Gas mixing in the two-phase flow decreased with increasing liquid
mass flow velocity.

The effect is illustrated in figures 33 and 34. At higher mass flow velo-
cities the transit time of the gas in the channels decreased and less
time is available for the bubbles to move in the direction of a lower
concentration. Similar effects of the mass flow rate have been reported
by Rowe and Angle (7) and by Bowring and Levy (11).
Enthalpy exchange by turbulent mixing in a single-phase system increases
with mass flow velocity, the eddy diffusivity being a function of the
level of turbulence. During two-phase flow mixing the enthalpy exchange
will depend on the total rate of heat exchange by gas (diffusion) and
by liquid (cross-flow). The former carrying along heat of evaporation,
decreased at higher mass flow velocities, but the liquid cross-flow
with its subsequent enthalpy exchange depended on both the gas exchange
and the momentum conditions in the subchannels, and is not such a simple
function of the mass flow velocity like the turbulent liquid mixing, if
any. However, in cases of relatively large gas diffusion and cross-flow
between the subchannels, like during the described experiments, it is
felt that the effect of the turbulent liquid mixing on the total enthalpy
exchange will be overshadowed by the effects of the other mechanisms.

(4) The gas diffusion rate between subchannels in the two-phase flow in-
creased with wider gap.

See figures 35 and 36. This behaviour was to be expected from a diffusion
exchange since the rate of diffusion in general is proportional to the
area perpendicular to the pathway of the diffusing property. Larger
mixing rates were also reported by Rowe and Angle (7), who widened the
gap by increasing the rod pitch.

(5) No lateral pressure difference larger than the experimental error of
± 1 mm water column, nor significant momentum exchange within the
experimental uncertainty of ± 2% of the total axial pressure drop
between the subchannels, could be observed during the experiments.

The relatively low local cross-flow velocity in the gap even during the largest mixing flow rates did not give rise to a measurable pressure difference, contrary to observations by Bestenbreur and Spigt (13) in air-water experiments mainly performed in the slug flow regime. Momentum exchange will probably be so small that more refined measuring techniques will have to be used instead of the data reduction analysis reported.

(6) The total axial pressure drop over the test section decreased by widening the gap between the subchannels.

The magnitude of this effect of changing the gap width (which affects the rate of mixing) can be seen in figure 37. From the data given in the tables 4.1. and 4.2. it can be derived that usually both the hydrostatic head and the friction loss decreased in the case of the larger gap width. The largest contribution was made by the friction term as a result of the lower average liquid velocity in the test section during comparable experiments with the 4 mm - gap than in the case of the 2 mm - gap.

It is often said that by lifting the tip of the veil that covers the riches of new knowledge, one wonders about the few possessions gathered so far.
This is certainly true of the complex subject of two-phase flow in general as well as of the topic of subchannel analysis. The observations described in this study only increases the need for more experimental work on the two-phase flow mixing. Further fundamental studies in scaled-up models would make a large contribution towards the general understanding of the mechanism of mixing, as would comparative studies of mixing in adiabatic air-water and steam-water systems, and of the mixing mechanism in different two-phase flow regimes. The effect of a great number of system and geometrical conditions over a large range of parameters should be investigated systematically to obtain usable qualitative and quantitative results.

ACKNOWLEDGEMENTS

NOMENCLATURE

A   cross section, area $\qquad$ L^2

C   pressure loss coefficient of the transverse cross
flow in the gap, $\qquad$ diml
coefficients in eq. (5.11)

c   heat capacity of liquid or gas at constant pressure
per unit mass $\qquad$ $L^2 t^{-2} T^{-1}$

D   diffusion coefficient, $\qquad$ $L^2 t^{-1}$
rod diameter $\qquad$ L

d   coefficient in diffusion expression $\qquad$ $L^3 t^{-2}$

d_h hydraulic diameter $\qquad$ L

E   coefficient in eq. (5.11)

e   latent heat of evaporation at constant volume $\qquad$ $L^2 t^{-2}$

F   wall friction force, per unit cross sectional area,
per unit length, eq. (5.9) $\qquad$ $ML^{-2} t^{-2}$

        coefficient in eq. (5.11)

F_1 constant in eq. (5.4b)

f   single-phase friction factor $\qquad$ diml

G   coefficient in eq. (5.11)

g   gravitational acceleration $\qquad$ Lt^{-2}

h   specific enthalpy $\qquad$ $L^2 t^{-2}$

k   conductance, eq. (2.1)

l   Prandtl mixing length $\qquad$ L

M   mass flow $\qquad$ Mt^{-1}

Mc	rate of mass exchange between subchannels, per unit length	$ML^{-1}t^{-1}$
Me	rate of enthalpy exchange between subchannels, per unit length	MLt^{-3}
Mg	rate of gaseous enthalpy exchange between subchannels, per unit length	MLt^{-3}
m	number of subchannels	diml
n	number of neighbouring subchannels	diml
p	local pressure	$ML^{-1}t^{-2}$
pitch	distance between centres of rods	L
q'	heat exchange between subchannels per unit length	MLt^{-3}
q'''	heat input per unit cross sectional area, per unit length	$ML^{-1}t^{-3}$
R	two-phase friction multiplier	diml
Re	Reynolds number	diml
S	slip ratio, gap shape factor, eq. (1.10)	diml diml
s	gap width	L
T	temperature	T
T_b	liquid temperature at which bubbles detach from the wall	T
T_{sat}	saturation temperature	T
v	velocity	Lt^{-1}
w'	rate of turbulent mass exchange, per unit length, eq. (1.9)	$ML^{-1}t^{-1}$
X_{tt}	Martinelli-Nelson correlator	diml
x	weight quality	diml
y	co-ordinate in radial direction, distance between the centres of the subchannels	L L
z	co-ordinate in the axial direction	L

GREEK SYMBOLS

α	void fraction	diml
β	mixing coefficient	diml
Δ	increment ($\Delta p, \Delta z$)	
ε	eddy diffusivity,	$L^2 t^{-1}$
	numerical value, eq. (5.13)	diml
$\varkappa$	heat division parameter	diml
λ	$= dp/dV_1$,	
	mixing coefficient eq. (1.5)	diml
ρ	density	ML^{-3}
$\Phi_{1,tt}$	two-phase friction multiplier	diml

SUBSCRIPTS

a	injected air
acc	acceleration
c	cross flow
e	evaporation
exch	exchange
exp	experimental
fr	friction
g	gas

hydr   hydro static

i,j   subchannel identification

in   inlet

l   liquid

tot   total

UNITS

temperature   degree centigrade ($^{\circ}$C)

heat input   Watt (W)

length   meter (m) or millimeter (mm)

mass   kilogram (kg) or gram (g)

time   seconds (s)

pressure   absolute pressure (bar)
               Newton per square meter (N/m^2)

LIST OF REFERENCES

1. J.G. Knudsen, The effect of mixing on burnout in multirod bundles, HW-84525, December 1964.

2. L. Ingesson, Heat transfer between subchannels in a rod bundle, July 1969.

3. J.T. Rogers and N.E. Todreas, Coolant interchannel mixing in reactor fuel rod bundles single-phase coolants, Presented at the Winter Annual Meeting of the A.S.M.E. in New York, December 1968.

4. N.E. Todreas and L.W. Wilson, Coolant mixing in sodium cooled fast reactor fuel bundles, WASH-1096, April 1968.

5. J.T. Rogers and W.R. Tarasuk, A generalized correlation for natural turbulent mixing of coolant in fuel bundles, Trans. A.N.S. 11, No. 1, p. 346, June 1968.

6. D.S. Rowe, Cross flow mixing between parallel flow channels during boiling, BNWL-371 PT1, March 1967.

7. D.S. Rowe and C.W. Angle, Cross flow mixing between parallel flow channels during boiling, BNWL-371 PT2, December 1967.

8. T. van der Ros and M. Bogaardt, Mass and heat exchange between adjacent channels in liquid-cooled rod bundles, Nucl. Eng. and Design, vol. 12, no. 2, p. 259, May 1970.

9. R. Nijsing, I. Gargantini and W. Eifler, Analysis of fluid flow and heat transfer in a triangular array of parallel heat generating rods, Nucl. Eng. and Design, vol. 4, p. 375, 1966.

10. D.S. Rowe and C.W. Angle, Cross flow mixing between parallel flow channels during boiling, BNWL-371 PT3, January 1969.

11. R.W. Bowring and J. Levy, Freon 7-rod cluster subchannel mixing experiments, AEEW-R663, 1969.

12. A. Rosuel and A. Beghin, Etude de la repartition des debits dans une section d'essais a deux caneaux, Rapport Euratom no. 25, 1966.

13. T.P. Bestenbreur and C.L. Spigt, Study on mixing between adjacent channels in an atmospheric air-water system, THE report WW030-R103, May 1970.

14. D.S. Rowe, Cobra-II: A digital computer program for thermal-hydraulic subchannel analysis of rod bundle nuclear fuel elements, BNWL-1229 VC-80, February 1970.

15. R.W. Bowring, Hambo, a computer programme for the subchannel analysis of the hydraulic and burnout characteristics of rod-clusters, part 1: general description, AEEW-R524, 1967, and part 2: the equations, AEEW-R582, 1968.

16. C.L. Spigt, On the hydraulic characteristics of a boiling water channel with natural circulation, Doctorate thesis, Eindhoven University of Technology, 1966.

17. F.J.M. Dijkman, Some hydro-dynamic aspects of a boiling water channel, Doctorate thesis, Eindhoven University of Technology, 1969.

18. H.O. Olsen, Theoretical and experimental investigation of impedance void meters, Institutt for Atomenergi, Kjeller KR-118, August 1967.

19. J.C. Maxwell, A treatise on electricity and magnetism, Clarendon Press, Oxford, 1881.

20. N. Zuber et al, Steady state and transient void fraction in two-phase flow systems, final report, Euraec GEAP-5417, January 1967.

21. R. Wisman, Metingen aan damp- en drukverdeling van een versneld twee-phasen mengsel, Delft University of Technology, KR-226, December 1969.

22. J.R.S. Thom, Prediction of pressure drop during forced circulation boiling of water, Int. J. Heat Mass Transfer, vol. 7, p. 709, 1964.

23. R.C. Martinelli and D.B. Nelson, Prediction of pressure drop during forced-circulation boiling of water, Trans. A.S.M.E. vol. 70, 1948.

24. R. Bird, W. Steward and E. Lightfoot, Transport phenomena, Wiley, New York, 1965.

25. Mixing m x n, Rescona-Dynaflow report 338-3-217-01, July 1969.

26. S.G. Bankoff, A variable density single-fluid model for two-phase flow with particular reference to steam-water flow, Trans. A.S.M.E., J. of Heat Transfer, vol. 82, p. 265, 1960.

27. N. Zuber and J.A. Findlay, Average volumetric concentration in two-phase flow systems, Trans. A.S.M.E., J. of Heat Transfer, vol. 87, p. 453, 1965.

28. J.F. Marchaterre and B.M. Hoglund, Correlation for two-phase flow, Nucleonics, vol. 20, no. 8, p. 142, 1962.

29. W.H. Jens and P.A. Lottes, Analysis of heat transfer, burnout, pressure drop and density data for high pressure water, ANL-4627, 1951.

30. R.W. Bowring, Physical model, based on bubble detachment, and calculation of steam voidage in the subcooled region of a heated channel, HPR 10, December 1962.

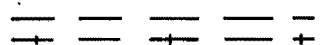31. Mixing m x n, Rescona-Dynaflow report 338-3-217-03, September 1969.

LIST OF ILLUSTRATIONS

95

Note : the key for the figures 39, 40, 42, 43, 44 and 45
       is as follows :

} experimental data

} calculated

} injected channel

} non-injected channel

SAMENVATTING (SUMMARY IN DUTCH)

Een experimenteel onderzoek is verricht naar het hydraulisch gedrag van
een twee-fase-mengsel in twee aanliggende, gesimplificeerde subkanalen
van een kernreactor tijdens menging in een doorzichtige testsectie, ten-
einde inzicht te verkrijgen in het mengmechanisme.
Koken werd gesimuleerd door het injecteren van luchtbellen door een po-
reuze glaswand in een van de subkanalen. Aan de uitlaat van de testsectie
werd het lucht-water mengsel in separators gescheiden zonder de menging
in de kanalen te beïnvloeden.
De hoeveelheid uitgewisselde massa als een functie van de kanaallengte
werd voor iedere component afzonderlijk bepaald door metingen van de
voidfractie, massastroom en drukverdeling in de kanalen. De onafhankelijk
instelbare grootheden waarvan de invloed op het systeem nagegaan is, zijn
het gesimuleerde kanaalvermogen, de massastroomvloeistof en de breedte
van de verbinding tussen de subkanalen; van elk van deze parameters werd
een grote invloed op het mengproces verwacht.

Teneinde de metingen te analyseren - met behulp van een dataverwerkings-
programma - waren behalve de experimentele gegevens, correlaties nodig
voor de slip en voor de twee-fase-frictie. Daarom werden onder gelijke
omstandigheden als tijdens de mengmetingen experimenten verricht. De
belangrijkste conclusie verkregen uit de meetgegevens is geweest het be-
palen van het mengmechanisme gedurende de metingen. Deze vonden alle
plaats onder belstroming. De menging van gas gedroeg zich als een diffusie-
proces, de uitwisseling van vloeistof was zodanig dat gelijke drukgradien-
ten in stand werden gehouden in de lengterichting van beide kanalen.
De vloeistof uitwisseling vertoonde geen interventie met de gasdiffusie,
hoewel de stromingsrichting vaak tegengesteld was.

Echter, wij zijn ons bewust van het begrensde gebied van de parameters,
zoals de druk, gewichtskwaliteit, Reynolds' nummer, type stromingsgebied
en testsectie-geometrie, gedurende de proeven, zodat wij er alleen aan-
spraak op maken, het gedrag van het systeem in kwalitatief opzicht en
het effect van de gebruikte variabelen, verklaard te hebben voor de tij-
dens het onderzoek heersende condities.
Toegevoegd is een mathematische beschrijving van het thermisch-hydraulisch
stationair gedrag van subkanalen tijdens menging. De theoretische studie
was gebaseerd op een oplossing van de behoudswetten van ieder subkanaal
waaraan een uit metingen verkregen uitdrukking voor twee-fase-menging
was toegevoegd. De vergelijkingen werden numeriek geprogrammeerd en opge-
lost met behulp van een computer. De kwalitatieve resultaten van de bere-
keningen waren in redelijke overeenstemming met de experimenten.

98

CURRICULUM VITAE

Op aanbeveling van de senaat volgt hier een kort levensbericht van
de schrijver van dit proefschrift.

Hij werd geboren te Rotterdam op 23 mei 1939. Na de lagere school
bezocht hij een M.U.L.O. school, waar het eindexamen M.U.L.O.-b
werd afgelegd in 1957, en een Hogere Technische School, beide te
Den Haag. Na het behalen van het H.T.S. diploma werktuigbouwkunde
in 1961 vestigde hij zich in Canada. Daar vervolgde hij aan the
University of Western Ontario zijn studie in de werktuigbouwkunde.
Zijn afstudeerwerk in Heat Transfer and Fluid Mechanics voerde hij
uit onder leiding van Prof.dr. E.S. Nowak. De graad van Master of
Science in Engineering werd uitgereikt in oktober 1965.

Hierna trad hij als wetenschappelijk medewerker in dienst van de
Technische Hogeschool Eindhoven, waarbij een deel van zijn onder-
zoek, verricht in het laboratorium voor Warmtetechniek en Reaktor-
bouw, heeft geleid tot het schrijven van dit proefschrift.
Sedert kort is hij in dienst van de N.V. Philips te Eindhoven.

STELLINGEN

1. De veel verbreide mening, dat gedurende cross-flow tussen subkanalen
   een mengsel van een gemiddelde dichtheid oversteekt, is niet juist.
   Zie o.a.: D.S. Rowe, BNWL-1229 VC-80, 1970
   R.W. Bowring, AEEW - R582, 1968.

2. Bij de berekening van de cross-flow tussen subkanalen zoals beschreven
   in dit proefschrift zal de richting van de cross-flow fysisch niet
   altijd overeenkomen met de radiale drukgradient.

3. De mening van Spigt, dat bij de berekening van de menging van de koel-
   vloeistof van twee belendende kanalen het niet toelaatbaar is dat de
   dwarsstroming tengevolge van radiale drukverschillen zo groot wordt
   gekozen, dat het verloop van de statische druk in axiale richting voor
   beide kanalen dezelfde is, is door de resultaten van de metingen, be-
   schreven in dit proefschrift, niet bewezen.
   C.L. Spigt, proefschrift TH Eindhoven, 1966.

4. Bij het ontwerp van meerstaafs testbundels wordt veelal onvoldoende
   aandacht besteed aan de plaatsing van de omringende wand t.o.v. de
   randstaven waardoor veelal de reactorconditie niet juist wordt gesimu-
   leerd.
   T. van der Ros, TH Eindhoven, rapport V-422, 1969.

5. Een herwaardering van de bekende experimentele burn-out data in bundels
   zou, indien rekening werd gehouden met het mogelijk optreden van menging
   tussen de subkanalen, kunnen leiden tot meer algemeen toepasbare burn-out
   correlaties.

6. Het is opmerkelijk dat de twee fasen frictie correlatie van Martinelli-
   Nelson die gebaseerd is op resultaten van adiabatische lucht-water expe-
   rimenten in een horizontale pijp verricht in 1941 een nog steeds veel
   gebruikte rekenmethode is om het frictieverlies te berekenen in een niet
   adiabatische twee fasen stroming in opwaartse richting.
   R.C. Martinelli en D.B. Nelson, Trans. A.S.M.E., vol. 70, 1948.

7. Het isoleren van het Technisch Hoger Onderwijs van andere richtingen van
   hoger onderwijs, ontstaan door het oprichten van technische hogescholen,
   heeft vele bezwaren.

8. De interpretatie van burn-out metingen met onderkoelde uitlaatcondities
   dient met zorg te geschieden omdat de vereiste hogere eisen die gesteld
   moeten worden aan de instrumentatie, t.o.v. metingen in het gebied van
   positieve uitlaatkwaliteiten, veelal niet worden onderkend.

9. Vaak wordt door fabrikanten van stoomgenererende warmtewisselaars bij het ontwerp onvoldoende gebruik gemaakt van de kennis die in de verschillende van toepassing zijnde vakgebieden bestaat.

10. Het verdient aanbeveling te onderzoeken of het geven van onderwijs in de engelse of spaanse taal i.p.v. de nederlandse taal in de overzeese rijksdelen de ontwikkeling van deze gebieden ten goede zou komen.

T. van der Ros
10 november 1970